Study about the Employing both Hydrogen and Microwave Irradiation for a Novel Pre-treatment of High Sulfur Iron Ore

アフマドレザ, アミニ

Kyushu University

Materials Science and Engineering

Study about the employing both Hydrogen and Microwave Irradiation for a Novel Pre-treatment of High Sulfur Iron Ore

A Thesis Submitted in Partial Fulfillment of the Requirement for the Degree of Ph.D. in Materials Process Engineering

By:

Ahmadreza AMINI

Supervisors:

Prof. Kazuya KUNITOMO

Associate Prof. Ko-ichiro OHNO

Assistant Prof. Takayuki MAEDA

December 19, 2018

In the name of the only engineer of the universe who created it and managing everything well.

Table of Index

Table of Figures

Tables

Chapter 1: INTRODUCTION

Ironmaking processes can be classified into different generations including the blast furnace (BF) process, the direct reduction ironmaking (DRI) process, and the Ironmaking Technology Mark 3 (ITmK3) in which the materials stay in the furnace for ~480, 360, and 10 min, respectively [1]. In all of these processes, iron ore plays an important role as the main iron source. Hence, the characterization and treatment of iron ore are determining steps for an efficient ironmaking process.

1-1. Iron Ore

Iron ore is a natural mineral containing iron oxides and accompanied by gangues. Iron can be found in iron ores in the form of hematite, magnetite, and/or iron carbonate [2]. Hematite, Fe_2O_3 (red iron ore), with a specific gravity of 5.26 is an anhydrous ferric oxide which can be either earthy, compact or crystalline [3] with a major gangue of silica, SiO_2. Hydrous ferric oxide is limonite (brown iron ore) with major gangues of alumina (Al_2O_3), silica (SiO_2), and lime (CaO) [2]. Magnetite, Fe_3O_4, with a specific gravity, 5.16 to 5.18 is strongly magnetic [3] and contains silica, lime and magnesia (MgO) as main gangues. Iron carbonate, $FeCO_3$, is known as siderite or sparry iron ore [2] with a specific gravity of 3.83 to 3.88 containing calcium, manganese, and magnesium [3].

An important parameter for attaining a high quality product is the amount of impurities such as sulfur (S) and phosphorous (P) that needs to be as small as possible. For a high-efficient treatment of these impurities (sulfur, in the present study), we need to know sources of these impurities during the ironmaking process.

1-1-1. Sulfur sources during reduction of iron ore

Iron forms three binary sulfides: FeS, FeS_2, and Fe_2S_3. FeS (magnetic pyrite) and FeS_2 (pyrite) are found naturally. In industry, FeS is obtained by melting scrap iron with sulfur ($Fe + \frac{1}{8}S_8 = FeS$) or pyrite ($Fe + FeS_2 = 2FeS$) [4].

Sulfur is also present in coal, both as organic and inorganic sulfur [5]. The total sulfur in coal varies in the range of 0.2−11 mass %, mostly in the form of FeS_2. Generally, the amount of sulphate sulfur cannot exceed 0.1 mass % except when the coal is exposed to air [6]. Sulfur can decrease the rate of carbon dissolution from graphite owing to either a decrease of carbon diffusivity, surface blockage, or a reduction of contact area due to poor wetting [7].

Not only, a coal-iron ore mixture contains sulfur which contaminates the reduced iron during the ironmaking process [8], but also iron ore may contain sulfur. Sulfur makes iron brittle, prone to cracking and failure, and has effect on reactions which are related to surface owing to the surface – active characteristic of this impurity.

Therefore, sulfur behavior during reduction of iron ore is a vital parameter for an efficient treatment in ironmaking process. However, for an accurate understanding of the sulfur behavior during reduction reaction, a sufficient information is required about the behavior of pure iron oxide during reduction reaction.

1-1-2. Reduction of Iron Ore

The iron production by the conventional methods is extensively energy and time consuming in addition to the consumption of a large quantity of natural resources. To overcome these issues, one approach is to employ methods with a shorter time and/or a lower temperature than the blast furnace methods. For example, using the fine iron ore powder with larger ratio of the

surface area to the volume is very effective to accelerate the reduction reaction whereas in the blast furnace, the fine particles fly away with hot air blasted from tuyers and prevent hot gas to flow in the furnace [9].

Moreover, microwave processing has been widely developed as alternative methods for ironmaking owing to its advantages as follows [10]:

1. Small amount of waste gas due to burner-less process.
2. Rapid, volumetric, and selective heating of materials.
3. High energy efficiency owing to the volumetric heating.
4. Reactions can be catalyzed because the heating occurs on a molecular or atomic level.
5. The temperature of the refractory can be minimized.

1-2. Microwaves

Electromagnetic (EM) radiation is a form of energy comprising both electric and magnetic fields perpendicular to each other. Generally, EM radiation is classified by the wavelength into radio waves, microwaves, infrared radiation, visible light, ultraviolet radiation, X-rays and gamma rays [11], as shown in **Figure 1-1**.

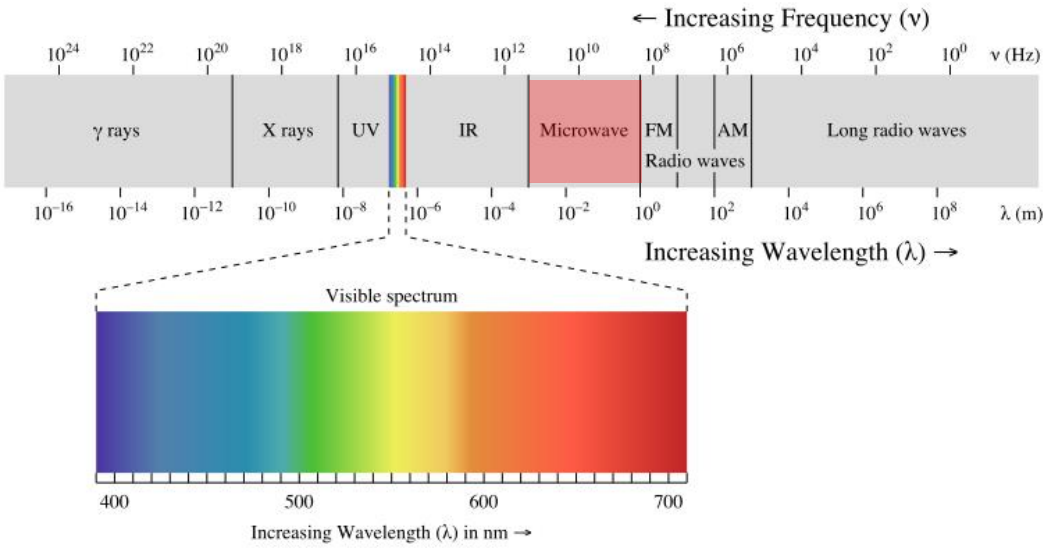

Figure 1-1 The electromagnetic spectrum [12].

Microwaves are the electromagnetic waves with frequencies in the range of 300 MHz to 300 GHz and wavelengths of 1 m to 1 mm [11]. Such frequencies and wavelengths make the microwaves suitable for different applications.

1-2-1. Microwaves in communications

Microwaves are used extensively in satellite communication for the transmission of signals and information because of their ability to penetrate Earth's atmosphere with minimum losses. Also, high frequency and greater bandwidth of microwaves provide more capability of information transmission [11].

1-2-2. Microwaves in radio detection and ranging (Radar)

Radars, such as the Global Positioning System (GPS), transmit the microwave signals and receive the reflected signals from the target. Comparing the transmitted and reflected microwave signals determines the velocity, elevation and shape of the target [11].

1-2-3. Microwaves in medical applications

Microwaves are used in hyperthermia treatment of cancer to create intense heat in the cancerous tissue and kill it. The other example of microwave application is MRI and promising application in the detection of tumors [11].

1-2-4. Microwaves in industrial and commercial applications

Microwaves are used in semiconductor processing techniques to enhance chemical vapor deposition (CVD) via generating plasma. Microwaves are also used for inspection purposes such as the nondestructive testing (NDT) [11].

1-2-5. Microwave–Material Interactions

The interaction of microwaves with materials can be generally classified into four categories, as illustrated in **Figure 1-2** [11]:

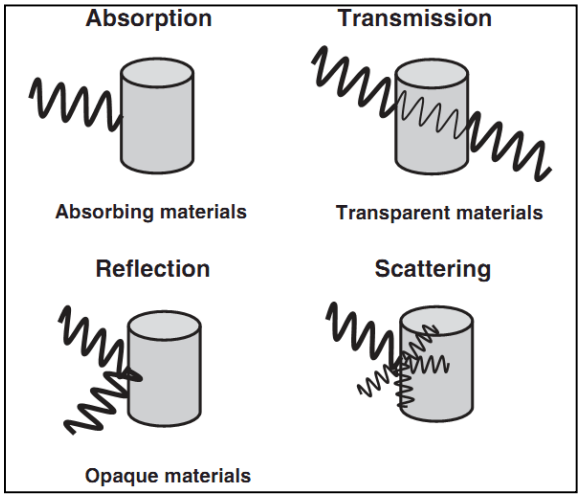

Figure 1-2 Interaction of the electromagnetic waves with materials [11].

Conducting materials, such as metals, reflect electromagnetic waves and act as opaque materials while low dielectric loss materials or insulating materials, such as glass, ceramics and air, let the microwaves to pass through. High dielectric loss materials can absorb electromagnetic energy and convert it to heat.

In microwave processing of materials, the interaction between the electric and magnetic field components of the microwaves and the materials can result in heating owing to the dielectric and magnetic losses. Dielectric loss is owing to the redistribution of charges or polarization under the influence of an alternating external electric field. The dielectric polarization loss includes electronic polarization, dipolar polarization, atomic (or ionic) polarization and interfacial polarization. Conduction loss is dominant mechanism for heating in materials with high conductivity, such as metals. In magnetic materials, magnetic losses such as hysteresis, eddy currents, domain wall and electron spin resonance contribute to the heating.

However, the different interactions between materials to microwaves cannot be explained by single theory [11].

1-2-1. Microwave heating

An increase in the conductivity of insulating materials such as oxide ceramics with temperature leads to an increase in the dielectric properties allowing better coupling with microwaves. Heating of high-conductivity materials such as metals is mainly affected by magnetic induction or induced eddy currents which move the electrons to an area near the surface. However, the density of the induced currents is decreased with increasing depth, known as the skin effect. The distance from the surface to a point inside the material where the power of the exposed electromagnetic waves decreases to 1/e (36.8%) of the surface value [13,14] is called penetration depth, or skin depth.

In conventional heating, thermal energy is usually transferred to the material by infrared radiation from the heating elements. Since the penetration depth of the infrared radiation is restricted to the surfaces of the material, heat transfer to the rest of the material is based on conduction from surface (hotter part) to the center (colder part). In microwave irradiation, heat can be generated from within the material owing to the penetrative power of microwaves. Therefore a temperature profile from center (hotter) toward the surface (colder) is expected during microwave heating owing to the heat loss from surface to the surroundings [11].

1-3. Reduction of Iron Ore during Microwave Heating

The energy required for the chemical reactions, such as endothermic deoxidation reaction, needs to be volumetrically transported into the iron oxide [13]. Therefore, the volumetric microwave heating has been considered as an energy source to speed up the chemical reactions [15–18]. Stir *et al*. [19] showed that the magnetite reduction to Fe during microwave heating is mediated by wüstite which forms as a nonstoichiometric reaction layer at the surface of unreacted Fe_3O_4 cores and propagates toward the inner volume of the magnetite particles. Hayashi *et al*. [20] showed that the magnetite is rapidly reduced to wüstite with increasing temperature from 850 °C to 950 °C followed by endothermic reduction of wüstite to iron from 950 °C to 1400 °C during microwave heating of mechanically mixed iron ore and graphite powder. It is also reported [9] that in the case of the conventional heating, samples started to reduce at ~1000 °C and carburized at ~1300 °C while by microwave heating, the reduction can initiate at ~820 °C and the carburization at ~1250 °C.

1-4. Behavior of Impurities during Microwave Heating

Hara *et al.* [21] reported that the phosphorus in magnetite ore can be removed in off-gas during microwave heating of mechanically mixed iron ore and graphite powder owing to the low oxygen partial pressure and the absence of lime to make little slag. They showed that the phosphorous content of produced pig iron during this process is lower than that of pig iron in blast furnace. Further, they demonstrated that the sulfur content dissolved into pig iron during microwave treatment is higher than in pig iron of blast furnace owing to the lack of lime and slag.

1-5. The Purpose of the Present Study

Demand for high-grade iron ores is increasing to produce high-quality steels whereas the purity of iron ore is decreasing with time, as shown in **Figure 1-3** [22].

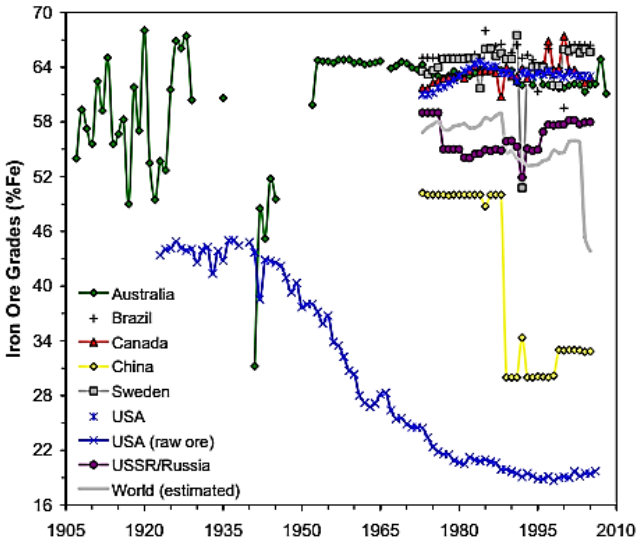

Figure 1-3 Estimated iron ore grades with time for selected countries [22].

Therefore, treatment of low-grade iron ores is unavoidable in the recent ironmaking processes. For example, Iranian iron ore in the Sangan, Gol-e-Gohar, and Chadormalu mines (~80% of Iranian iron ore are produced from these mines [23]) are considered as high sulfur iron ores, as presented in **Table 1-1**.

Table 1-1 Characteristics of the Sangan, Gol-e-Gohar, and Chadormalu iron ore mines

Mine	**Magnetite**	**Hematite + Limonite /Apatite**	**Pyrite /Pyrrhotite**	**TFe** (wt %)	**FeO** (wt %)	**S** (wt %)	**P** (wt %)
Sangan [24]	Mostly		Main source of sulfur (1-8 %)	66.4*		0.72*	<0.01*
Gol–e–Gohar [25]	30-45 %	5 %	1-8 %	50.91	15.29	1.62	0.075
Gol–e–Gohar [26]	Mostly	Apatite: Main Source of P	Pyrite: Main Source of S	67.7	17.7	0.5	0.08
Chadormalu [27]	~ 75 %	Apatite: Main Source of P		55.9		0.19	0.94

* After low intensive magnetic separation

On the other hand, processing of high sulfur iron ores is an important issue regarding the environmental considerations such as SO_2 and CO_2 emissions. To mitigate the emission of these gases, a novel process is required to decrease either carbon consumption or SO_2 emission.

Carbothermic reduction of iron oxide can be accomplished at a lower temperature and in a shorter time during microwave treatment compared to the conventional heating. This energy-efficient process decreases the carbon consumption during iron ore treatment. A further CO_2 mitigation is also expected by using H_2, instead of carbonaceous materials, as a reducing agent. On the other hand, a good desulfurizer such as CaO is required to prevent SO_2 emission in treatment of a high-sulfur iron ore.

In the present study, microwave treatment of high sulfur iron ore in the presence of CaO in H_2 is proposed as a novel approach for mitigating both CO_2 and SO_2 emissions during desulfurization and reduction reactions.

In almost all previous investigations about reduction reactions via microwave heating, a mixture of iron oxide and carbonaceous materials has been used owing to a great microwave absorbability of carbonaceous materials which accelerate the heating of the sample during treatment; however, in the absence of the carbonaceous materials (in this study, H_2 will be used as a reducing agent, instead of using carbonaceous materials), only initial material can act as a microwave absorber to heat up the sample. Therefore, the magnetite (Fe_3O_4) was selected as the initial material in the present study because of its higher microwave absorbability than other oxide-states of iron. Moreover, the interaction between microwaves and Fe_3O_4 particles plays a vital role in the microwave treatment, especially in the absence of a good microwave susceptor such as carbonaceous materials. Therefore, in the first step, the interaction between microwaves and magnetite particles will be studied in N_2 at both high temperatures (T>585 °C) and temperatures lower than the Curie point (T<585 °C) to have a comprehensive understanding about effective parameters, such as magnetite particle size and apparent density, on microwave heating. As mentioned before, a novel eco-friendly process is proposed in this study for microwave treatment of magnetite to combine the advantages of both microwave heating and using H_2 as a reducing agent for the first time in the world. Therefore, to investigate the H_2-reduction behaviour of magnetite particles during microwave irradiation, the atmosphere will be changed from N_2 to H_2 and the effect of magnetite particle size and microwave characteristics, such as penetration depth, will be investigated.

Up to here, the reduction reaction behavior of the magnetite in H_2 during microwave irradiation will be clarified; however, the main purpose of the present study is the reduction and desulfurization of a high-sulfur iron ore.

To investigate the effect of sulfur on the reduction reaction of a high-sulfur iron ore, a mixture of Fe_3O_4 and FeS (as sulfur source) will be used to prepare a high-sulfur magnetite sample similar to the actual high-sulfur iron ore. In addition, to study simultaneous desulfurization and reduction reaction of the high-sulfur magnetite sample during microwave treatment in H_2, CaO will be added, as a good desulfurizer, to the mixture.

Finally, to expand our understanding of the dominant mechanism in the simultaneous desulfurization and H_2-reduction of high sulfur iron ore, a kinetic study will be conducted using FeS-CaO mixture. For this purpose**,** the microwave heating system will be equipped with thermobalance to prepare a unique apparatus for a continuous study of the hydrogen reduction during microwave irradiation. In addition, the simultaneous desulfurization and carbothermic reduction of FeS in the presence of CaO in N_2 will be performed to compare the effect of reducing agent (graphite and H_2) on the reaction during microwave treatment.

1-6. References

[1] C. Wu, V. Sahajwalla, Dissolution rates of coals and graphite in Fe-C-S melts in direct ironmaking: Influence of melt carbon and sulfur on carbon dissolution, Metall. Mater. Trans. B. 31 (2000) 243–251.

[2] K. Bugayev, Y. Konovalov, E. Tretyakov, Y. Bichkov, V. Kovalenko, Iron and Steel Production, Book for Business, 2001.

[3] J. Poveromo, The Making, Shaping and Treating of Steel, The AISE Steel Foundation, Pittsburgh, PA, 1999.

[4] A. Holleman, E. Wiberg, Inorganic Chemistry, Academic Press, 2001.

[5] S. KIKUCHI, S. ITO, I. KOBAYASHI, O. TSUGE, K. TOKUDA, ITmk3 Process, KOBELCO Technol. Rev. 29 (2010) 77–84.

[6] A. Ghosh, Ironmaking and Steelmaking Theory and Practice, 2008.
[7] A. Attar, Chemistry, thermodynamics and kinetics of reactions of sulphur in coal-gas reactions: A review, Fuel. 57 (1978) 201–212.
[8] S. Inaba, Y. Kimura, Behavior of Sulfur in the Carbon-bearing Iron Oxide Pellet during Heating, ISIJ Int. 44 (2004) 2112–2114.
[9] K. Ishizaki, K. Nagata, T. Hayashi, Production of pig iron from magnetite ore-coal composite pellets by microwave heating, ISIJ Int. 46 (2006) 1403–1409.
[10] K. Nishioka, T. Taniguchi, Y. Ueki, K. Ohno, T. Maeda, M. Shimizu, Gasification and Reduction Behavior of Plastics and Iron Ore Mixtures by Microwave Heating, ISIJ Int. 47 (2007) 602–607.
[11] M. Gupta, E. Wong Wai Leong, Microwaves and Metals, John Wiley & Sons, 2007.
[12] Electromagnetic radiation, Free Encycl. Wikipedia. (2016). https://en.wikipedia.org/wiki/Electromagnetic_radiation#/media/File:EM_spectrum.svg (accessed February 3, 2016).
[13] M. Hayashi, Y. Yokoyama, K. Nagata, Effect of particle size and relative density on powdery Fe_3O_4 microwave heating, J. Microw. Power Electromagn. Energy. 44 (2010) 198–206.
[14] C.A. Crane, M.L. Pantoya, B.L. Weeks, M. Saed, The effects of particle size on microwave heating of metal and metal oxide powders, Powder Technol. 256 (2014), 113.
[15] A. Ferrari, J. Hunt, A. Lita, B. Ashley, A.E. Stiegman, Microwave-Specific Effects on the Equilibrium Constants and Thermodynamics of the Steam − Carbon and Related Reactions, J. Phys. Chem. C. 118 (2014) 9346–9356.
[16] J. Hunt, A. Ferrari, A. Lita, M. Crosswhite, B. Ashley, A.E. Stiegman, Microwave-specific enhancement of the carbon-carbon dioxide (Boudouard) reaction, J. Phys. Chem. C. 117 (2013) 26871–26880.
[17] J. Zhou, W. Xu, Z. You, Z. Wang, Y. Luo, L. Gao, C. Yin, R. Peng, L. Lan, A new type of power energy for accelerating chemical reactions: the nature of a microwave-driving force for accelerating chemical reactions, Sci. Rep. 6 (2016) 25149.
[18] K. Kashimura, M. Sato, M. Hotta, D. Kumar Agrawal, K. Nagata, M. Hayashi, T. Mitani, N. Shinohara, Iron production from Fe_3O_4 and graphite by applying 915 MHz microwaves, Mater. Sci. Eng. A. 556 (2012) 977–979.
[19] S.B. Lee, P.C.H. Rhee, Reduction behavior of iron ore by reducing gas containing H_2S, Scand. J. Metall. 32 (2003) 203–210.
[20] S. HAYASHI, Y. IGUCHI, J. HIRAO, Effects of the oxygen and sulphur potentials in reducing gas on the reduction rate of wustite and morphology of reduced iron., Trans. Iron Steel Inst. Japan. 24 (1984) 143–146.
[21] K. Hara, M. Hayashi, M. Sato, K. Nagata, Pig Iron Making by Focused Microwave Beams with 20 kW at 2.45 GHz, ISIJ Int. 52 (2012) 2149–2157.
[22] G.M. Mudd, The limits to growth and "finite" mineral resources: re-visiting the assumptions and drinking from that half-capacity glass, Int. J. Sustain. Dev.16(2013) 204.
[23] 2014 MINERALS YEARBOOK—IRAN, US deological survey, December 2017.
[24] B. Rezaee, A. Sarvi, A. Eslamian, S.M. Jebraeeli, A. Zabihi, Sulfur reduction in Sangan iron ore by flotation, E3S Web of Conferences, 18 (2017), 01023.
[25] T. Zhao, X. Wang, H. Ai, A. Sobhy, Process Mineralogy of Iranian High Sulfur Iron Ore, J. Minerals and Materials Characterization and Engineering, 6 (2018), 498–506.
[26] V. Soltanmohammadi, M. Noaparast, A. Hossein Kohsari, F. Zamani, Determination of optimum conditions to remove sulfur and phosphor from Gol-e-Gohar iron ore concentrate, IRAN J SCI TECHNOL B, Vol. 33, No. B3, pp 267-278.
[27] http://www.chadormalu.com/en-us/AboutMine

Chapter 2: Effect of particle size and apparent density on the initial stages of temperature increase during the microwave heating of Fe_3O_4

2-1. Abstract

Effect of the particle size and apparent density on the time required for the initial temperature increase during the microwave heating of Fe_3O_4 was investigated [1][2] to clarify the mechanism of interaction between the magnetite powder and microwave at temperatures lower than the Curie point of Fe_3O_4 (585 °C). Samples in the form of powders and briquettes (density, 3.3 g/cm^3) with particle sizes of 75–150 μm, 45–75 μm, and <45 μm were heated in multi-mode and maximum E- and H-field modes using a microwave generator at a frequency of 2.45 GHz. Results reveal that the microwave absorption capability of a sample with higher apparent density is lower because of its higher electrical conductivity, which causes a shallower penetration depth. Further, the effect of the particle size on the microwave heating of Fe_3O_4 at temperatures higher than the Curie point is different in the presence and absence of a strong electric field. This is attributed to a change in the heating mechanism from dielectric loss in the presence of the E-field to Joule loss in its absence. At temperatures lower than the Curie point, some of the small particles would be transparent owing to a greater penetration depth of the microwaves, which causes an early onset of temperature increase in the magnetite sample with a larger particle size. Moreover, the mechanism for the formation of spark and plasma during the microwave-induced heating is discussed by applying a novel approach to analyse the interactions between the powdery materials and microwaves.

2-2. Introduction

Iron production with microwave heating is considered a possible solution to mitigate the CO_2 emission. Reduction of iron oxide using highly efficient microwave heating is reported as a new method for energy conservation and also for decreasing the CO_2 emission [3–5]. Although bulk metals reflect most of the microwaves owing to the shallow penetration depth, sufficiently small-sized metal particles can couple with microwaves [6], and therefore, microwave-assisted sintering of fine metal powders is possible, as reported previously [7,8]. In addition, a higher reduction rate of iron oxide in H_2 than in CO [9–12] and also a higher interdiffusion coefficient of H_2/H_2O gas than that of CO/CO_2 [13] for diffusion into iron ore particles sintered at 500 °C have increased the demand for using H_2 as the reducing agent, instead of carbonaceous materials, to mitigate CO_2 emissions from the iron-making process. This has prompted research into cleaner and more efficient methods of iron production. One possibility is to employ microwaves as the heating source [3,14–18] during reduction with H_2; meanwhile, because the reduction reaction can be conducted at low temperatures of ca. 450–570 °C under H_2 atmosphere [10], it is important to expand our knowledge on the interaction between microwaves and iron resources such as magnetite in this range of temperature, which is lower than the Curie point of magnetite (585 °C). Further, the magnetic properties of magnetite can influence the interaction between the electromagnetic microwaves and Fe_3O_4. Therefore, for a more efficient use of the microwave irradiation, it is important to understand the heating mechanism and also find effective parameters for the microwave heating of powdery materials at both high temperatures and temperatures lower than the Curie point.

Magnetite is one of the most important resources for the production of iron via microwave heating because of its good coupling with microwaves. Considering the relatively low band

gap of ca. 0.1 eV of magnetite, it can be regarded as a semi-metal [19] (band gaps for metals, semiconductors, and insulators are in the range of 0.0, 0.2–3.0, and >3.0 eV, respectively [20]).

The microwave-power absorption by materials, P (W/m^3), can be evaluated using **Eq. (1)**:

$$P = \frac{1}{2}\sigma|E|^2 + \pi f \varepsilon_0 \varepsilon_r''|E|^2 + \pi f \mu_0 \mu_r''|H|^2 \quad (1)$$

where σ (S/m) is the electrical conductivity, E (V/m) is the electric field amplitude, H (A/m) is the magnetic field amplitude, f (Hz) is the microwave frequency, ε_0 (F/m) and μ_0 (N/A^2) are the permittivity and permeability of vacuum, respectively; ε_r'' (dimensionless) and μ_r'' (dimensionless) are the imaginary parts of permittivity and permeability, respectively. According to Eq. (1), three different mechanisms including Joule loss (first term, W/m^3), dielectric loss (second term, W/m^3), and magnetic loss (third term, W/m^3) would contribute to microwave heating. The effect of each mechanism is discussed in the following sections.

Previous studies [21,22] have shown that the imaginary part of the complex permittivity of magnetite increases significantly with temperature, from ca. 400–470 °C, whereas it is approximately zero at lower temperatures. Moreover, a considerable decrease in the imaginary part of the complex permeability of magnetite with temperature, from ca. 575 °C was reported. The measurements indicated that the main mechanisms for the heating of magnetite at temperatures lower than the Curie temperature of ca. 585 °C [23,24] would be the magnetic loss, whereas at elevated temperatures, the mechanism changes to the dielectric loss [25,26]. Hotta *et al*. [22] showed that the real part of the complex permittivity, ε' of Fe_3O_4 is affected by the specific surface area of the powder. Crane *et al.* [27] showed that an increase in the particle size of the conductive metals, such as aluminium, leads to an increase in the microwave absorption of the compacted powder because of an increase in the resistivity, ρ (Ω·m). They reported that in non-conductive oxides such as Fe_2O_3, a decrease in the particle size leads to an increase in both the effective surface area and effective conductivity, causing a better coupling of the microwave to the compacted powder. In addition, it has been reported [5] that pre-heating to 400 °C is required for the microwave heating of Fe_2O_3 with a high electrical resistivity of 1.0×10^7 Ω·m [27]. This is due to an increase in both the electrical permittivity and conductivity of hematite with an increase in temperature [28], resulting in a better coupling to microwaves.

Hayashi *et al*. [23] observed that absorption of microwave by magnetite at the steady state hardly depends on the particle size, and speculated that it is because of the great penetration depth of Fe_3O_4, ca. 80 μm, at room temperature at 2.45 GHz. However, such great penetration depth should be considered in case of the interaction between Fe_3O_4 and microwaves at temperatures lower than the Curie point, ca. 585 °C [23]. At the steady state, the penetration depth would be significantly shallower than 80 μm owing to an increase in the conductivity with temperature.

Moreover, there is a lack of sufficient information on the initial stages of temperature increase during the microwave heating. In fact, microwave absorption at the steady state is related to higher temperatures whereas the initial stages of temperature increase depend on the low-temperature (T< 585 °C) interaction between the microwaves and materials.

However, no clear standard is defined for the steady state attained during the microwave heating; therefore, the stagnation of the temperature increase, which would be due to the heat loss from the sample, could be considered as the steady state [23]. In the present study, the temperature of the steady state is defined as the average temperature of the sample from 100 s following the beginning of microwave heating in the multi-mode and maximum E-field mode to the end time of the experiment. For heating in the maximum H-field mode, the average temperature of the sample from 65 s to the end time of the experiment, where the temperature increased was found to stagnate, is considered as the steady state.

In this study, the effect of the apparent density and particle size on the microwave absorptivity of Fe_3O_4 is investigated by focusing on the initial stages of temperature increase for a better understanding of the interaction between the microwaves and materials at temperatures lower than the Curie point. Moreover, a novel mechanism for the formation of spark and plasma during the microwave heating is proposed by a unique approach based on the interactions between the powdery materials and microwaves.

2-3. Experimental Procedure

2-3-1. Materials

Six types of magnetite samples were prepared, including three powder samples and three briquette samples with grain sizes of 75−150 μm, 45–75 μm, and less than 45 μm, as follows:

Magnetite powder (ca. 1 μm, purity of 99%, Mitsuwa's pure chemicals) was pressed into a tablet (diameter, 30 mm; thickness, 20 mm) at a pressure of 42 MPa and then heated under a flow of Ar at 1350 °C for 1 h in an electric resistance furnace. The heat-treated tablets were crushed and ground to a certain grain size, as mentioned above. To prepare the briquette samples, ~0.02 g of a 5 mass% solution of polyvinyl alcohol in water (Tokyo chemical industry CO., LTD.) was added as a binder to 3 g of the crushed magnetite powder. Cylindrical briquette samples (diameter, 15 mm and thickness, 5 mm) were formed by cold-pressing followed by drying at 120 °C for 10 h. The properties of the samples are presented in **Table 2-1**. The apparent density of the briquette sample was calculated by dividing the weight of the sample by its apparent volume (height × π × [radius]^2) at 25 °C and pressure of 1 atm. To evaluate the density of the powder sample, 3 g of the powder was loaded into a 2.5 mL graduated cylinder followed by vibrating for 3 min using an ultrasonic cleaner (USM, AS ONE, JAPAN). Then, the bulk density of the powder sample was calculated by dividing the mass (g) of the powder, 3 g, by the volume occupied in the cylinder [29]. The electrical conductivity of the briquette samples was evaluated using an Analog tester (CX-270N, Custom) at 25 °C. The average electrical conductivity of the sample was calculated from the electrical conductivity along two directions: Along the pressure direction and orthogonal to the pressure direction. To evaluate the electrical conductivity of the powder samples, 3 g of each sample was loaded into a silica tube (20.6 mm outer diameter (OD), 15.4 mm inner diameter (ID), and 35.5 mm height). Then, the conductivity was measured between the two end of the tube occupied by the sample using an Analog tester (CX-270N, Custom) at 25 °C.

Table 2-1 Properties of magnetite samples

Sample No.	MP45	MP75	MP150	MB45	MB75	MB150
Particle size (μm)	< 45	45–75	75–150	< 45	45–75	75–150
Form	Powder	Powder	Powder	Briquette	Briquette	Briquette
Apparent density × 10^{-3} (kg/m^3)	2.1	2.4	2.6	3.3	3.3	3.3
σ in a direction orthogonal to the press direction at 25 °C (S/m)	-	-	-	6.0×10^{-3}	7.2×10^{-3}	9.5×10^{-3}
σ along the press direction at 25 °C (S/m)	-	-	-	2.5×10^{-2}	3.2×10^{-2}	5.7×10^{-2}
Average σ at 25 °C (S/m)	a	a	1.7×10^{-5}	1.6×10^{-2}	2.0×10^{-2}	3.3×10^{-2}

[a] The value is lower than the measurement limitation of ca. 8.3×10^{-6} S/m.

2-3-2. Microwave heating

The samples were subjected to microwave irradiation under multi- and single-mode operation using a microwave generator with a maximum output power of 1.5 kW at 2.45 GHz under N_2 atmosphere. For microwave heating under each mode (multi- and single-), a specific cavity was designed by the manufacturer. **Figure 2-1** illustrates the schematic of the set-up used for microwave heating in the multi-mode, whereby both the magnetic field (H) and the electric field (E) perpendicular to it contribute to heating, see **Figure 2-3**. Typically, the sample was loaded in an alumina crucible (41 mm OD, 36.5 mm ID, and 49 mm height) surrounded by ceramic wool and covered with an insulating ceramic fibre. The crucible was placed in a quartz chamber (95 mm OD, 85 mm ID, 96 mm height) and the sample was protected from oxidation by flowing N_2 during the experiments. The ceramic wool and insulation fibre, which do not absorb microwaves, served as thermal insulators preventing heat loss during heating as well as protectors of the quartz chamber.

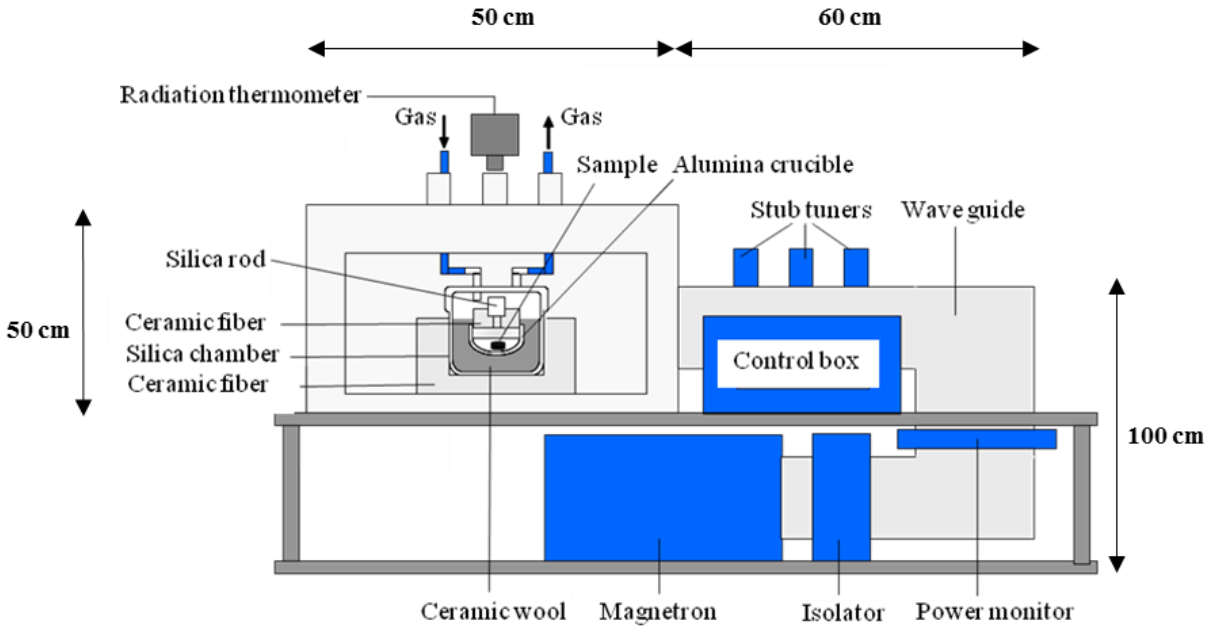

Figure 2-1 Schematic set-up of microwave heating in the multi-mode.

In case of the single mode, the H- or E-field has maximum amplitude, whereas the amplitude of the other is ca. 0, see **Figure 2-3**. For heating in the single-mode, a cavity different from that of the multi-mode one was used, as shown in the schematic of the set-up of microwave heating in the single-mode (**Figure 2-2**). An adjusting plunger was used to define the maximum magnetic or electric field position. For example, the sample was heated in the maximum E-field mode by adjusting the plunger to the sign indicating the E-field mode (red sign in **Figure 2-2**). The sample was placed on a piece of ceramic fibre and placed inside a quartz tube, and it was protected from oxidation by flowing N_2 during the experiments.

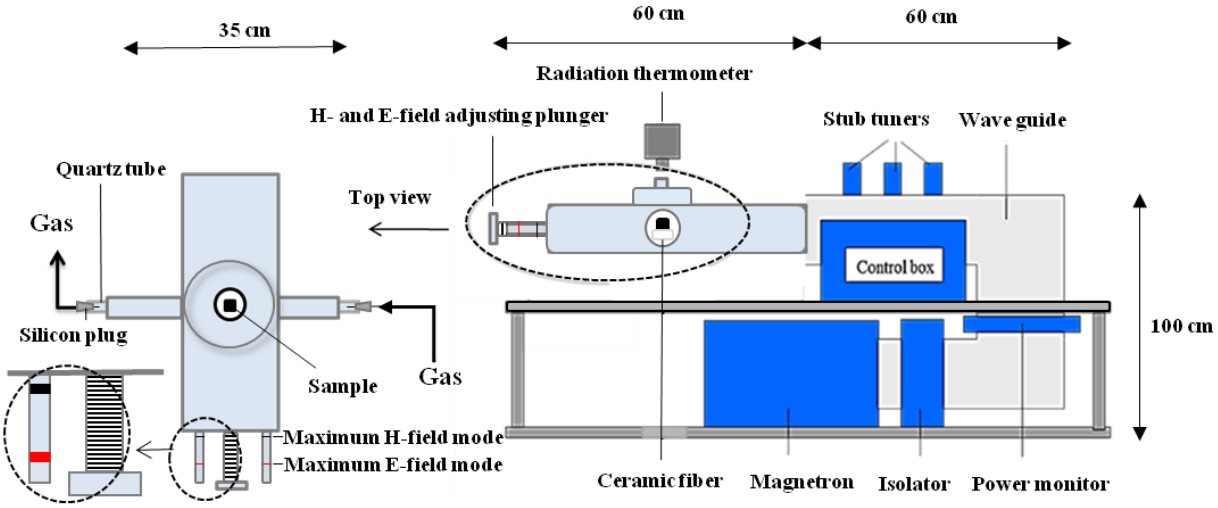

Figure 2-2 Schematic set-up of microwave heating in the single-mode (maximum E- or H-field mode).

A constant power of 1050 W was manually set using three tuning stubs until the end of the heating process in all the experiments. The temperature of the sample was measured through a window above the sample using an infrared radiation thermometer. The measurement temperature range is 330–1500 °C.

Figure 2-3 shows the schematic of single-mode and multi-mode during microwave treatment.

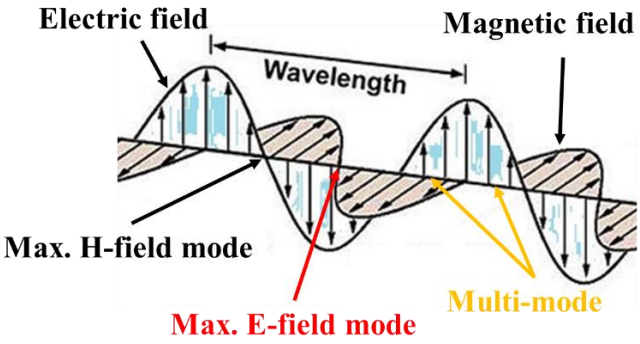

Figure 2-3 Schematic of single-mode (maximum E- or H-field mode) and multi-mode.

2-3-3. Sample analysis

To investigate the possibility of any phase change during the microwave treatment, all samples were subjected to phase analysis using X-ray diffraction (XRD, Cu-$K\alpha$; λ = 1.54 Å; scan speed, 51.9 °/min; power, 3 kW; RIGAKU Smartlab, ZOTK, JAPAN) before and after microwave heating. To prepare the samples for XRD analysis, briquette samples were crushed using a ceramic pestle.

2-4. Results and Discussion

2-4-1. Powder sample <45 μm in size

Figure 2-4 (a) shows the variation in the temperature of samples MP45 during the microwave heating in the multi-mode and maximum E- and H-field modes. Its magnitude during the initial stages of temperature increase is illustrated in **Figure 2-4** (b).

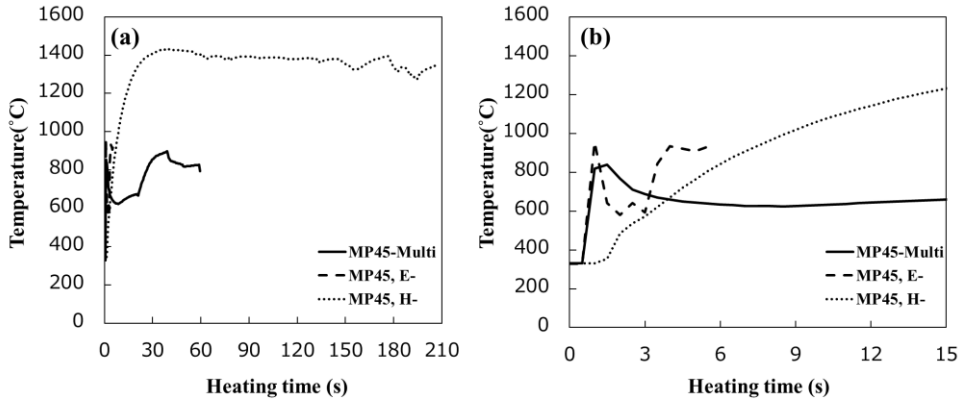

Figure 2-4 Variation in the temperature of MP45 samples during the microwave heating in the multi-mode (solid line) and maximum E- (dashed line) and H-(dotted line) field modes at 1050 W (a) and its magnitude during the initial stages of temperature increase (b).

In the maximum E-field mode, bright bluish purple plasma formed over the sample precisely after the onset of irradiation and a rapid temperature increase was observed. It seems that the infrared thermometer recorded the temperature of the plasma formed over the surface of the sample rather than the actual temperature of the sample. Moreover, a sudden increase in the temperature of the sample during the microwave heating was observed in previous studies [23,27,30], which could be due to the formation of plasma or an electric discharge. Yoshikawa *et al.* [30] reported the observation of a metallic colour in some regions over scales ranging from several hundred micrometres to millimetres in a loosely hand-pressed Fe_3O_4 sample heated in the maximum H-field mode. However, the detailed mechanism of this phenomenon could not be understood because of its occurrence inside the material; they explained it by a phenomenon called hot-spot formation due to temperature fluctuations in the sample. Bao *et al.* [31] explained that hot spots are the cause of local overheating resulting in the formation of a local liquid phase. Reportedly, these hot spots are different from thermal runaway, which is global overheating of the sample. Menendez *et al.* [32] observed two different plasmas, ball lightning and arc discharge, during the microwave heating of different kinds of carbon materials.

To explain the mechanism of spark formation, a clear definition of spark and plasma is required, as follows: An electric spark is a sudden discharge of electricity that occurs when a high electric field creates an ionized, electrically conductive channel through an insulating medium. This is created when the applied electric field exceeds the dielectric breakdown strength of the insulating medium and leads to the emission of light and a snapping sound [33]. Repeated formation of spark could generate a high-temperature region required for the ionization of gases within the voids between the particles. This ionized gas is referred to as plasma, which is one of the four states of matter.

In powdery materials, the voids among the particles form a kind of non-conducting gaps. These gaps seem to play a prominent role in the formation of spark. Particles that are affected by the electric field (the electric field is generated in the multi-mode and maximum E-field mode or induced by an alternating magnetic field in the maximum H-field mode) would act as an electrode during the microwave heating. When the electric field is sufficiently strong, the gaps between the particles, which are normally insulating mediums, transit rapidly from a non-conducting to a conducting state. Such transition could induce the formation of a spark. Meanwhile, a high-temperature region generated by the spark among the particles could induce certain changes in the appearance of the powder, as observed in this work and also reported by other researchers [3,6,30].

The formation of spark and plasma precisely after the onset of microwave irradiation in the maximum E-field mode would be due to the existence of a sufficiently high-amplitude electric field that generates sparks among the particles and provides the conditions required for the formation of plasma.

In the maximum H-field mode, the temperature increased rapidly to ca. 483 °C in 2 s and then gradually to ca. 1018 °C at a lower rate. These temperatures were measured on the surface of the sample using the radiation thermometer; however, a higher temperature is expected in the centre of the sample because of a higher thermal loss from the surface. The rapid temperature increase via the magnetic loss mechanism up to approximately the Curie point was also reported by other researchers [23]. A decrease in the rate of temperature increase would be related to the magnetic loss, which does not contribute to heating above the Curie temperature of ca. 585 °C [23], and the heating mechanism of Fe_3O_4 at these elevated temperatures is due to conduction loss [30] or dielectric loss [22].

Although no spark was observed in the beginning of heating in the multi-mode and maximum H-field mode, the spark was observed when the temperature reached ca. 890 °C after 38 s in the multi-mode and ca. 1366 °C after 150 s in the maximum H-field mode. On one hand, in the maximum H-field mode, the weak electric field induced by the alternating H-field at the beginning of the heating is apparently not high enough to generate a spark. On the other hand, a weaker electric field is required for spark formation at elevated temperatures owing to a decrease in the dielectric strength of the gaps between the particles. It seems that the electric field induced by the alternating H-field would be sufficiently high to generate a spark at ca. 1366 °C, in the present study. In the multi-mode operation, the spark was observed at a lower temperature, ca. 890 °C, compared to the temperature at which sparking was observed in the H-field maxima mode. The electric field amplitude corresponding to the multi-mode operation is not as high as that of the maximum E-field mode operation; however, it is higher than the electric field induced by the alternating magnetic field in the maximum H-field mode operation. Therefore, a lower temperature is required for the formation of spark in the multi-mode operation than that required in the maximum H-field mode.

2-4-2. Briquette sample with particle sizes less than 45 μm

Figure 2-5 (a) shows the temperature of the MB45 samples during the microwave heating in the multi-mode and maximum E- and H-field modes. Its magnitude during the initial stages of temperature increase is illustrated in **Figure 2-5** (b).

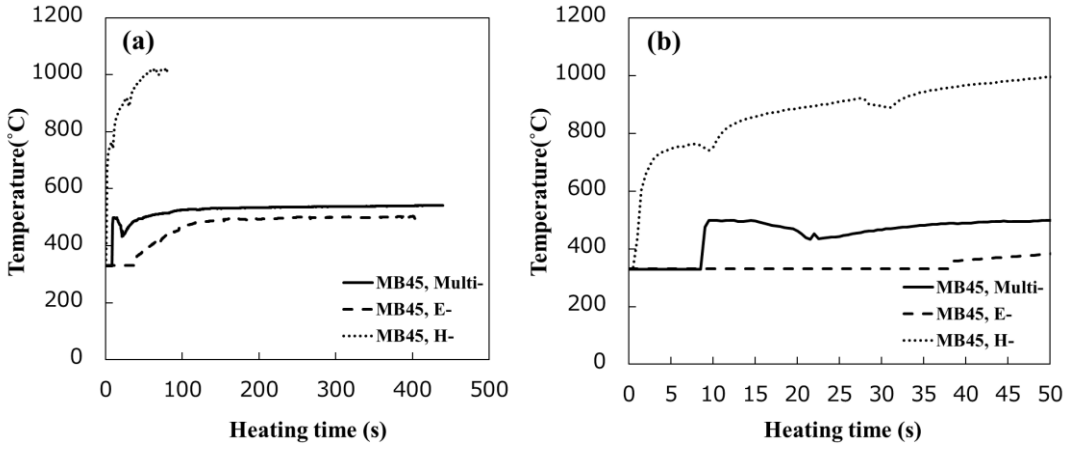

Figure 2-5 Variation in the temperature of MB45 samples during the microwave heating in the multi-mode (solid line) and maximum E- (dashed line) and H- (dotted line) field modes at 1050 W (a) and its magnitude during the initial stages of temperature increase (b).

The required time for the initial temperature increase in the sample heated in the maximum H-field mode is quite shorter than that in the sample heated in the maximum E-field mode. This indicates that the magnetic loss is the main heating mechanism at the beginning of heating, as reported by Peng *et al*. [21]. Meanwhile, no increase in temperature is observed during the heating in the multi-mode and maximum E-field mode after the surface temperature of the sample reached ca. 475 °C (the temperature of the centre would be close to the Curie temperature of ca. 585 °C [23], as explained in section **2-4-1**). Peng *et al*. [21] showed that the real and imaginary parts of the complex permittivity of magnetite noticeably increase with temperature, from ca. 470 °C, whereas those of the complex permeability decrease with temperature, from ca. 500–570 °C. This implies that the microwave absorption via dielectric loss would increase gradually due to the increase in the permittivity at elevated temperatures. However, it seems that the lower heat generated via magnetic loss and also the heat loss from the sample during the microwave heating cause the temperature increase to stagnate, as has been previously reported [23].

In case of heating in the maximum H-field mode, the temperature increased rapidly to ca. 690 °C via the magnetic loss mechanism and then increased gradually at a lower rate to ca. 1020 °C. The magnetic loss does not contribute to the heating at temperatures higher than the Curie point [21,23] and an increase in the electrical conductivity due to the temperature increase [23] would be the reason for the increase in the temperature of the sample via Joule loss.

Moreover, no spark was observed during the microwave heating of the briquette samples. It has been reported that the electrical conductivity of powdery materials could increase with an increase in their compaction [23,27]. A higher electrical conductivity of the briquette sample implies a shorter conductive path through the connected particles, instead of the path via the gaps between the particles, which could prevent spark generation.

2-4-3. X-ray diffraction analysis

Figure 2-6 shows the XRD patterns of the powder and briquette samples before and after microwave heating.

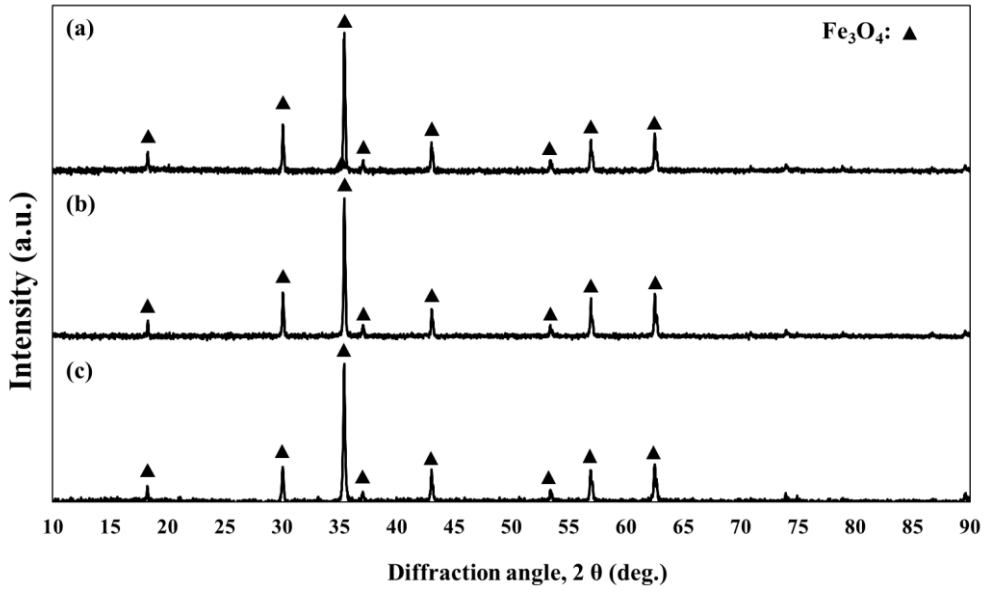

Figure 2-6 XRD patterns of the briquette (a) and powder (b) samples after the microwave heating compared to that obtained before microwave heating (c).

In the present study, no phase change was detected after the microwave heating, either in the powder or in the briquette samples. This is possibly due to the microwave photon energy, ca. 10^{-5} eV, being quite lower than the energy required for exciting the valence electrons of the metal oxides from their orbitals, at low temperatures [3,34]. This result is in good agreement with the results of other studies [35], although the de-oxidation of magnetite due to microwave heating in an inert atmosphere or in air has also been reported somewhere else [30].

2-4-4. Comparison of the powder samples

Figure 2-7 shows the average temperature of samples MP45, MP75, and MP150 at the steady state during their heating in the multi-mode and maximum E- and H-field modes. The temperature of the samples heated in the multi-mode and maximum E-field mode are related to the temperature of the spark generated before the steady state is reached and is indicated by the × symbol in **Figure 2-7**.

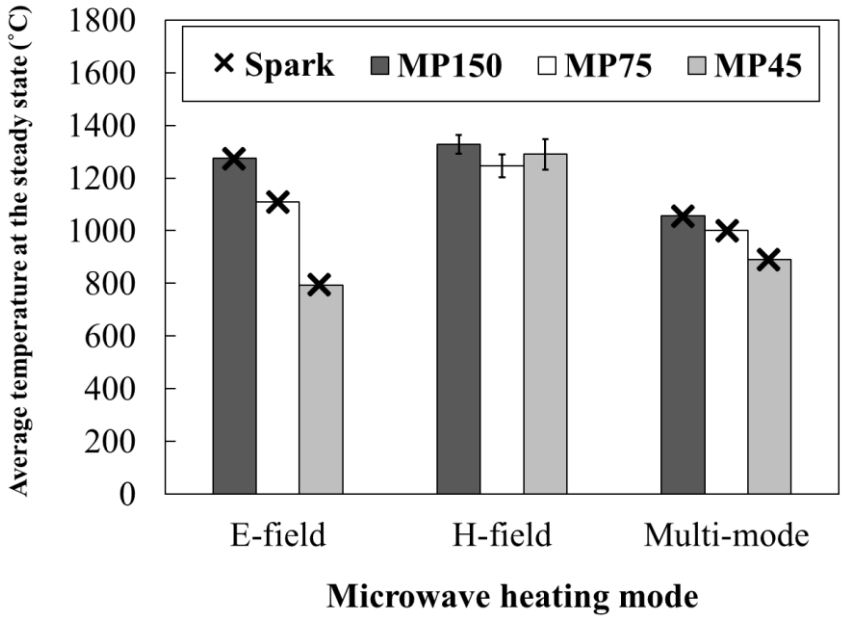

Figure 2-7 Average temperatures of samples MP45, MP75, and MP150 at the steady state during their heating in the multi-mode and maximum E- and H-field modes. The temperature of all the samples heated in the multi-mode and maximum E-field mode are related to the sparking that occurred before the steady state was reached and is indicated by × symbol. Error bars represent the standard deviations of the average temperatures at the steady state.

Figure 2-8 shows the average time required for the initial temperature increase in samples MP45, MP75, and MP150 heated in the multi-mode and maximum E- and H-field modes.

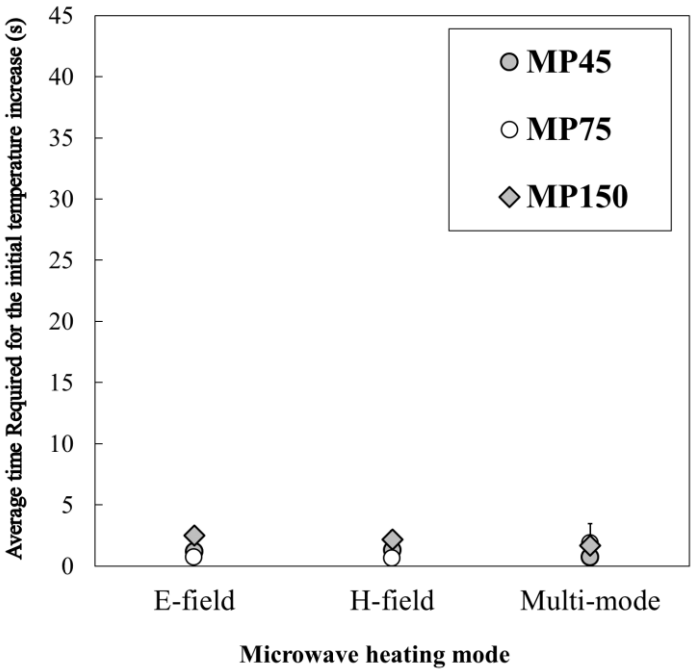

Figure 2-8 Average time required for the initial temperature increase in samples MP45, MP75, and MP150 heated in the multi-mode and maximum E- and H- field modes. Error bars represent the standard deviations of the required times.

A similar behaviour was observed for samples MP75 and MP150 compared to the sample MP45 heated in the multi-mode and maximum E-field mode (**Figure 2-7**), in which case the spark was formed. Moreover, a similar time was required for the temperature increase in samples MP75, MP150 compared to sample MP45 (**Figure 2-8**) heated in the multi-mode, E- and H-field modes, which would be due to the competition between the effect of particle size and apparent density on the microwave absorptivity of each sample.

Both the particle size and apparent density of samples MP45, MP75, and MP150 are different with respect to each other, as presented in **Table 2-1**. Therefore, it is quite complicated to explain which of the two parameters (apparent density or particle size) is dominant in these samples while comparing their behaviour with those of other samples, and this would lead to inaccurate conclusions. Therefore, to clarify the effect of particle size on microwave absorption independent of the apparent density, briquette samples with the same apparent density but different particle sizes were selected for investigating the particle size. Further, powder and briquette samples with the same particle size but different apparent density were chosen to investigate the effect of the apparent density on microwave absorption, independent of the particle size.

2-4-5. Effect of apparent density

Figure 2-9 shows the average temperature of samples MP45 and MB45 at the steady state during the microwave heating in the multi-mode and maximum E- and H-field modes. The temperature of sample MP45 heated in the multi-mode and maximum E-field mode are related to the temperature of the spark generated before the steady state is reached and is indicated by the × symbol in **Figure 2-9**.

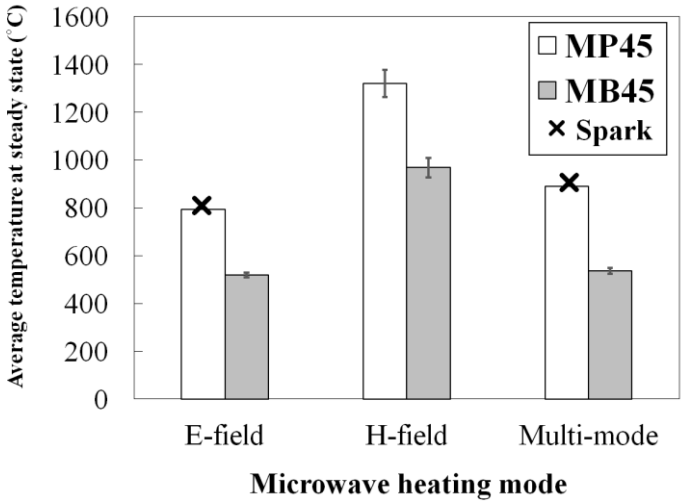

Figure 2-9 Average temperatures of samples MP45 and MB45 at the steady state during heating in the multi-mode and maximum E- and H-field modes. The temperature of sample MP45 heated in the multi-mode and maximum E-field mode are related to the spark that occurred before reaching the steady state and is indicated by × symbol. Error bars represent the standard deviations of the average temperatures at the steady state.

The powder sample, MP45, was observed to heat to a higher temperature compared to the briquette sample, MB45, demonstrating the higher microwave absorption capability of the former at the steady state. This result agrees well with the results of previous studies [23,36], wherein lower microwave absorption were observed for samples with a larger relative density.

To investigate the effect of the apparent density on the initial stages of temperature increase during the microwave heating, each experiment was conducted at least twice and the average time required for the initial temperature increase for each sample is plotted in **Figure 2-10**, with the standard deviation represented as error bars.

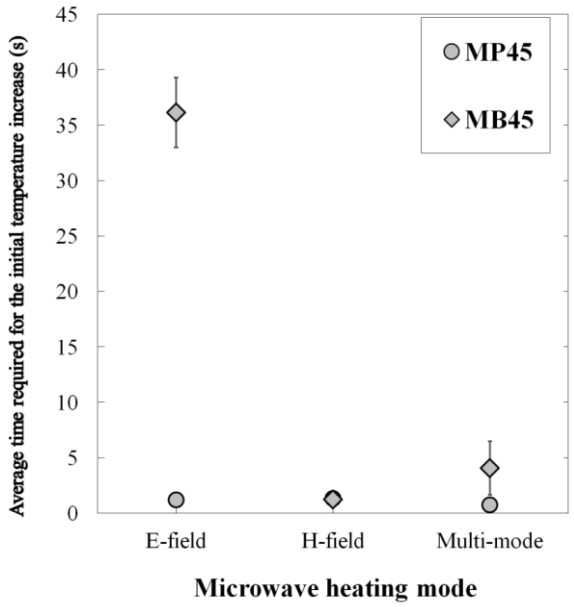

Figure 2-10 Average time required for the initial temperature increase in samples MP45 and MB45 heated in the multi-mode and maximum E- and H- field modes. Error bars represent the standard deviations of the required times.

A shorter time was required for the initial temperature increase in sample MP45, indicating better microwave absorption by this sample compared to sample MB45 even at low temperatures.

Microwave absorption is directly related to the penetration depth, δ (m). It presents the distance from the surface to a point inside the material where the power of the exposed electromagnetic waves decreases to 1/e, 36.8%, of the surface value [23,27]. It can be calculated according to **Eq. (2)** [23]:

$$\delta = \left[\frac{\omega^2 \varepsilon' \mu'}{2}\left(\sqrt{1+\frac{\sigma^2}{\omega^2 \varepsilon'^2}}-1\right)\right]^{-\frac{1}{2}} \quad (2)$$

where ω (rad/m) is the angular frequency of the microwave ($2\pi f$), σ (S/m) is the electrical conductivity, and ε' and μ' are the real parts of permittivity and permeability, respectively.

At high temperatures, such as the steady state, the main mechanisms for the microwave heating of Fe_3O_4 would be dielectric loss combined with Joule loss owing to an abrupt increase in both permittivity and electrical conductivity with temperature [21–23,28,37]. The magnetic loss could be neglected at these elevated temperatures, because of a dramatic decrease in the permeability with temperature from ca. 575 °C, as reported by Hotta *et al*. [22]. Therefore, the most effective parameters affecting the microwave absorption at high temperatures would be the permittivity and electrical conductivity. For acicular magnetite powders at room temperature and a frequency of 2.45 GHz, δ has been calculated to be ~80 μm by Hayashi *et al*. [23], with ε' = ~40, μ' = ~1.7, and σ = ~1.0×10^2 (S/cm). According to Eq. (2), an increase in the electrical conductivity causes a decrease in the penetration depth, whereas an increase in the permittivity has an inverse effect. If the values of both σ and ε' increase to the same extent, the effect of the electrical conductivity would be dominant, causing a decrease in δ. This explanation is in excellent agreement with that provided by Peng *et al*. [26]; they reported a decrease in the penetration depth of Fe_3O_4 from 0.0153 to 0.0023 m despite a significant increase in ε'' from 1.0976 to 83.3109 with an increase in the temperature from 24 to 880 °C. The penetration depth of a compacted magnetite sample would be shallower than 80 μm owing to the increases in both the permittivity and electrical conductivity with an increase in the relative density, as reported by other researchers [21–23,27,37,38]. Therefore, a lower temperature of sample MB45 at the steady state compared to that of MP45 could be attributed to the smaller amount of heat that could be generated in the former sample, owing to a shallower penetration depth.

At low temperatures, such as the initial stages of temperature increase, the dielectric loss could be neglected because of the very low permittivity of magnetite ($\varepsilon'' \simeq 0$) [22]. Moreover, Hotta *et al*. [38] reported an increase in the permeability of Fe_3O_4 with an increase in the relative density. As mentioned above, an increase in the permeability leads to a decrease in δ; moreover, an increase in the electrical conductivity also causes a decrease in the penetration depth (Eq. (2)). Therefore, an early onset of temperature increase in sample MP45 compared to the onset of temperature increase in sample MB45 could be related to the shallower penetration depth of the latter even at low temperatures.

Further, the behaviours of samples MP75 and MP150 were found to be similar those of samples MB75 and MB150, respectively.

2-4-6. Effect of particle size

According to **Figure 2-11**, no significant difference is observed between the steady state temperature of samples MB45, MB75, and MB150 heated in the multi-mode and maximum E-

field mode, where a strong electric field exists. This result is in a good agreement with that of Hayashi *et al.* [23] who reported that the microwave heating of magnetite is hardly affected by the particle size. However, in the present study, the steady state temperature of MB150 is observed to be respectively ca. 15 and 70 °C higher than those of MB75 and MB45 when heated in the maximum H-field mode.

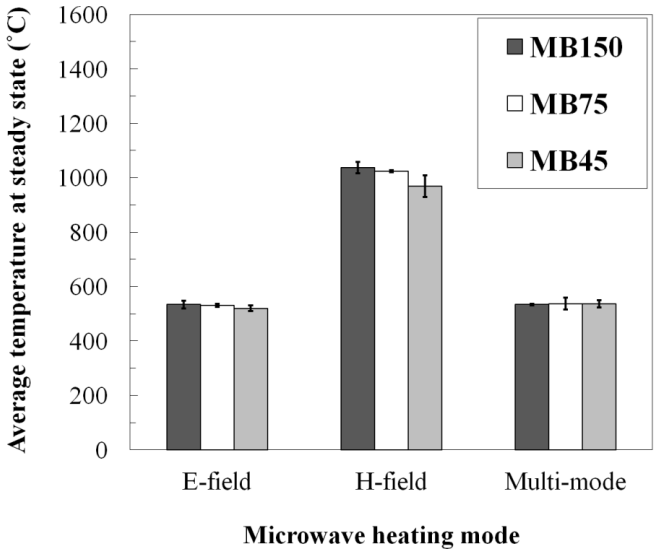

Figure 2-11 Average temperatures of samples MB150, MB75, and MB45 at the steady state during the microwave heating in the multi-mode and maximum E- and H-field modes.

In the presence of an electric field, at high temperatures, the dielectric loss is the dominant mechanism for heating [25,26] because of a significant increase in the imaginary part of the permittivity with temperature [21,22]. Therefore, the similar temperatures observed at the steady state in the presence of the E-field could be due to the complex permittivity of the sample, which is independent of the particle size [38]. In the absence of a strong electric field at high temperatures, Joule loss could be the main mechanism for microwave heating; here, magnetic loss cannot contribute to the microwave heating at temperatures higher than the Curie point. Therefore, a higher temperature of sample MB150 compared to samples MB75 and MB45 at the steady state corresponding to the maximum H-field mode could be owing to the higher electrical conductivity of the former sample, as presented in **Table 2-1**.

A different heating mechanism is expected at temperatures lower than the Curie point, where the magnetic loss can also contribute to heating.

According to **Figure 2-12**, there is no considerable difference between the times required for the initial temperature increase in samples MB45, MB75, and MB150 heated in the multi-mode and maximum H-field mode. This result indicates that in the presence of H-field, where the magnetic loss is the dominant mechanism for heating at temperatures lower than the Curie point (ca. 585 °C) [23], microwave heating is not affected by the particle size of the sample. This is possibly due to the permeability, which is independent of the particle size, as reported by Hotta *et al*. [38].

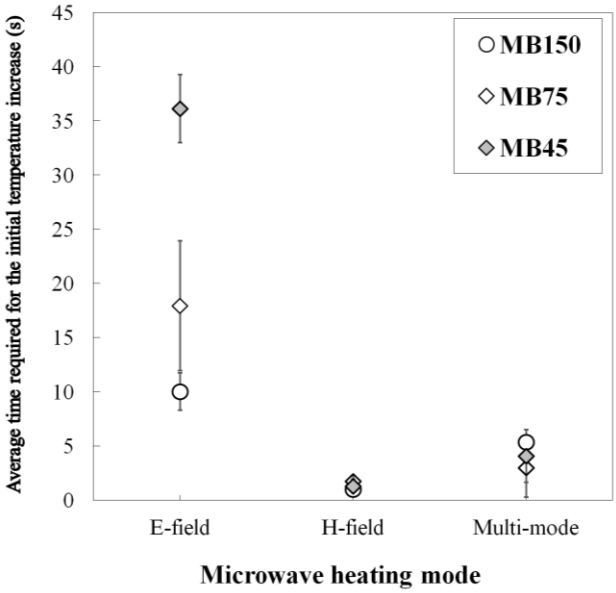

Figure 2-12 Average time required for the initial temperature increased in samples MB45, MB75, and MB150 heated in the multi-mode and maximum E- and H- field modes. Error bars represent the standard deviation of the required times.

In the absence of a high H-field at temperatures lower than the Curie point, neither magnetic loss nor dielectric loss can contribute to microwave heating and only Joule loss would be an effective mechanism for heating, according to Eq. (1). It seems that the Joule loss of sample MB150 is higher than that of MB75. Further, Joule loss of MB75 seems to be higher than that of MB45 because of the higher electrical conductivity of the sample with a larger particle size, as presented in **Table 2-1** (the lower electrical conductivity in sample with smaller particle size is likely attributed to the larger number of grain boundaries which act as a barrier for transport of electric charges in sample with smaller particle size). In addition, a greater penetration depth is expected owing to a significant decrease in μ' in the maximum E-field mode, according to Eq. (2), which would affect its microwave absorption. It has been reported that the ratio of the particle size (d) to the penetration depth (δ) is a critical factor for optimum microwave absorption by conductive materials [7,27]. For a very low d/δ ratio, the particle acts as a transparent material and cannot couple with the microwaves. For a very high d/δ ratio, most of the microwaves will be reflected and the sample cannot heat well. For instance, a d/δ ratio of ca. 2.4 is suggested for maximum microwave absorption in nonmagnetic metal particles [7,27]. Thus, larger particles can absorb more of the microwave power owing to their higher d/δ ratios whereas some of the smaller particles cannot couple with the microwaves and behave like a transparent material, owing to their low d/δ ratio. **Figure 2-13** shows the mechanism of the interaction between the microwaves and magnetite particles of different sizes at high and low temperatures.

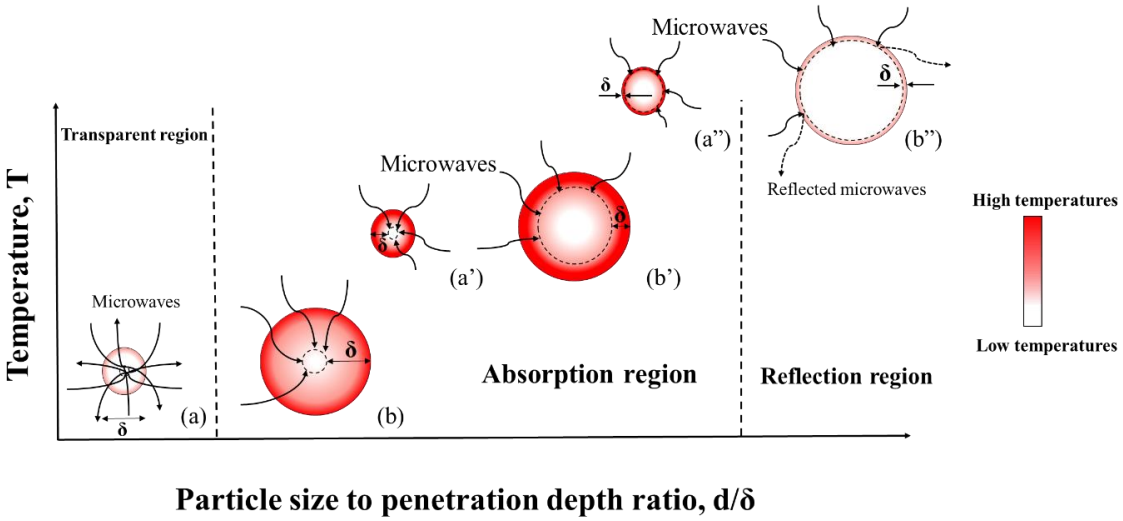

Figure 2-13 Interaction between microwaves and magnetite particles with different d/δ ratio at different temperatures.

It seems that most of the particles in sample MB45 fall in the transparent region at temperatures lower than the Curie point (**Figure 2-13** (a)), whereas the particles in samples MB75 and MB150 fall in the absorption region for the same temperature range (**Figure 2-13** (b)). Therefore, an early onset of temperature increase in samples MB150 and MB75 compared to the onset of temperature increase of sample MB45 would be due to both higher Joule loss and higher d/δ ratio of the samples with a larger particle size, MB150 and MB75. This result proves the considerable impact of the particle size on microwave absorption at temperatures lower than the Curie point.

2-5. Conclusions

To expand our understanding of the interaction between the microwaves and magnetite particles at both high temperatures and temperatures lower than the Curie point, the effect of the apparent density and particle size of Fe_3O_4 on their microwave absorption was studied using a microwave generator at 2.45 GHz at 1050 W. The results can be summarized as follows:

1. A lower apparent density leads to a shorter time required for the initial temperature increase and also to a higher temperature at the steady state owing to higher microwave absorption caused by the higher electrical resistivity of the material.
2. At high temperatures, the particle size of Fe_3O_4 has no effect on the microwave absorption in the presence of the E-field because the permittivity is independent of the particle size. In the maximum H-field mode, Joule loss is the dominant mechanism for heating, causing a higher temperature in a sample with larger particles, because of their higher electrical conductivity.
3. At temperatures lower than the Curie point, the particle size of Fe_3O_4 has no effect on the time required for the initial temperature increase in the presence of the H-field. In the maximum E-field mode, Joule loss is the dominant mechanism for heating, leading to a higher temperature in a sample with larger particles, because of their higher electrical conductivity.

2-6. References

[1] A. Amini, K. Ohno, T. Maeda, K. Kunitomo, Effect of particle size and apparent density on the initial stages of temperature increase during the microwave heating of Fe_3O_4, Powder Technol. 338 (2018) 101–109.

[2] A. Amini, K. Ohno, T. Maeda, K. Kunitomo, Coupling of Magnetite Particles with Microwaves at Temperatures lower than the Curie Point, IOP Conf. Ser. Mater. Sci. Eng. 424 (2018) 012042.

[3] K. Kashimura, M. Sato, M. Hotta, D. Kumar Agrawal, K. Nagata, M. Hayashi, T. Mitani, N. Shinohara, Iron production from Fe_3O_4 and graphite by applying 915 MHz microwaves, Mater. Sci. Eng. A. 556 (2012) 977–979.

[4] K. Hara, M. Hayashi, Continuous Pig Iron Making by Microwave Heating with 12.5 kW at 2.45 GHz, J. Microw. Power Electromagn. Energy. 45 (2011) 137–147.

[5] M. Hayashi, K. Takeda, K. Kashimura, T. Watanabe, K. Nagata, Carbothermic Reduction of Hematite Powders by Microwave Heating, ISIJ Int. 53 (2013) 1125–1130.

[6] J. Sun, W. Wang, Q. Yue, Review on microwave-matter interaction fundamentals and efficient microwave-associated heating strategies, Materials (Basel). 9 (2016).

[7] M. Ignatenko, M. Tanaka, M. Sato, Absorption of microwave energy by a spherical nonmagnetic metal particle, Jpn. J. Appl. Phys. 48 (2009).

[8] O. Ertugrul, H.S. Park, K. Onel, M. Willert-Porada, Effect of particle size and heating rate in microwave sintering of 316L stainless steel, Powder Technol. 253 (2014) 703–709.

[9] W. Liu, J.Y. Lim, M.A. Saucedo, A.N. Hayhurst, S.A. Scott, J.S. Dennis, Kinetics of the reduction of wüstite by hydrogen and carbon monoxide for the chemical looping production of hydrogen, Chem. Eng. Sci. 120 (2014) 149–166.

[10] A. Pineau, N. Kanari, I. Gaballah, Kinetics of reduction of iron oxides by H_2. Part I: Low temperature reduction of hematite, Thermochim. Acta. 447 (2006) 89–100.

[11] A. Pineau, N. Kanari, I. Gaballah, Kinetics of reduction of iron oxides by H_2. Part II. Low temperature reduction of magnetite, Thermochim. Acta. 456 (2007) 75–88.

[12] K.Y. Kim, E.J. Jang, D.Y. Kim, S.M. Jung, Effect of magnetic field on reduction of magnetite, Ironmak. Steelmak. 44 (2017) 6–16.

[13] T. Murakami, Y. Kamiya, T. Kodaira, E. Kasai, Reduction Disintegration Behavior of Iron Ore Sinter under High H_2 and H_2O Conditions, ISIJ Int. 52 (2012) 1447–1453.

[14] T. Chun, H. Long, Z. Di, P. Wang, Q. Meng, Influence of microwave heating on the microstructures of iron ore pellets with coal during reduction, Ironmak. Steelmak. 44 (2017) 486–491.

[15] K. Ishizaki, K. Nagata, Microwave Induced Solid – Solid Reactions between Fe_3O_4 and Carbon Black Powders, ISIJ Int. 48 (2008) 1159–1164.

[16] K. Ishizaki, K. Nagata, T. Hayashi, Production of pig iron from magnetite ore-coal composite pellets by microwave heating, ISIJ Int. 46 (2006) 1403–1409.

[17] J. Zhou, W. Xu, Z. You, Z. Wang, Y. Luo, L. Gao, C. Yin, R. Peng, L. Lan, A new type of power energy for accelerating chemical reactions: the nature of a microwave-driving force for accelerating chemical reactions, Sci. Rep. 6 (2016) 25149.

[18] J. Li, B. Li, J. Han, Z. Cao, J. Wang, A Comparative Study on the Reduction Mechanism of Fe_2O_3 Under Different Heating Methods, Jom. 66 (2014) 1529–1536.

[19] J. Noh, O.I. Osman, S.G. Aziz, P. Winget, J.-L. Brédas, A density functional theory investigation of the electronic structure and spin moments of magnetite, Sci. Technol. Adv. Mater. 15 (2014) 044202.

[20] L. Blaney, L. Blaney, Magnetite (Fe_3O_4): Properties , Synthesis , and Applications, 15 (2007).

[21] Z. Peng, J.-Y. Hwang, J. Mouris, R. Hutcheon, X. Huang, Microwave Penetration Depth in Materials with Non-zero Magnetic Susceptibility, ISIJ Int. 50 (2010) 1590–1596.
[22] M. Hotta, M. Hayashi, K. Nagata, High Temperature Measurement of Complex Permittivity and Permeability of Fe_3O_4 Powders in the Frequency Range of 0.2 to 13.5 GHz, ISIJ Int. 51 (2011) 491–497.
[23] M. Hayashi, Y. Yokoyama, K. Nagata, Effect of particle size and relative density on powdery Fe_3O_4 microwave heating., J. Microw. Power Electromagn. Energy. 44 (2010) 198–206.
[24] H. Kobori, T. Asahi, A. Yamasaki, A. Sugimura, T. Taniguchi, A. Ando, H. Kawanaka, Y. Naitoh, T. Shimizu, Electrical- and magneto-resistance control for magnetite nanoparticle sinter by regulation of heat treatment temperature, J. Magn. Magn. Mater. 323 (2011) 686–690.
[25] N. Standish, H.K. Worner, D.Y. Obuchowski, Particle size effect in microwave heating of granular materials, Powder Technol. 66 (1991) 225–230.
[26] Z. Peng, Z. Li, X. Lin, M. Yang, J.Y. Hwang, Y. Zhang, G. Li, T. Jiang, Microwave Power Absorption in Materials for Ferrous Metallurgy, Jom. 69 (2017) 178–183.
[27] C.A. Crane, M.L. Pantoya, B.L. Weeks, M. Saed, The effects of particle size on microwave heating of metal and metal oxide powders, Powder Technol. 256 (2014) 113–117.
[28] Z. Peng, J.-Y. Hwang, C.-L. Park, B.-G. Kim, M. Andriese, X. Wang, Microwave Permittivity, Permeability, and Absorption Capability of Ferric Oxide, ISIJ Int. 52 (2012) 1535–1538.
[29] S.M. Jafari, M. Ghalegi Ghalenoei, D. Dehnad, Influence of spray drying on water solubility index, apparent density, and anthocyanin content of pomegranate juice powder, Powder Technol. 311 (2017) 59–65.
[30] N. Yoshikawa, G. Xie, Z. Cao, D. V. Louzguine, Microstructure of selectively heated (hot spot) region in Fe_3O_4 powder compacts by microwave irradiation, J. Eur. Ceram. Soc. 32 (2012) 419–424.
[31] R. Bao, J. Yi, Densification and alloying of microwave sintering WC–8wt.%Co composites, Int. J. Refract. Met. Hard Mater. 43 (2014) 269–275.
[32] J.A. Menéndez, E.J. Juárez-Pérez, E. Ruisánchez, J.M. Bermúdez, A. Arenillas, Ball lightning plasma and plasma arc formation during the microwave heating of carbons, Carbon N. Y. 49 (2011) 346–349.
[33] Electric spark, Wikipedia, Free Encycl. (2017). https://en.wikipedia.org/wiki/Electric_spark (accessed December 25, 2017).
[34] M. Gupta, E. Wong Wai Leong, Microwaves and Metals, John Wiley & Sons, 2007.
[35] R. Rajavaram, J. Lee, J.S. Oh, H.G. Kim, J. Lee, Microwave heating characteristics of magnetite ore, Met. Mater. Int. 22 (2016) 1116–1120.
[36] A. Mondal, A. Shukla, A. Upadhyaya, D. Agrawal, Effect of porosity and particle size on microwave heating of copper, Sci. Sinter. 42 (2010) 169–182.
[37] M. Hotta, M. Hayashi, K. Nagata, Complex Permittivity and Permeability of α-Fe_2O_3 and $Fe_{1-x}O$ Powders in the Microwave Frequency Range between 0.2 and 13.5 GHz, ISIJ Int. 50 (2010) 1514–1516.
[38] M. Hotta, M. Hayashi, A. Nishikata, K. Nagata, Complex Permittivity and Permeability of SiO_2 and Fe_3O_4 Powders in Microwave Frequency Range between 0.2 and 13.5 GHz, ISIJ Int. 49 (2009) 1443–1448.

Chapter 3: Effect of the Ratio of Magnetite Particle Size to Microwave Penetration Depth on Reduction Reaction Behaviour by H_2

3-1. Abstract

In this study [1], we investigated reduction of magnetite by H_2 during microwave irradiation. This process combines the advantages of microwave irradiation and using H_2 as a reducing agent to mitigate CO_2 emissions during the ironmaking process. Weight change measurements showed that a reduction of 75% was achieved after treatment under H_2 for 60 min. For better understanding of the effective parameters in microwave chemistry, scanning electron microscopy, combined with energy-dispersive X-ray spectroscopy (SEM-EDX), was performed, which demonstrated a greater reduction of large particles (> 40 μm) than small particles. This behaviour could be attributed to the higher microwave absorption capability of large particles with a higher ratio of particle size to penetration depth (d/δ). Small particles behave as transparent material and are heated via conduction and/or convection; thus, there is no contribution from the catalytic effect of microwaves to the reduction reaction. Moreover, the reduction of Fe_3O_4 to $Fe_{0.94}O$, followed by transformation to Fe, seems to proceed from the surface toward the centre of the particle despite the volumetric microwave heating. This could be due to the higher gas accessibility of iron oxide on the particle surface than in the particle centre.

3-2. Introduction

Microwave irradiation has the potential to decrease the amount of carbonaceous materials required for eco-friendly chemistry owing to its specific characteristics such as non-thermal effect (catalytic effect) [2–5], volumetric heating, rapid and selective heating [4], and high-efficiency heating [6]. For example, the theoretical carbon consumption in conventional heating such as blast furnace is ~380 kg per t of pig iron production, where ~230 kg is used for iron oxide reduction, and the remainder (150 kg) is used for heating and preparing the reaction energy [7]. The energy required to break the iron–oxygen bonds is 10^5 times higher than the energy that can be provided by microwave photons, i.e. 10^{-5} eV. In an antibonding state of an unpaired spin, the microwave can vibrate the state causing enhancement in deoxidation [5]. Moreover, Hayashi *et al*. [8] reported that the flow of conductive heat from the surface to the centre is the rate controlling step during the reduction of powdery iron oxides. They employed the volumetric heating characteristics of microwave heating to overcome this problem. Kashimura *et al*. [5] took advantage of the high efficiency of microwave heating to produce iron from an Fe_3O_4 and graphite mixture. They found that the combined effect of thermal energy and magnetic field of microwaves improves deoxidation during carbothermic reactions. Chun *et al*. [9] showed that using microwave heating for iron oxide reduction by carbon leads to a porous structure due to the rapid heating of both iron oxide and carbon by microwave irradiation. Stir *et al*. [10] studied the reduction behaviour of magnetite by carbon black at the E-field maxima position of a microwave generator, and found that formation of primary and secondary wüstite represents intermediate steps in the reduction of Fe_3O_4 to Fe.

Previously, a mixture of iron oxide and carbonaceous material has typically been used to study iron production during microwave heating due to the susceptibility of carbon to microwaves. The amount of carbonaceous material required in this method is less than that of the conventional ironmaking process [7,11]. Demand for reduced CO_2 emissions during the ironmaking process has prompted research into a cleaner and more efficient method of iron

production. One possibility is to employ H_2 ($Fe_3O_{4(s)}+4H_{2(g)}=3Fe(s)+4H_2O$), instead of carbonaceous materials, as the reducing agent [12,13] to mitigate CO_2 emissions. The reduction rate of iron oxide in H_2 is much higher than that in CO [13–17], and Murakami *et al*. [18] showed that the interdiffusion coefficient of H_2/H_2O gas in iron ore sintered particles at 500 °C is three times higher than that of CO/CO_2. Considering these advantages of using H_2 as the reducing agent, several previous studies have investigated iron oxide reduction by H_2. Fruehan *et al*. [19] studied the final stage of iron ore reduction by H_2 and showed that formation of an iron layer around large grains causes a change in the reaction mechanism, from a gas reaction to solid state oxygen diffusion. Pineau *et al.* [15] demonstrated that Fe_3O_4 is reduced directly by H_2 to Fe at temperatures lower than 420 °C whereas, in the temperature range of 450–570 °C, magnetite, wüstite, and iron can co-exist due to a decrease in the apparent activation energy of the reduction reaction. This was explained by decreased defects in the crystalline structure of magnetite, which can be annealed at ~420 °C. Other researchers [17,20–22] reported an increase in the reduction of magnetite powder by H_2 in the presence of a strong external magnetic field. Kim *et al*. [17] and Raw *et al*. [22] theorized that the reduced iron particles became rearranged in the magnetic field, preventing their agglomeration and increasing the access of the reducing reagent H_2 to the unreacted magnetite powders.

Therefore, eco-friendly ironmaking would involve non-carbonaceous materials, such as H_2, in the reduction reaction via microwave irradiation. In this case, only magnetite is employed as the initial microwave absorber and its transformation to wüstite or metallic iron via the reduction reaction could have a significant effect on microwave absorption. Furthermore, the non-thermal effect of microwave irradiation on the rate of chemical reactions, referred to as the catalytic effect of microwaves, has attracted the attention of researchers on microwave irradiation energy in terms of speeding up chemical reactions [2–5]. However, such an effect cannot be considered when target particles cannot absorb microwaves and behave like transparent materials. Therefore, to improve our understanding of microwave chemistry, effective parameters of microwave absorption and the subsequent reaction should be identified, and the extent of each effect needs to be investigated. For instance, it has been reported that the ratio of the particle size, d, to the microwave penetration depth, δ, is a critical factor for optimum microwave absorption by conductive materials [23,24]. The penetration depth, δ (m), represents the distance from the surface to a point inside the material where the power of the exposed electromagnetic waves decreases to 1/e (36.8%) of the surface value [24,25], which can be calculated using equation (2) [25,26].

At a very low d/δ ratio, the particle acts as a transparent material and cannot couple with the microwaves. By contrast, at a very high d/δ ratio, most of the microwaves will be reflected and the sample cannot heat well. For example, a d/δ value of ~2.4 has been suggested for optimum microwave absorption in non-magnetic metal particles [23,24]. In our previous study [26], the interaction between microwaves and magnetite particles was investigated in neutral atmosphere (N_2) to clarify the effect of particle size and apparent density of a magnetite sample on microwave absorption.

In this study, the potential for magnetite reduction by H_2 with microwave heating is investigated using a multi-mode microwave generator operated at an output power of 1050 W. Moreover, the effect of new-phase formation during Fe_3O_4 reduction on microwave heating is determined, and the effect of the d/δ ratio on the reduction reaction is elucidated.

3-3. Experimental Procedure

3-3-1. Materials

The purpose of this study is to investigate the effect of the ratio of the magnetite particle size to microwave penetration depth on the reduction reaction by H_2. Thus, a magnetite sample with known grain size distribution is required. At the laboratory scale, larger particles with known range of grain size can be prepared by heat treatment of finer particles followed by crushing, grinding, and sieving. Therefore, to prepare a magnetite sample with a grain size of less than 45 μm, a procedure similar to that used in our previous study [26] was employed, wherein the reagent magnetite powder (particle size ≈ 1 μm, purity 99%, Mitsuwa's Pure Chemicals, JAPAN) was pressed into a tablet shape (30 mm in diameter, 20 mm in height), followed by heating in flowing Ar at 1350 °C for 60 min in an electric resistance furnace. Ar was used to provide an inert atmosphere to avoid variation in the oxidation state of magnetite. The heat-treated tablets were crushed and ground to a grain size less than 45 μm. Then, to prepare the briquette samples, ~0.02 g of a 5 mass% aqueous solution of polyvinyl alcohol (Tokyo Chemical Industry CO., LTD., JAPAN) was added as a binder to 3 g of the crushed magnetite powder. Then, a cylindrical briquette sample (15 mm in diameter, 5 mm in height, 37% porosity) was formed by a cold press and was dried at 120 °C for 10 h. Pure H_2 gas was used as the reducing agent after removing its humidity by passing it through a silica gel column.

3-3-2. Microwave irradiation

Prepared briquette samples were subjected to microwave irradiation using a multi-mode microwave generator with a maximum output power of 1.5 kW at 2.45 GHz under N_2 (1 NL/min) atmosphere, in which both the perpendicular magnetic (H) and electric (E) fields contribute to heating (**Figure 3-1** (a)). The atmosphere was changed to H_2 (1 NL/min) after 6 min, which was designated as time zero for reduction degree calculations. A constant power of 1050 W was manually set until the end of heating in all experiments using three tuning stubs.

The Fe_3O_4 sample was contained in an alumina crucible (41 mm outer diameter (OD), 36.5 mm inner diameter (ID), and 49 mm height) surrounded by ceramic wool (Al_2O_3: 35 %, SiO_2: 50 %, and ZrO_2: 15 %, Isolite Insulating Products CO., LTD., Japan). The crucible was then placed in a silica chamber (95 mm OD, 85 mm ID, 96 mm height). Ceramic wool, which cannot absorb microwaves, served as a thermal insulator to prevent heat loss during heating and to protect the silica chamber. The sample temperature was measured using an infrared thermometer capable of measuring a temperature range from 330–1500 °C. The silica chamber was purged by pure N_2 gas before the experiment. Each experiment was conducted for a certain time, and then microwave irradiation was stopped and the atmosphere was changed to N_2 for the cooling step. The cooled sample was subjected to weight change measurement, XRD, SEM-EDX, and optical microscopy.

3-3-3. Sample analysis

To identify the phase transformations during heat treatment, briquette samples were subjected to phase analysis using X-ray diffraction (XRD, Cu-$K\alpha$; λ = 1.54 Å; scan speed, 51.9°/min; power, 3 kW; RIGAKU Smartlab, ZOTK, JAPAN) before and after the reduction reaction. For this purpose, a portion of the treated sample was ground in a ceramic mortar with a pestle to a fine powder (93 mass% under 32 μm, 5 mass% 32–45 μm, and 2 mass% 45–75 μm). Further, the microstructure of the remaining parts of reduced samples was analysed using an optical microscope (BX 50, OLYMPUS, JAPAN) and SEM-EDX (SU 3500, HITACHI, JAPAN).

3-4. Results and Discussion

3-4-1. Temperature profile and reduction degree

Figure 3-1 (b) shows typical temperature profiles of microwave-heated Fe_3O_4 samples during reduction by H_2 for 15, 30, and 60 min. A similar temperature profile was observed for all samples, confirming the reproducibility of the method. An unsteady temperature profile after changing the atmosphere to H_2 demonstrated some variation in the microwave absorption of the samples at different stages of reduction. Such unsteady heating behaviour had also been observed in previous studies [5,27–29]. However, in those studies, a gradual increase in temperature during microwave heating was reported, which would be due to the presence of carbonaceous materials as a microwave susceptor in their samples. In this study, each significant change in the heating behaviour of the sample was considered a distinct stage (stages I, II, III, and IV) and was used to study the effect of new phases formed via the reduction reaction on the microwave absorption capability of the sample.

The reduction degree % (dimensionless), was calculated according to **Eq. (3)**:

$$\text{Reduction degree (\%)} = \frac{W_i - W_t}{W_O \times W_i} \quad (3)$$

where W_i (g) is the initial weight of the sample, W_t (g) is the weight of the sample after treatment for t min, and W_O (dimensionless) is the stoichiometric weight ratio of oxygen in magnetite, which is 0.2766. **Figure 3-1** (c) shows the reduction degree of magnetite samples after different treatment durations in the present report and that achieved by other researchers [17,30]. To validate the results, each experiment was conducted at least twice. The average reduction degree was used as the reduction degree for a certain treatment duration in **Figure 3-1** (c), in which the error bars represent the standard deviations. Evaluations of the reduction degree based on weight change measurements (**Figure 3-1** (c)) indicate that the reduction reaction began soon after changing the atmosphere to H_2. Therefore, as mentioned above, phase transformation during the reduction reaction was responsible for the unsteady heating behaviour of the sample. The XRD patterns of the samples before, during, and after reduction by H_2 during microwave irradiation are illustrated in **Figure 3-1** (d) for different treatment durations.

According to the XRD pattern of the sample treated in the first 6 min under N_2, no phase transformation was detected, demonstrating heating of the sample without any reduction.

In stage I, $Fe_{0.94}O$ was detected in the XRD pattern, confirming the initial stage of the reduction reaction. An increase in the sample temperature after changing the atmosphere to H_2 showed some variation in microwave coupling with the sample owing to wüstite formation during this stage. For improved coupling of materials with irradiated microwaves, microwave power absorption, P (W/m^3), and microwave penetration depth, δ (m), could be considered the most effective parameters.

The P (W/m^3) value of a material represents its ability to convert microwave power into thermal energy, which can be evaluated using **Eq. (1)** [25,26,31]:

According to **Eq. (1)**, three different mechanisms, i.e. Joule loss (first term), dielectric loss (second term), and magnetic loss (third term), contribute to microwave heating.

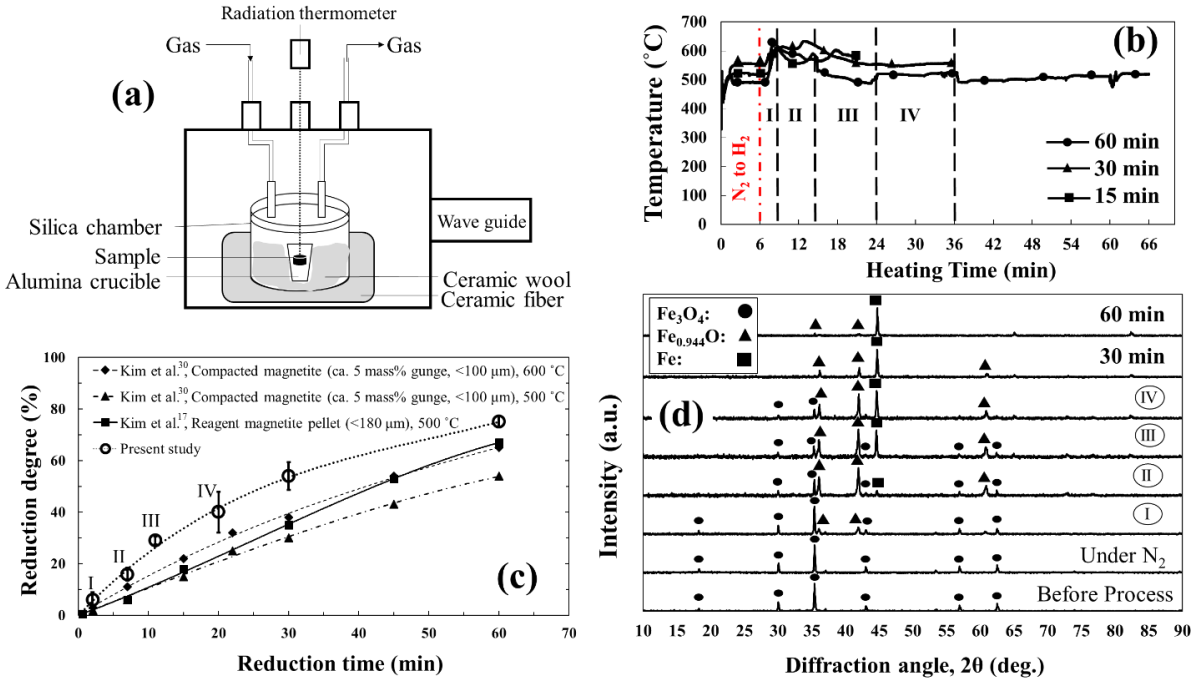

Figure 3-1 (a) Schematic setup for microwave irradiation. (b) Typical temperature profiles of microwave-heated magnetite samples during reduction by H_2 for 15, 30, and 60 min. The dash-dotted line shows the time the atmosphere was changed from N_2 to H_2. Dashed lines delineate the four heating stages (I, II, III, and IV) determined during the experiment. (c) Reduction degree of the magnetite samples reduced by pure H_2 in the present study (microwave irradiation) and reported by other researchers (conventional heating). Error bars represent the standard deviation of the average reduction degree for a certain treatment duration. (d) XRD patterns of magnetite samples before, during, and after reduction by H_2 during microwave irradiation.

The Joule loss in wüstite is reportedly higher than that in magnetite owing to the higher electrical conductivity of wüstite (9.1 S/cm) than that of magnetite (1.0×10^{-3} S/cm) [5,32]. Moreover, Hotta *et al.* [33] showed that not only the electrical conductivity but also the permittivity (real part) of wüstite is higher than that of magnetite. This leads to greater penetration depth in wüstite than in magnetite, as also reported by Peng *et al.* [34]. Therefore, higher microwave absorption is expected by wüstite, causing an increase in temperature after wüstite formation during stage I. This result is in good agreement with that of Ishizaki *et al.* [28], where wüstite formation is considered responsible for an increase in temperature during microwave heating.

Metallic iron formed in stage II (**Figure 3-1** (d)), which would be responsible for a decrease in sample temperature. It is well known that the penetration depth of metals like copper (δ_{Copper} = 1.3 μm) is substantially less than that of metal oxides such as magnetite ($\delta_{Magnetite}$ = 80 μm) [25] because of the higher electrical conductivity of the former materials [24]. The formation of metallic iron in stage II resulted in less absorption of microwaves [28] due to a shorter penetration depth than either wüstite or magnetite. Lower microwave absorption then led to a decrease in sample temperature during this stage.

In stage III, the intensity of the Fe peak increased, demonstrating greater reduction, which was also confirmed by weight change measurements (**Figure 3-1** (c)). In stage IV, the sample temperature reached a steady state due to heat loss via conduction from the reaction chamber, equal to the heat generated in the sample via microwave irradiation. This phenomenon was also observed by Hayashi *et al.* [25], who reported a constant temperature during microwave heating of magnetite and theorized that the rate of microwave absorption is equal to the rate of thermal

energy dissipation. Moreover, comparing the reduction degree obtained in the present study with that reported by other researchers [17,30] demonstrates that a greater reduction is achievable by employing microwave irradiation during magnetite reduction by pure H_2 than by using conventional heating methods. Such behaviour is attributed to both thermal and non-thermal (catalytic) effects of microwave irradiation when speeding up chemical reactions, as demonstrated by other researchers [2–5].

3-4-2. Microstructural observations

To identify the reduction mechanism of different particles, microscope observations were conducted. The SEM-EDX map and line analysis of particles in the Fe_3O_4 sample reduced by H_2 during 30 min of microwave heating are shown in **Figure 3-2**.

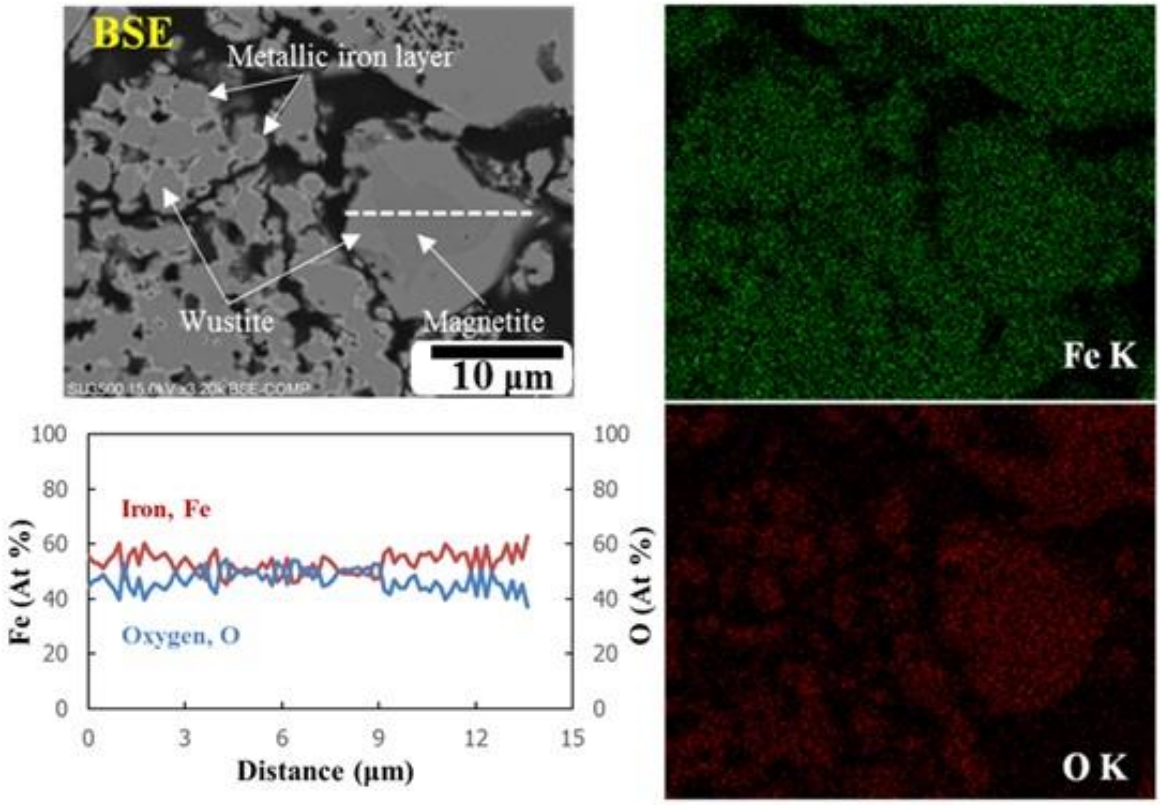

Figure 3-2 SEM-EDX map and line analysis of particles in the Fe_3O_4 sample reduced by H_2 during 30 min microwave heating.

Very small particles (2–5 µm) were completely reduced to wüstite and the reduction reaction progressed via formation of a thin metallic iron layer on the particle surface. In small particles (~15 µm), the complete reduction of magnetite to wüstite required longer treatment time and no metallic iron was observed in these particles. These observations demonstrate that metallic iron can only form after the complete reduction of Fe_3O_4 to $Fe_{0.94}O$. This result is in good agreement with that of Pineau *et al.* [15], who reported that Fe_3O_4 was completely reduced to wüstite before reduction to Fe at temperatures above 570 °C. Moreover, reduction in small particles proceeded from the particle surface toward the particle centre in spite of the microwave irradiation. As mentioned above, the optimum d/δ ratio is known as an essential factor for optimum microwave coupling of conductive materials [23,24]. A penetration depth of ~80 µm was calculated by Hayashi *et al.* [25] for magnetite powders at room temperature at a frequency of 2.45 GHz, where ε' is ~40, μ' is ~1.7, and σ is 1.0×10^2 (S/cm), according to **Eq.**

(2). The penetration depth for a compacted magnetite sample, as employed in this study, is less than 80 μm due to an increase in both permittivity and electrical conductivity with increasing relative density, as reported by other studies [24,25,33,35–37]. Therefore, the mechanism of magnetite reduction by H_2 during microwave heating is a function of the d/δ ratio, as illustrated in **Figure 3-3**.

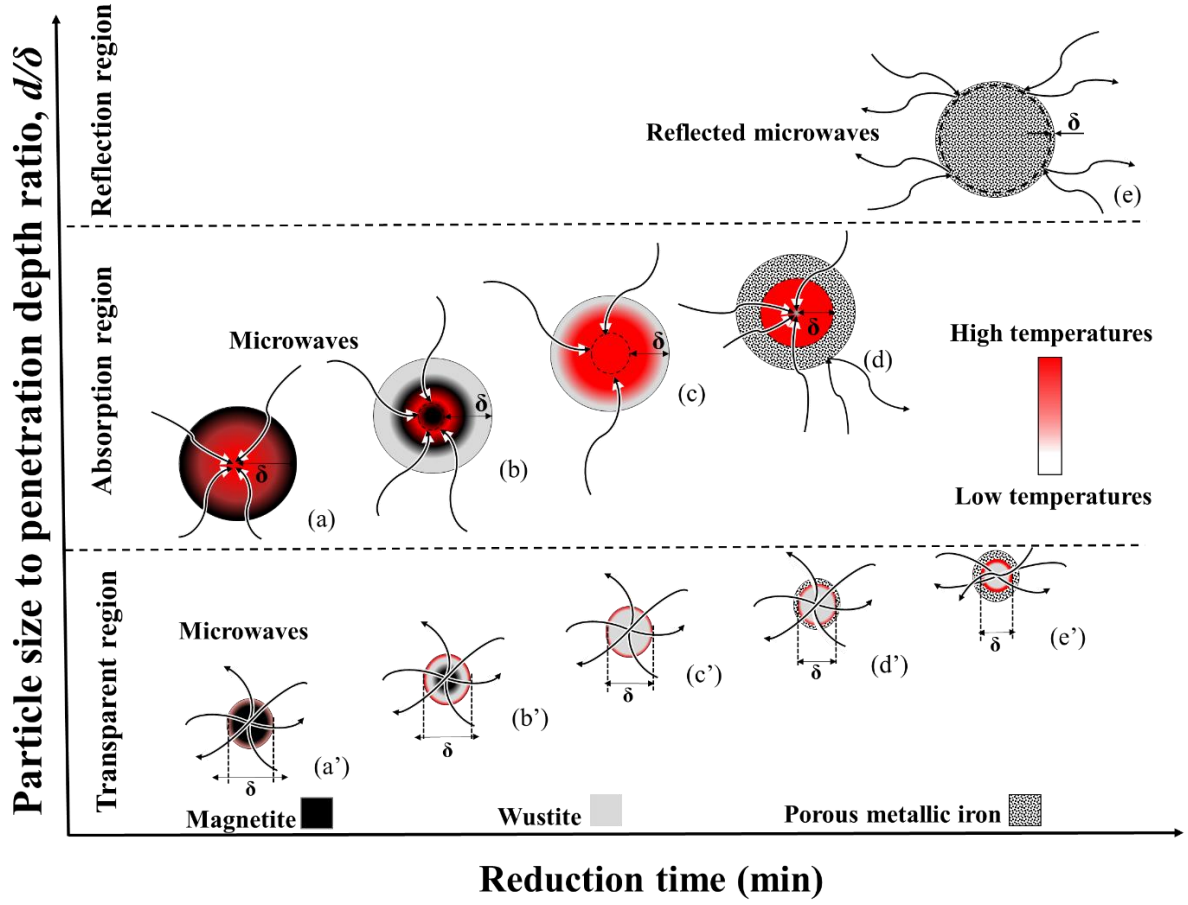

Figure 3-3 Mechanism of magnetite reduction by H_2 during microwave heating. Dark grey: magnetite (Fe_3O_4). Bright grey: wüstite ($Fe_{0.94}O$). Speckled pattern: porous metallic iron (Fe).

In particles larger than ~40 μm, magnetite was completely reduced to wüstite and then transformed to porous metallic iron. In these large particles, better microwave absorption is expected due to a higher d/δ ratio than that of small particles (**Figure 3-3** (a) and (a')). However, because of higher gas accessibility on the particle surface than the particle centre, as also reported by other studies [17], it is expected that, even in large particles, the reduction of magnetite to wüstite (**Figure 3-3** (b) and (c)) and of wüstite to porous metallic iron (**Figure 3-3** (d) and (e)) proceeds from the surface toward the centre despite their good microwave absorption. This reduction direction has also been observed in previous studies [5,17,27,28,38]. This mechanism was confirmed by optical microscopy observations of a partially reduced sample after 30-min treatment under H_2 (**Figure 3-4** (a)), where an iron layer was observed around the wüstite.

Small particles with a very low d/δ ratio behaved as a transparent material during microwave irradiation in this study (**Figure 3-3** (a')) and were heated by transferring the heat from well-heated large particles via conduction and/or convection, instead of by microwave absorption. In addition, the catalytic effect of microwaves (non-thermal effect) [4] on iron oxide reduction [5] should be ignored in these small particles. In this case, a wüstite layer forms

on the surface of the magnetite because of the reduction direction of magnetite to wüstite (**Figure 3-3** (b') and (c')) and that of wüstite to porous metallic iron (**Figure 3-3** (d') and (e')). This mechanism was confirmed by SEM observations (**Figure 3-2**) of a wüstite layer on the surface of the magnetite in particles of ~15 μm, as well as a thin metallic iron layer detected on the surface of small particles.

On the other hand, Stir *et al*. [10] demonstrated that the reduction kinetics of Fe_3O_4 to wüstite are controlled by the phase boundary while those of wüstite to Fe are affected by cation vacancies and structural defects. Thus, microwave irradiation would improve the reduction of wüstite particles, which are cubic crystal with Fe^{+2} defects [9]. Therefore, a higher temperature of the large particles (thermal effect) and a larger catalytic effect of microwaves (non-thermal effect) [4] on iron oxide reduction [5] would cause greater reduction in large particles than in small particles. Optical microscope observations of a reduced sample after 60 min of treatment under H_2 (**Figure 3-4** (b)) confirmed that the reduction progressed more in large particles than in small particles.

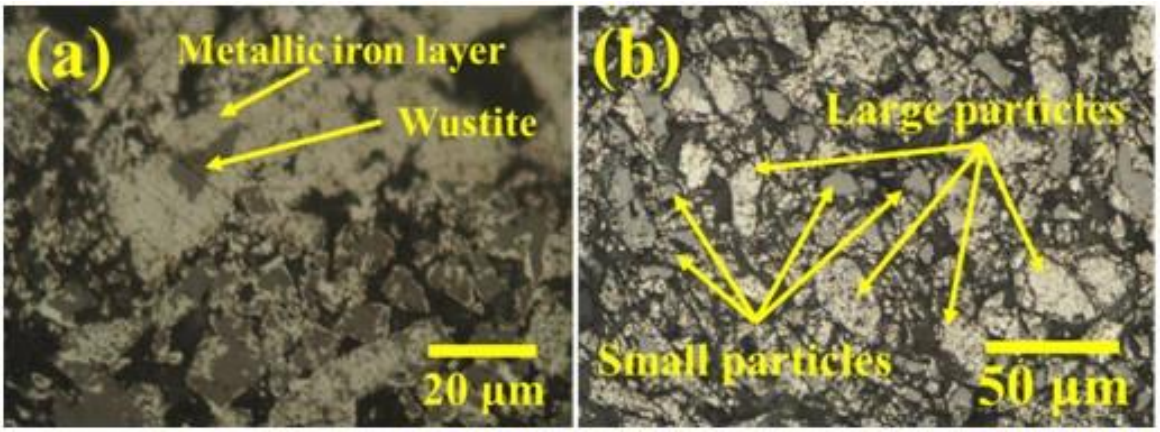

Figure 3-4 Optical microscope images of large particles in the Fe_3O_4 sample after treatment in H_2 with microwave irradiation for (a) 30 min, partially reduced particle, and (b) 60 min, fully reduced large particle.

As mentioned in Section 3, the formation of metallic iron causes a significant decrease in penetration depth [25] owing to the higher electrical conductivity of metals than oxides [24]. Therefore, the d/δ ratio increases noticeably, causing reflection of microwaves, as shown in **Figure 3-3** (e). Thus, microwave absorption should decrease with formation of metallic iron, as reported by other researchers [28]. This mechanism is confirmed by the decrease in sample temperature in stage II shown in **Figure 3-1** (b), where the XRD patterns demonstrate the formation of metallic iron (**Figure 3-1** (d)).

3-5. Conclusions

The possibility of magnetite reduction by H_2 during microwave heating was investigated for the first time using a multi-mode microwave generator operated at an output power of 1050 W, to combine the advantages of microwave heating and using H_2 as a reducing agent to mitigate CO_2 emissions during the ironmaking process. In addition, the microstructure of the reduced samples was analysed to clarify the effect of the ratio of magnetite particle size to microwave penetration depth (d/δ) on the reduction reaction behaviour by H_2. The results are summarized as follows:

1. The Joule loss in wüstite is higher than that in magnetite due to the higher electrical conductivity of wüstite (9.1 S/cm) than that of magnetite (1.0×10^{-3} S/cm). Therefore,

wüstite formation via reduction reaction causes an increase in microwave absorption of the sample, leading to an increase in temperature.

2. Large particles, which have a high d/δ ratio, could couple with the microwaves, producing higher temperature and higher catalytic effect of microwaves on the reduction reaction progress in large particles. However, small particles, which have very low d/δ ratio, behave as a transparent material, and are heated via convection and/or conduction in the absence of either the thermal or non-thermal effects of microwave irradiation.
3. During microwave heating in a H_2 atmosphere, the reduction of Fe_3O_4 to $Fe_{0.94}O$ and that of $Fe_{0.94}O$ to Fe proceeds from the particle surface toward the particle centre due to the higher gas accessibility of iron oxide on the particle surface.
4. The formation of metallic iron results in less absorption of microwaves owing to a shorter penetration depth than the case of either wüstite or magnetite. Lower microwave absorption then leads to a decrease in the sample temperature during microwave heating.

3-6. References

[1] A. Amini, K. Ohno, T. Maeda, K. Kunitomo, Effect of the Ratio of Magnetite Particle Size to Microwave Penetration Depth on Reduction Reaction Behaviour by H_2, Sci. Rep. 8 (2018) 15023.

[2] A. Ferrari, J. Hunt, A. Lita, B. Ashley, A.E. Stiegman, Microwave-Specific Effects on the Equilibrium Constants and Thermodynamics of the Steam − Carbon and Related Reactions, J. Phys. Chem. C. 118 (2014) 9346–9356.

[3] J. Hunt, A. Ferrari, A. Lita, M. Crosswhite, B. Ashley, A.E. Stiegman, Microwave-specific enhancement of the carbon-carbon dioxide (Boudouard) reaction, J. Phys. Chem. C. 117 (2013) 26871–26880.

[4] J. Zhou, W. Xu, Z. You, Z. Wang, Y. Luo, L. Gao, C. Yin, R. Peng, L. Lan, A new type of power energy for accelerating chemical reactions: the nature of a microwave-driving force for accelerating chemical reactions, Sci. Rep. 6 (2016) 25149.

[5] K. Kashimura, M. Sato, M. Hotta, D. Kumar Agrawal, K. Nagata, M. Hayashi, T. Mitani, N. Shinohara, Iron production from Fe_3O_4 and graphite by applying 915 MHz microwaves, Mater. Sci. Eng. A. 556 (2012) 977–979.

[6] X. Qiao, X. Xie, The effect of electric field intensification at interparticle contacts in microwave sintering, Sci. Rep. 6 (2016) 32163.

[7] K. Hara, M. Hayashi, Continuous Pig Iron Making by Microwave Heating with 12.5 kW at 2.45 GHz, J. Microw. Power Electromagn. Energy. 45 (2011) 137–147.

[8] M. Hayashi, K. Takeda, K. Kashimura, T. Watanabe, K. Nagata, Carbothermic Reduction of Hematite Powders by Microwave Heating, ISIJ Int. 53 (2013) 1125–1130.

[9] T. Chun, H. Long, Z. Di, P. Wang, Q. Meng, Influence of microwave heating on the microstructures of iron ore pellets with coal during reduction, Ironmak. Steelmak. 44 (2017) 486–491.

[10] M. Stir, K. Ishizaki, S. Vaucher, R. Nicula, Mechanism and kinetics of the reduction of magnetite to iron during heating in a microwave E-field maximum, J. Appl. Phys. 105 (2009) 124901.

[11] K. Kashimura, K. Nagata, M. Sato, Concept of Furnace for Metal Refining by Microwave Heating -A Design of Microwave Smelting Furnace with Low CO_2 Emission-, Mater. Trans. 51 (2010) 1847–1853.

[12] S.K. Kuila, R. Chatterjee, D. Ghosh, Kinetics of hydrogen reduction of magnetite ore fines, Int. J. Hydrogen Energy. 41 (2016) 9256–9266.

[13] A.A. Barde, J.F. Klausner, R. Mei, Solid state reaction kinetics of iron oxide reduction using hydrogen as a reducing agent, Int. J. Hydrogen Energy. 41 (2016) 10103–10119.
[14] W. Liu, J.Y. Lim, M.A. Saucedo, A.N. Hayhurst, S.A. Scott, J.S. Dennis, Kinetics of the reduction of wüstite by hydrogen and carbon monoxide for the chemical looping production of hydrogen, Chem. Eng. Sci. 120 (2014) 149–166.
[15] A. Pineau, N. Kanari, I. Gaballah, Kinetics of reduction of iron oxides by H2. Part I: Low temperature reduction of hematite, Thermochim. Acta. 447 (2006) 89–100.
[16] A. Pineau, N. Kanari, I. Gaballah, Kinetics of reduction of iron oxides by H2. Part II. Low temperature reduction of magnetite, Thermochim. Acta. 456 (2007) 75–88.
[17] K.Y. Kim, E.J. Jang, D.Y. Kim, S.M. Jung, Effect of magnetic field on reduction of magnetite, Ironmak. Steelmak. 44 (2017) 6–16.
[18] T. Murakami, Y. Kamiya, T. Kodaira, E. Kasai, Reduction Disintegration Behavior of Iron Ore Sinter under High H_2 and H_2O Conditions, ISIJ Int. 52 (2012) 1447–1453.
[19] R.J. Fruehan, Y. Li, L. Brabie, E.-J. Kim, Final Stage of Reduction of Iron Ores by Hydrogen, Scand. J. Metall. 34 (2005) 205–212.
[20] M.W. Rowe, S.M. Lake, R. Fanick, Effect of magnetic field on reduction of iron oxides: magnetite and wüstite, Nature. 266 (1977) 612–614.
[21] D. Aylmer, M.W. Rowe, Effects of a strong external magnetic field on the reduction of cobalt and iron oxides: Confirmation, J. Chem. Phys. 78 (1983) 2094–2095.
[22] M.W. Rowe, P.K. Gallagher, E.M. Gyorgy, Establishing the absence of any influence by an external magnetic field upon the intrinsic rate of reduction of magnetite by hydrogen, J. Chem. Phys. 79 (1983) 3534–3536.
[23] M. Ignatenko, M. Tanaka, M. Sato, Absorption of microwave energy by a spherical nonmagnetic metal particle, Jpn. J. Appl. Phys. 48 (2009) 067001.
[24] C.A. Crane, M.L. Pantoya, B.L. Weeks, M. Saed, The effects of particle size on microwave heating of metal and metal oxide powders, Powder Technol. 256 (2014) 113–117.
[25] M. Hayashi, Y. Yokoyama, K. Nagata, Effect of particle size and relative density on powdery Fe_3O_4 microwave heating., J. Microw. Power Electromagn. Energy. 44 (2010) 198–206. http://www.ncbi.nlm.nih.gov/pubmed/21721468.
[26] A. Amini, K. Ohno, T. Maeda, K. Kunitomo, Effect of particle size and apparent density on the initial stages of temperature increase during the microwave heating of Fe_3O_4, Powder Technol. 338 (2018) 101–109.
[27] K. Hara, M. Hayashi, M. Sato, K. Nagata, Pig Iron Making by Focused Microwave Beams with 20 kW at 2.45 GHz, ISIJ Int. 52 (2012) 2149–2157.
[28] K. Ishizaki, K. Nagata, T. Hayashi, Production of pig iron from magnetite ore-coal composite pellets by microwave heating, ISIJ Int. 46 (2006) 1403–1409.
[29] K. Nishioka, T. Taniguchi, Y. Ueki, K. Ohno, T. Maeda, M. Shimizu, Gasification and Reduction Behavior of Plastics and Iron Ore Mixtures by Microwave Heating, ISIJ Int. 47 (2007) 602–607.
[30] W.-H. Kim, S. Lee, S.-M. Kim, D.-J. Min, The retardation kinetics of magnetite reduction using H_2 and H_2–H_2O mixtures, Int. J. Hydrogen Energy. 38 (2013) 4194–4200.
[31] Y. Wada, S. Fujii, E. Suzuki, M.M. Maitani, S. Tsubaki, S. Chonan, M. Fukui, N. Inazu, Smelting Magnesium Metal using a Microwave Pidgeon Method, Sci. Rep. 7 (2017) 46512.
[32] N. Yoshikawa, G. Xie, Z. Cao, D. V. Louzguine, Microstructure of selectively heated (hot spot) region in Fe_3O_4 powder compacts by microwave irradiation, J. Eur. Ceram. Soc. 32 (2012) 419–424.

[33] M. Hotta, M. Hayashi, K. Nagata, Complex Permittivity and Permeability of α-Fe_2O_3 and $Fe_{1-x}O$ Powders in the Microwave Frequency Range between 0.2 and 13.5 GHz, ISIJ Int. 50 (2010) 1514–1516.
[34] Z. Peng, Z. Li, X. Lin, M. Yang, J.Y. Hwang, Y. Zhang, G. Li, T. Jiang, Microwave Power Absorption in Materials for Ferrous Metallurgy, Jom. 69 (2017) 178–183.
[35] M. Hotta, M. Hayashi, K. Nagata, High Temperature Measurement of Complex Permittivity and Permeability of Fe_3O_4 Powders in the Frequency Range of 0.2 to 13.5 GHz, ISIJ Int. 51 (2011) 491–497.
[36] Z. Peng, J.-Y. Hwang, J. Mouris, R. Hutcheon, X. Huang, Microwave Penetration Depth in Materials with Non-zero Magnetic Susceptibility, ISIJ Int. 50 (2010) 1590–1596.
[37] M. Hotta, M. Hayashi, A. Nishikata, K. Nagata, Complex Permittivity and Permeability of SiO_2 and Fe_3O_4 Powders in Microwave Frequency Range between 0.2 and 13.5 GHz, ISIJ Int. 49 (2009) 1443–1448.
[38] S. Takayama, G. Link, M. Sato, J. Jelonnek, Possibility for Iron Production Using High-Power Millimeter Waves, IEEE Trans. Plasma Sci. 43 (2015) 3517–3521.

Appendix:

3-7. Sulfur behavior in iron oxide reduction by H_2 during microwave heating

3-7-1. Introduction

To investigate the effect of sulfur on the reduction reaction of magnetite during microwave heating in H_2, a mixture of Fe_3O_4:FeS:CaO with a mole ratio of 13:1:1 was used to prepare a high sulfur (~1 mass%) magnetite sample containing a good desulfurizer component (CaO).

3-7-2. Materials

Reagent $CaCO_3$ powder (purity, 99.5%) was calcined at 1300 °C for 600 min followed by crushing and grinding to the grain size of less than 45 μm. Formation of CaO after calcination process was confirmed by X-ray diffraction analysis; however, small amount of $CaCO_3$ possibly remain which cannot be detected in the XRD pattern. Reagent FeS (purity, 99%) was crushed and ground to the grain size of less than 45 μm. The prepared magnetite powder (purity, 99%, grain size, <45 μm), CaO, and FeS were mixed well to prepare a mixture powder containing 13:1:1 stoichiometric mole ratio of Fe_3O_4:FeS:CaO. To prepare the briquette samples, approximately 0.02 g of a 5 mass% aqueous solution of polyvinyl alcohol was added as a binder to 3 g of the mixture powder. A cylindrical briquette sample (15 mm diameter, 5 mm high) was formed by a cold-press followed by drying at 120 °C for 600 min. Prepared briquette samples were subjected to microwave heating.

3-7-3. Results and discussion

Figure 3-5 shows temperature profiles of the sample during microwave heating for 15 and 30 minutes.

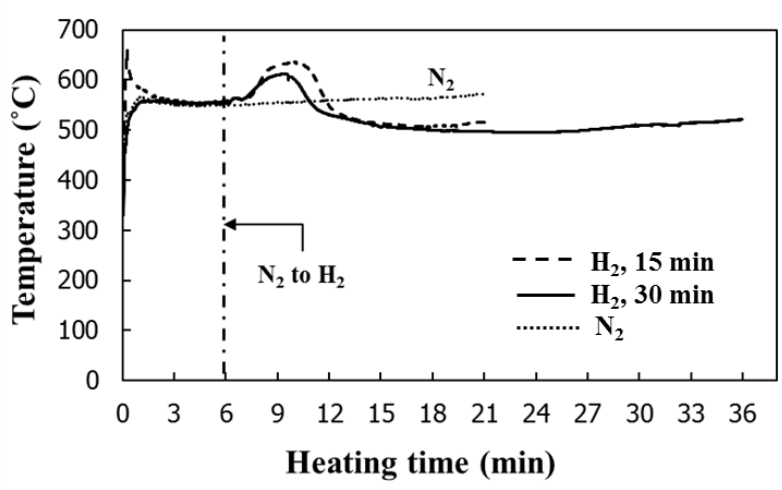

Figure 3-5 Temperature profiles of the sample reducing by H_2 during microwave heating. The vertical Dash-dotted line shows the moment of changing atmosphere from N_2 to H_2.

An unsteady temperature profile was observed after changing the atmosphere to H_2, see **Figure 3-5**. A similar pattern also observed in section **3-4-1** wherein the microwave absorption of the Fe_3O_4 sample varied during reduction reaction owing to the new-phase formation via reduction of magnetite to FeO and Fe.

XRD patterns of the sample after microwave heating under N_2 and H_2 atmosphere, illustrated in **Figure 3-6**, confirmed the reduction of magnetite to wüstite followed by reduction to metallic iron during treatment under H_2 for 15 and 30 minutes. In addition, no sulfur-containing phase was detected in the XRD patterns that is likely attributed to the small amount of sulfur in the sample, <1 mass%.

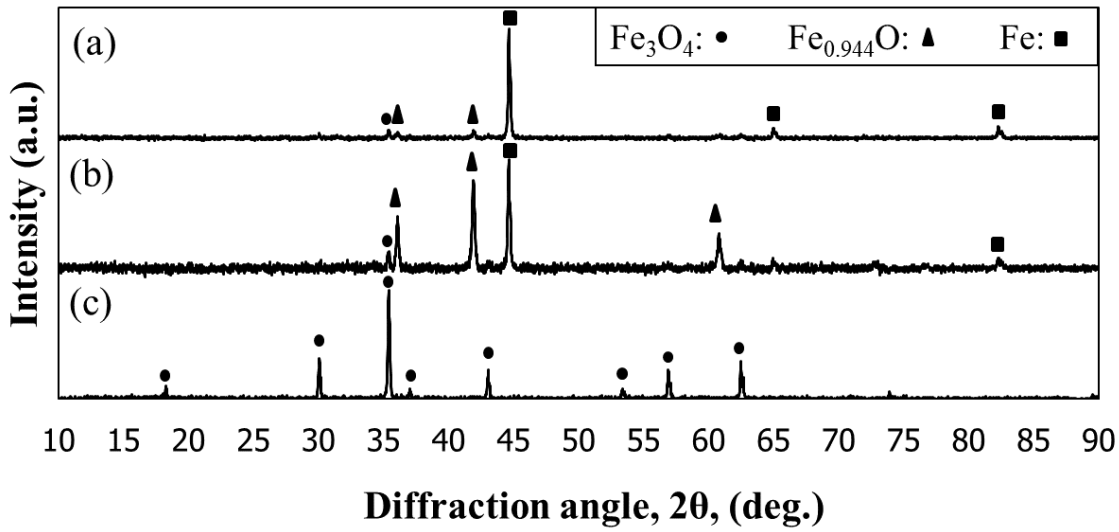

Figure 3-6 XRD patterns of Fe_3O_4:FeS:CaO=13:1:1 sample after microwave treatment in H_2 for (a) 30 min, (b) 15 min, and (c) in N_2 for 21 min.

Reduction degree, %R, was also calculated according to **Eq. (3)** where W_O is the stoichiometric weight ratio of oxygen in the sample, which is 0.269.

Figure 3-7 shows the reduction degree in Fe_3O_4:FeS:CaO samples with mole ratios of 13:1:1 and 1:0:0 reduced by H_2 for 15 and 30 min during microwave heating.

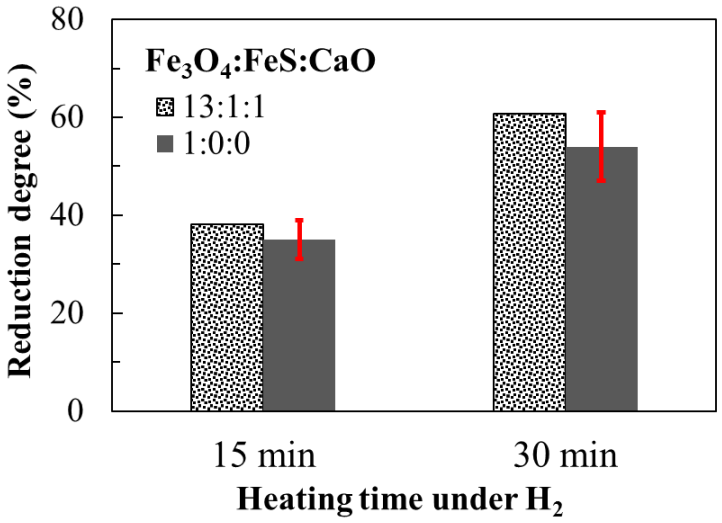

Figure 3-7 Reduction degree in Fe_3O_4:FeS:CaO samples with mole ratios of 13:1:1 and 1:0:0 reduced by H_2 for 15 and 30 min during microwave heating.

3-7-4. Microstructure observation

Partially reduced 13:1:1 sample after 30 min treatment (%R = 60.8) was subjected to the SEM observation and EDX analysis. The BSE image, map and point analysis are shown in **Figure 3-8**.

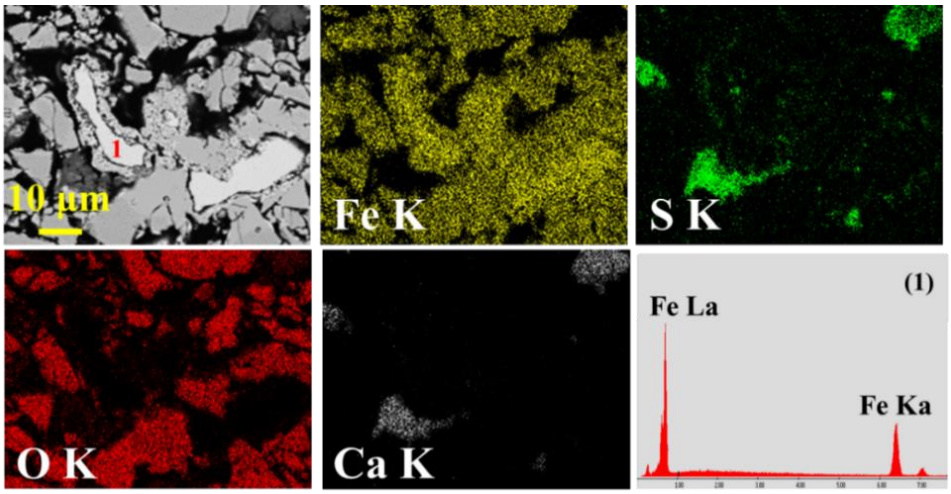

Figure 3-8 SEM-EDX observation of partially reduced 13:1:1 sample (%R = 60.8) after microwave treatment in H_2 for 30 min.

Point analysis of the reduced metallic iron, point (1), indicated that no sulfur was moved from sulfide phase to the reduced metallic iron during reduction. This result is in a good agreement with Yu *et al*. [1] where they also reported that most of the sulfur remain in the form of troilite (FeS) during the reduction and finally can be separated via magnetic separation after reduction.

It was observed that the metallic iron was enclosed by a porous FeS layer with a narrow gap between theme. The porous FeS layer is also observed by other researchers [2] [3] during reduction of iron oxide by H_2-H_2S gas mixture which encircled the metallic Fe phase during conventional heating; however, they reported no gap between porous FeS layer and metallic

Fe. Yu *et al*. [1] also reported no gap between FeS and reduced Fe after reduction of iron ore-coal composite briquette during conventional heating. Therefore, the gap between the metallic Fe and sulfide phase in the present study is likely owing to the selective heating characteristic of microwave irradiation. In fact, different magnetic and dielectric properties of metallic Fe and sulfide phase (such as electrical conductivity: σ_{Fe} = 1.04×10^{5} S/cm [4], σ_{FeO} = 9.1 S/cm [5], $\sigma_{Magnetite}$ = 1.0×10^{-3} S/cm [5], and σ_{FeS} = 2.0×10^{1} S/cm [6]) causes a variation in both microwave absorption and heating rate of these two phases making a gap between them during microwave treatment. Moreover, thermal stress can separate the metallic iron and wüstite in metal/oxide interface owing to the different thermal expansion coefficient of them. Such separation is more preferred in the presence of sulfur because of a decrease in surface energy that decreases the energy required for the void formation in wüstite/Fe interface [7].

On the other hand, the average temperature of the 1:0:0 sample during reduction by H_2 was ca. 573 °C while that of the 13:1:1 sample after 15 and 30 min treatment was 548 and 520 °C, respectively. Although the average temperature of the pure magnetite sample is higher than that of the sulfur-containing sample, a slightly higher reduction degree was attained in the latter sample. This is likely attributed to the improved surface diffusion in the presence of sulfur [7] owing to a decrease in surface energy by sulfur adsorption.

A progress in the desulfurization reaction is also confirmed by SEM observation shown in **Figure 3-8** wherein the CaS particles were detected; however, no CaS phase was detected in the XRD patterns (**Figure 3-6**) owing to the small amount of the sulfur containing phases in the samples.

To extend our understanding about the mechanism of desulfurization reaction, further experiments are required to focus on the reaction between FeS and CaO in the presence of a reducing agent.

3-7-5. References

[1] W. Yu, T. Sun, T. Hu, Desulfuration Behavior of Low-grade Iron Ore-coal Briquette during the Process of Direct Reduction Followed by Magnetic Separation, ISIJ Int. 55 (2015) 329–331.

[2] R. Kuwano, T. Oku, Y. Ono, Effects of Gaseous Sulfide on the Reduction of Iron Oxide Pellets, Trans. ISIJ. 66 (1981) 342–348.

[3] S.B. Lee, P.C.H. Rhee, Reduction behavior of iron ore by reducing gas containing H2S, Scand. J. Metall. 32 (2003) 203–210.

[4] J. Devi, M.J. Akhtar, P. Datta, Multiphysics Model of Iron Powder Compacts for Efficient Microwave Processing, 56 (2017) 11–23.

[5] K. Kashimura, M. Sato, M. Hotta, D. Kumar Agrawal, K. Nagata, M. Hayashi, T. Mitani, N. Shinohara, Iron production from Fe_3O_4 and graphite by applying 915 MHz microwaves, Mater. Sci. Eng. A. 556 (2012) 977–979.

[6] H. Kobayashi, N. Takeshita, N. Môri, H. Takahashi, T. Kamimura, Pressure-induced semiconductor-metal-semiconductor transitions in FeS, Phys. Rev. B - Condens. Matter Mater. Phys. 63 (2001) 115203.

[7] H.J. Grabke, D. Wiemer, H. Viefhaus, Segregation of sulfur during growth of oxide scales, Appl. Surf. Sci. 47 (1991) 243–250.

Chapter 4: Carbothermic Reduction Behavior of FeS in the Presence of CaO during Microwave Irradiation

4-1. Abstract

Carbothermic reduction of FeS in the presence of CaO was experimentally studied by employing a multi-mode microwave generator at 1050 W and 2.45 GHz as an external heat source to mitigate CO_2 and SO_2 emissions [1]. According to XRD analysis, an ion exchange reaction between FeS and CaO was initiated at temperatures lower than 645 °C and progressed by a further heating to 850 °C without any evidence for the onset of a reduction reaction. Detection of Fe phase in the XRD pattern of sample heated to 920 °C and existence of CO/CO_2 in the off-gas during microwave treatment demonstrated that the reduction reaction initiates at ca. 850 °C. It was found that the onset of reduction reaction promotes the ion exchange reaction by FeO consumption via reduction to Fe. Moreover, optical microscope and SEM-EDX observations showed that carbon can be absorbed by metallic iron to make molten iron particles at 1290 °C.

4-2. Introduction

Carbothermic reduction of iron sulfide cannot perform in the absence of a desulfurizer due to the thermodynamic reasons [2]. Lime (CaO) has a high tendency for reaction with sulfur to form $CaSO_4$ and CaS in the oxidizing and reducing atmosphere, respectively [3,4]. Hara *et al*. [4] reported the production of Cu, Co and Fe after a carbothermic reduction of sulfide concentrate containing copper, cobalt, and iron in the presence of CaO at 1000 °C. Also, Hara *et al*. [5] has studied the reduction of a mineral sulfide-CaO-C mixture and demonstrated that an increase in mole ratio of C:CaO improves magnetic separation of products into metal and CaS.

The carbothermic reduction of FeS in the presence of lime can be considered as a two-stage reaction [3,6]; desulfurization reaction, **Eq. (4)**, and reduction reaction, **Eqs. (5)** and/or **(6)**. The total reaction is represented by **Eq. (7)**.

$$FeS_{(s)} + CaO_{(s)} = FeO_{(s)} + CaS_{(s)} \qquad \Delta G_4° = -4615 - 0.205T \quad J.mol^{-1} \quad (4)$$

$$FeO_{(s)} + C_{(s)} = Fe_{(s)} + CO_{(g)} \qquad \Delta G_5° = +111500 - 147.93T \quad J.mol^{-1} \quad (5)$$

$$FeO_{(s)} + CO_{(s)} = Fe_{(s)} + CO_{2(g)} \qquad \Delta G_6° = -12615 + 20.40T \quad J.mol^{-1} \quad (6)$$

$$FeS_{(s)} + CaO_{(s)} + C_{(s)} = Fe_{(s)} + CaS_{(s)} + CO_{(g)} \qquad \Delta G_7° = +106885 - 148.14T \quad J.mol^{-1} \quad (7)$$

Considering the thermodynamic information presented in **Eqs (4)−(7)**, the desulfurization reaction is an exothermic reaction ($\Delta H<0$) which can proceed after providing the energy required for activation of this reaction whereas the reduction reaction is an endothermic reaction ($\Delta H>0$) which requires energy in form of heat to progress. The heat provided by exothermic desulfurization reaction is insufficient to initiate the reduction reaction regarding the total reaction, **Eq. (7)**, which is also endothermic ($\Delta H>0$). Therefore, an external heat source is required to generate a sufficient heat for the onset of both desulfurization and reduction reactions.

Recently, microwave heating is applied as a new heating method in order to eliminate CO_2 emission during treatment of powder materials [7,8]. Carbon, as a good microwave susceptor,

plays a vital role in microwave absorption. Such extraordinary characteristic of carbon has prompted research into the carbothermic reduction of iron oxides under microwave irradiation [9–15]. It is reported that the carbothermic reduction of iron oxide during microwave heating requires a shorter reaction time and a lower temperature than that in the conventional heating methods [10,16]. Such advantages are attributed to the specific characteristics of microwave heating such as rapid, selective, and volumetric heating [17–20].

On the other hand, higher stability of the metal oxide than metal sulfide demonstrates a greater reactivity of mineral sulfide in an ion exchange reaction [3]. For example, the Gibbs free energy of the ion exchange reaction between FeS and CaO is negative indicating higher stability of the FeO than FeS. Furthermore, metallization of Fe is restricted by the reduction reaction owing to a higher stability of FeO than metallic iron [3]. Kutsovskaya *et al*. [21] studied the reduction reaction in a mixture of FeS:CaO:C = 1:1.1:1.1 and showed that a reduction of 70 % attains in 120 min at 950 °C and that of 95 % in 30 min at 1050 °C. Hara [3] reported that the rate of reduction reaction should be higher than desulfurization reaction to prevent SO_2 emission which caused by a reaction between metal oxide and mineral sulfide. Therefore, C/CaO ratio should be greater than 1 during carbothermic reduction of mineral sulfides in the presence of CaO.

In the present study, carbothermic reduction of FeS in the presence of CaO is investigated by microwave heating of samples containing 1:1:2 stoichiometric mole ratio of FeS:CaO:C to mitigate CO_2 and SO_2 emissions during metallic iron production via desulfurization and reduction reactions.

4-3. Experimental Procedure

Reagent $CaCO_3$ powder (purity, 99.5%) was calcined at 1300 °C for 600 min followed by crushing and grinding to the grain size of less than 45 μm. Formation of CaO after calcination process was confirmed by X-ray diffraction analysis; however, small amount of $CaCO_3$ possibly remain which cannot be detected in the XRD pattern. Reagent FeS (purity, 99%) was crushed and ground to the grain size of less than 45 μm. Reagent graphite powder (purity, 99%, grain size, 75 μm) and prepared CaO and FeS were mixed well to prepare a mixture powder containing 1:1:2 stoichiometric mole ratio of FeS:CaO:C. To prepare the briquette samples, approximately 0.02 g of a 5 mass% water solution of polyvinyl alcohol was added as a binder to 3 g of the mixture powder. A cylindrical briquette sample (15 mm diameter, 8 mm high) was formed by a cold-press followed by drying at 120 °C for 600 min. Prepared briquette samples were subjected to microwave heating using a multi-mode microwave generator with a maximum output power of 1.5 kW at 2.45 GHz under N_2 (1 L/min) atmosphere in which both the perpendicular magnetic, H, and electric, E, fields contribute to heating, as shown in **Figure 4-1**. A constant power of 1050 W was manually set until the end of heating in all experiments using three tuning stubs.

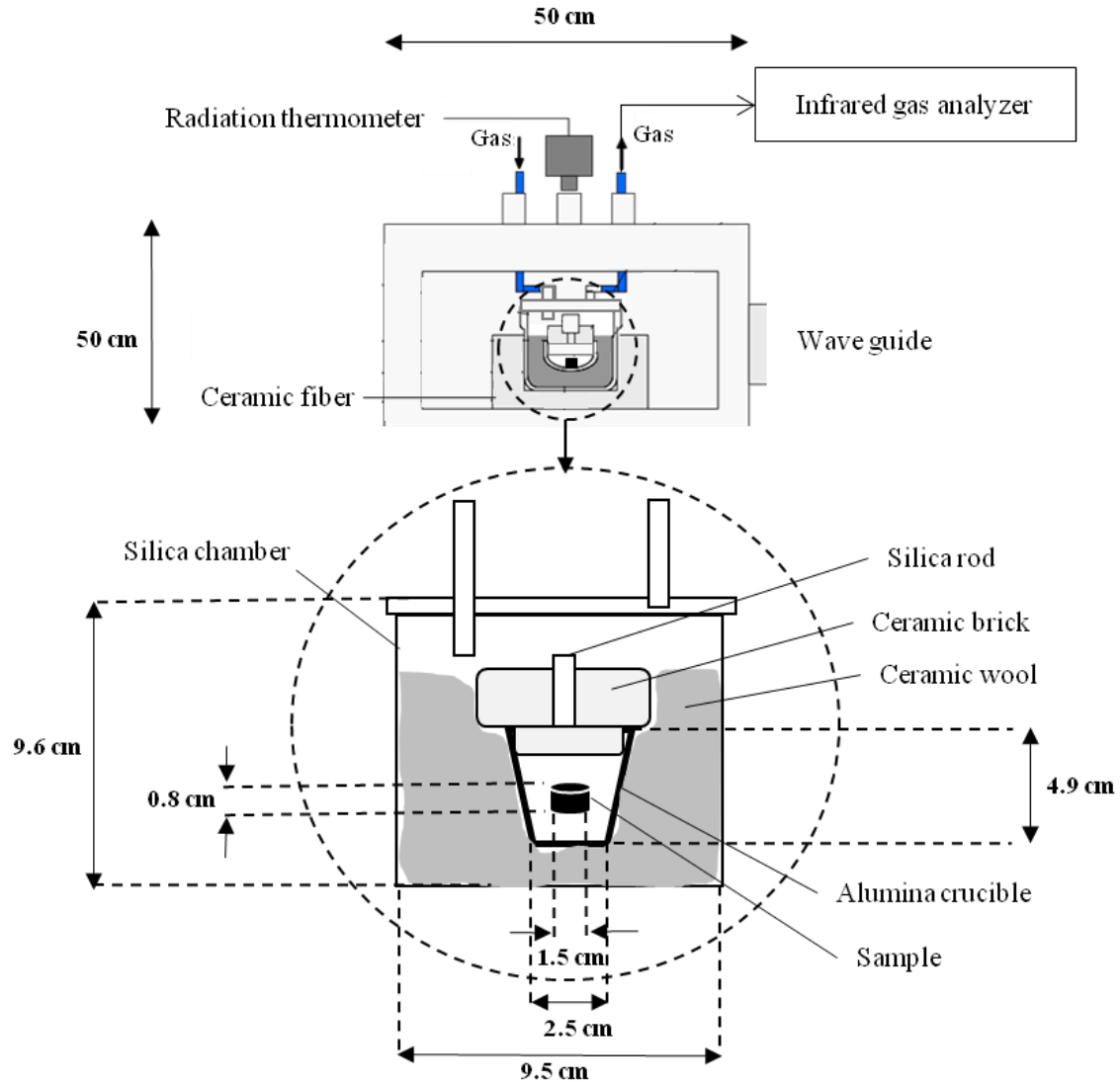

Figure 4-1 Schematic set-up for microwave heating.

The sample was contained in an alumina crucible (41 mm OD, 36.5 mm ID, 49 mm high) which surrounded by ceramic wool and covered by an insulation ceramic brick. The crucible was placed in a silica chamber (95 mm OD, 85 mm ID, 96 mm high) where the sample was protected from oxidation by flowing N_2 during the experiments. The ceramic wool and fiber were served as a thermal insulator to prevent heat loss during the heating and also used as a protector for silica chamber. The generated microwaves irradiated through the wave guide into the microwave box wherein the silica chamber was installed [22]. Sample's temperature was measured through a window above the sample using an infrared radiation thermometer. The measurement temperature range of the thermometer is 330-1500 °C. To identify the phase transformations during heat treatment, microwave irradiation was stopped after 2, 10, 25, 30, and 35 min, then treated samples were subjected to phase analysis using X-ray diffraction (XRD, Cu-$K\alpha$; λ = 1.54 Å; scan speed, 51.9 °/min; power, 3 kW; RIGAKU Smartlab, ZOTK, JAPAN). For this purpose, a portion of the treated sample was ground in a ceramic mortar and pestle. Further, XRD internal quantitative analysis method was applied to study reaction progress by quantitatively evaluation of final products after a certain treatment duration. For this purpose, 10 mass % reagent Si powder (purity, 99%, grain size, 75 μm) was added as

standard material to each sample then I_{CaS}/I_{Si} and I_C/I_{Si} were calculated after X-ray diffraction analysis of samples.

The microstructure of the remaining part of treated samples was analysed using optical microscope observation. Moreover, carbon and sulfur contents of the sample were measured before and after treatment using a carbon/sulfur analyzer (HORIBA Scientific EMIA-320V2 Carbon-Sulfur Analyzer). Also, amount of CO and CO_2 gases generated during microwave treatment were measured using an infrared off-gas analyzer (URA-208, SHIMADZU). To evaluate reaction progress, weight change ratio was calculated by dividing the weight change of the sample by its initial weight.

4-4. Results and Discussion

4-4-1. Heating Profile

Figure 4-2 shows the average temperature of samples heated via microwave irradiation for 2, 10, 25, 30, and 35 min with the standard deviation represented as error bars. A similar temperature profile was observed in all samples, confirming the reproducibility of the method.

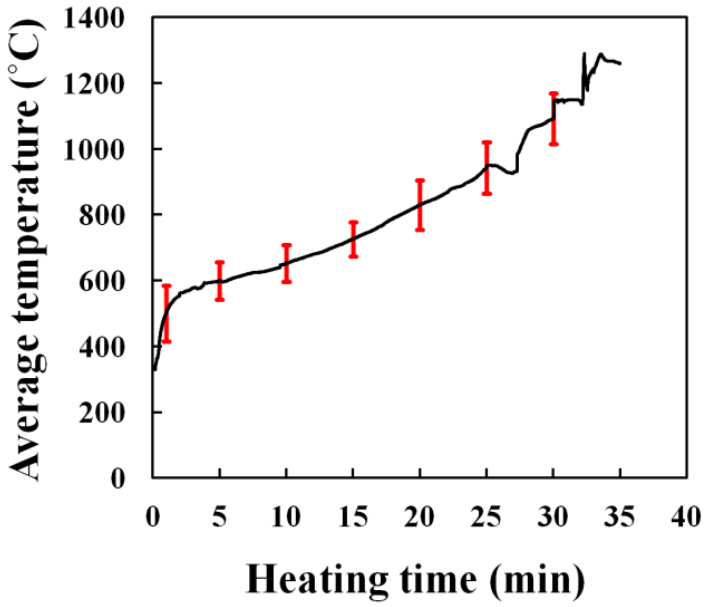

Figure 4-2 Average temperature of samples heated via microwave irradiation for 2, 10, 25, 30, and 35 min. Error bars represent the standard deviations of the average temperature.

A gradual increase in temperature was observed during microwave heating, which would be due to the presence of carbonaceous materials as a microwave susceptor in all samples. Such heating behaviour was also observed in previous studies [10,12,22,23].

Figure 4-3 illustrates XRD patterns of samples heated to 520, 645, 920, 1040, and 1290 °C in 2, 10, 25, 30, and 35 min, respectively.

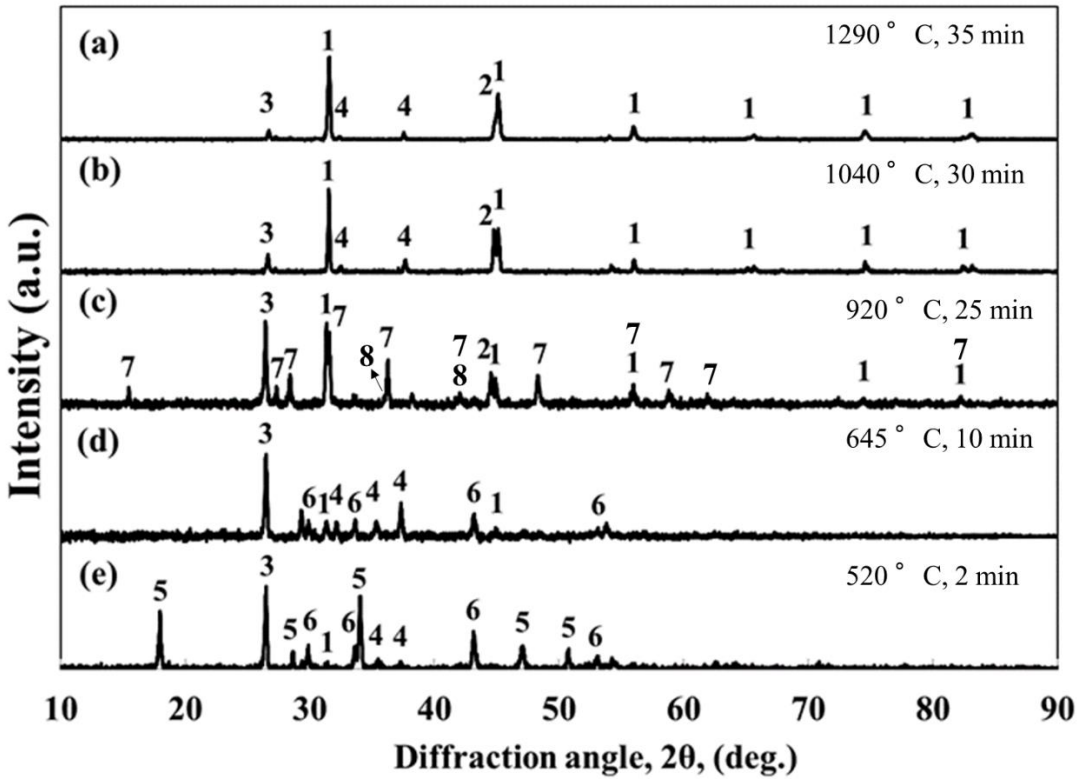

Figure 4-3 XRD patterns of samples heated to (a) 1290 °C in 35 min, (b) 1040 °C in 30 min, (c) 920 °C in 25 min, (d) 645 °C in 10 min, (e) 520 °C in 2 min. 1: CaS, 2: Fe, 3: C, 4: CaO, 5: $Ca(OH)_2$, 6: FeS, 7: FeO·CaS, 8: FeO.

Detecting $Ca(OH)_2$ phase in the pattern of sample heated to 520 °C in 2 min, see **Figure 4-3** (e), indicates that the sample was hydrated according to **Eq. (8)** before microwave processing, although the CaO powder was kept in a vacuum chamber to protect it from hydration. Therefore, formation of $Ca(OH)_2$ before microwave treatment is likely attributed to the hydration of a small portion of CaO in the mixture powder via a reaction with aqueous solution polyvinyl alcohol (the binder) according to **Eq. (8)**.

$$CaO + H_2O = Ca(OH)_2 \qquad \Delta G_8° = 63086 - 117.8T \quad J.mol^{-1} \qquad (8)$$

In addition, the desulfurization reaction, **Eq. (4)**, was initiated in sample heated to 520 °C regarding a weak CaS peak detected in the XRD pattern of this sample, see **Figure 4-3** (e).

XRD pattern of sample treated for 10 min, see **Figure 4-3** (d), demonstrated that a further heating to 645 °C causes fully dehydration of the sample at temperatures lower than 645 °C. The absence of iron oxide peaks despite detection of weak CaS peaks in the XRD pattern of samples heated to 520 and 645 °C will be explained at the end of section 3.1.

Presence of Fe phase in the XRD pattern of sample heated to 920 °C, see **Figure 4-3** (c), demonstrated the onset of reduction reaction, **Eqs. (5)** and/or **(6)**, at 645−920 °C. Further, a significant increase in the intensity of CaS peak at 31° was observed in the XRD pattern of sample heated to 920 °C, see **Figure 4-3** (c), compared to sample heated to 645 °C, see **Figure 4-3** (d). This indicates an extraordinary progress of desulfurization reaction via **Eq. (4)** in the former sample that is attributed to the consumption of FeO (as a product of the desulfurization reaction, **Eq. (4)**) via reduction to Fe at 645−920 °C, which increases the driving force for a further progress in **Eq. (4)**. On the other hand, an oxysulfide phase (FeO·CaS) was detected in

the XRD pattern of sample heated to 920 °C, **Figure 4-3** (c). This phase is considered as an intermediate phase during desulfurization reaction and its formation confirms the progress of this reaction. Formation of oxysulfide phases during carbothermic reduction of sulfide minerals in the presence of lime is also reported in previous studies [2,3,24].

In addition, formation of the intermediate oxysulfide phase was confirmed by SEM-EDX analysis of samples heated to 645 and 920 °C, as shown in **Figure 4-4** (a) and (b), respectively; however, no oxysulfide phase was detected in the XRD pattern of sample heated to 645 °C owing to the small amount of this phase.

The intermediate phase was transformed to final products (CaS and Fe) after a further heating to 1040 °C, see **Figure 4-3** (b), and no more phase change was observed at higher temperatures, **Figure 4-3** (a).

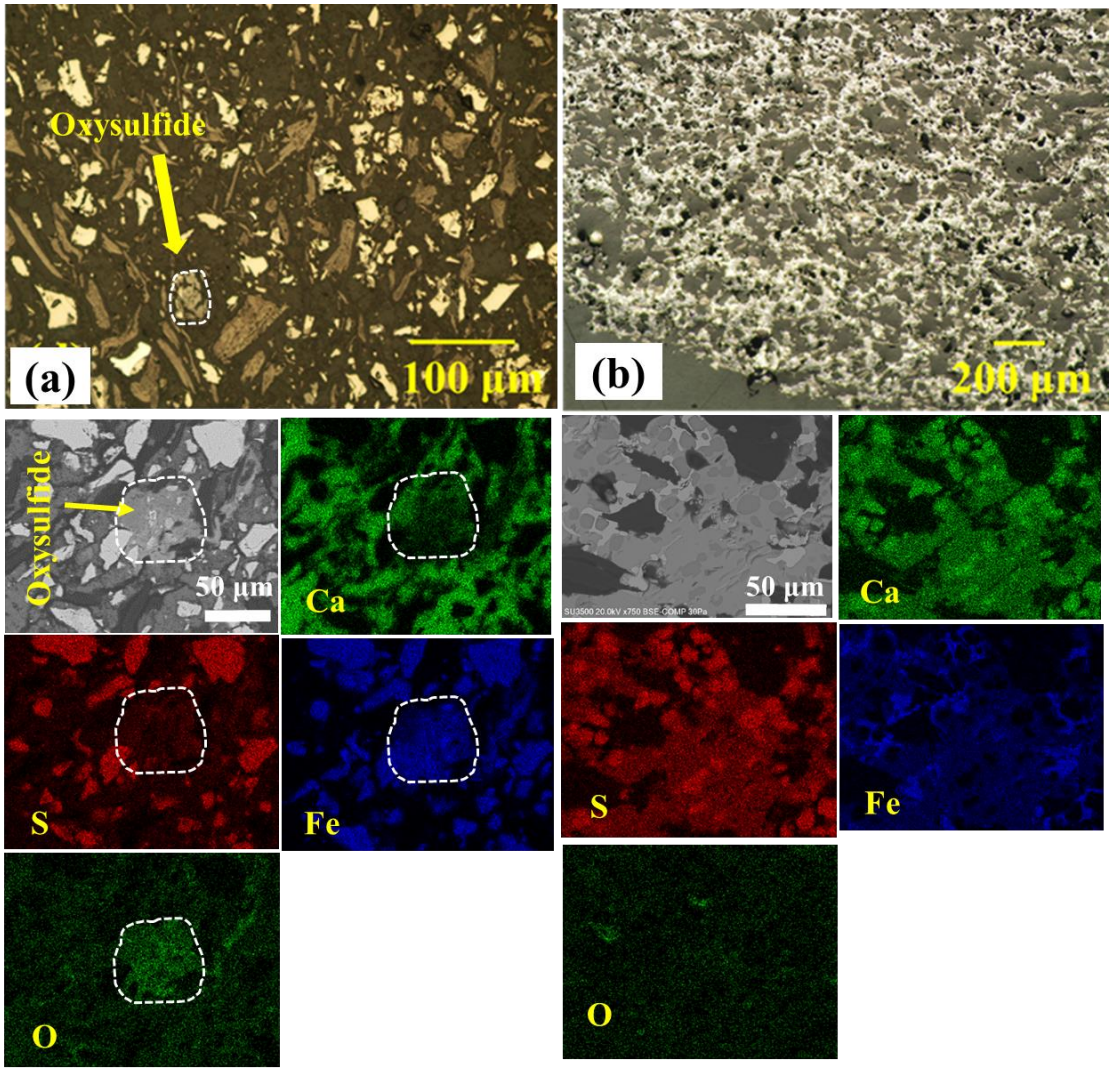

Figure 4-4 Optical microscope and SEM-EDX images of samples heated to (a) 645 °C in 10 min, and (b) 920 °C in 25 min via microwave irradiation.

Weight change ratio of treated samples for 2, 10, 25, 30, and 35 min was calculated according to **Eq. (9)** to confirm the progress in desulfurization and reduction reactions via phase transformations as mentioned above.

$$\Delta W_t = (W_i - W_t)/W_i \quad (9)$$

Where ΔW_t (dimensionless) is the total weight change ratio after treatment for t min, W_i (g) is the initial weight of sample, and W_t (g) is the weight of sample after treatment for t min.

Figure 4-5 shows carbon and sulfur contents and weight change ratio of samples heated for 2, 10, 25, 30, and 35 min during microwave treatment.

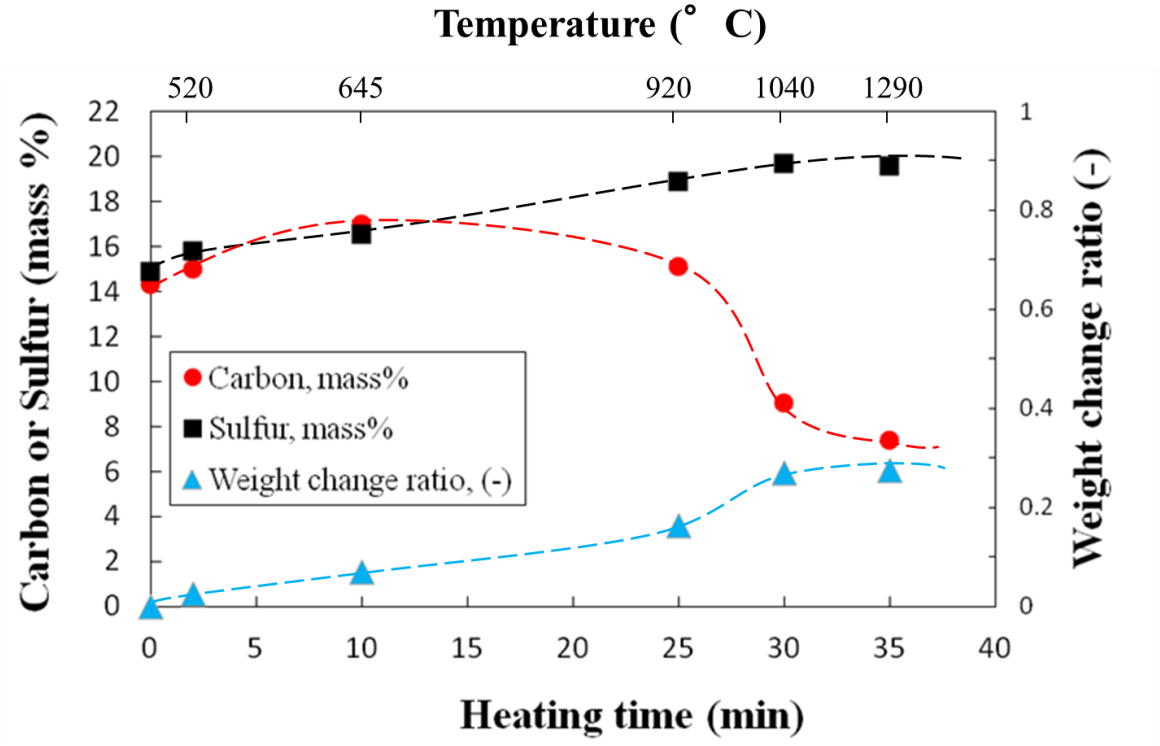

Figure 4-5 Carbon and sulfur contents and weight change ratio of samples heated for 2, 10, 25, 30, and 35 min.

As shown in **Figure 4-5**, a decrease in weight of the sample was observed after 2 min treatment whereas the absence of Fe phase in the XRD pattern of this sample, see **Figure 4-3** (e), indicates that the reduction reaction, **Eq. (5)**, cannot initiate at 520 °C. Therefore, the weight change of the sample at ca. 520 °C is attributed to either removal of volatile materials (the binder) or dehydration reaction regarding the Gibbs free energy of **Eq. (8)** obtained by FactSage® software. Accordingly, such weight loss is the cause of the increase in carbon and sulfur fraction of the mixture in the beginning of the treatment, as shown in **Figure 4-5**.

The absence of Fe phase in XRD pattern of sample heated to 645 °C, indicates that the reduction reaction, **Eqs. (5)** and/or **(6)**, cannot initiate at temperatures lower than 645 °C in the present study. Such behavior is in good agreement with the results of Marina *et al*. [21] and Rosenqvist [25] who also reported that the iron production from a mixture of FeS, CaO, and C is thermodynamically feasible above 650 and 730 °C, respectively. Therefore, the weight loss in sample heated to 645 °C in 10 min is attributed to either the fully dehydration reaction, as confirmed by XRD analysis (**Figure 4-3** (d)), or removing of volatile materials such as binder. The absence of $Ca(OH)_2$ in the XRD pattern of sample heated to 645 °C (**Figure 4-3** (d)) in 10 min indicates that the calcium hydroxide has no effect on overall reaction at temperatures >645 °C.

Further weight loss in sample heated to 920 °C in 25 min accompanied by a decrease in carbon contents of this sample is attributed to the onset of reduction reaction at 645−920 °C according to **Eqs. (5)** and/or **(6)**, as confirmed by detecting of Fe in XRD pattern of sample heated to 920 °C in 25 min, see **Figure 4-3** (c).

A significant decrease in carbon contents of sample heated to 1040 °C in 30 min is owing to either removing as CO and/or CO_2 via the reduction reaction which causes a greater weight loss in this sample, or consuming via the Boudouard reaction according to **Eq. (10)**.

$$C_{(s)} + CO_{2(g)} = 2\ CO_{(g)} \quad (10)$$

No significant weight loss after a further heating to 1290 °C demonstrates the accomplishment of reduction reaction at ca. 1040 °C.

Figure 4-6 shows the CO/CO_2 of the off-gas during microwave heating of sample heated to 1290 °C in 35 min.

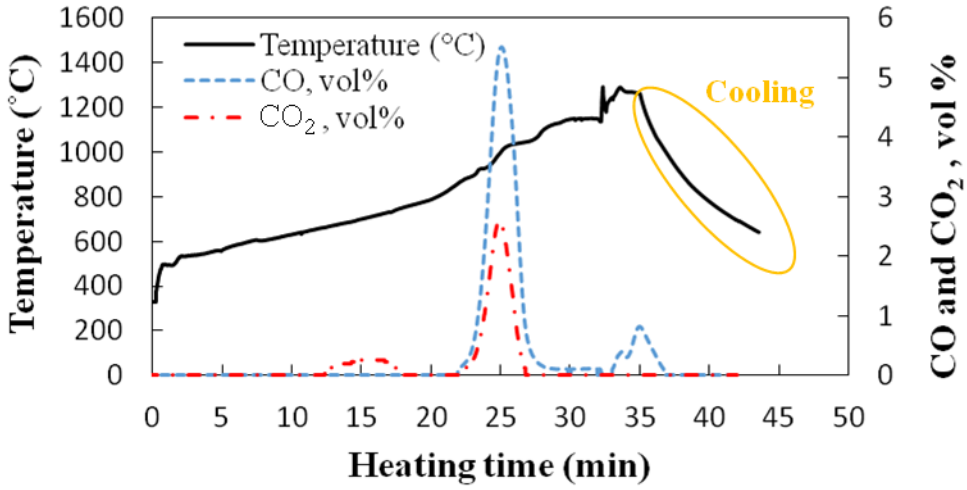

Figure 4-6 Off-gas analysis of sample heated to 1290 °C in 35 min during microwave irradiation.

Simultaneous dehydration of $Ca(OH)_2$ and binder removal at temperatures lower than 645 °C cause a significant decrease in vol. % of CO_2 in the off-gas. Therefore, no CO/CO_2 was detected in the off-gas at temperatures lower than 645 °C. On the other words, the presence of H_2O in the off-gas (resulted from dehydration reaction) up to 645 °C leads to a significant decrease in volume fraction of CO/CO_2 while at temperatures >645 °C, the H_2O has no effect on the off-gas measurements owing to the fully dehydration up to 645 °C. After binder removal and fully dehydration of sample at 645 °C, see **Figure 4-3** (d), an increase in the CO_2 of the off-gas (ca. 0.3 vol. % CO_2) followed by decreasing to zero vol. % at ca. 680 °C was detected. Although no calcium carbonate peak was detected in the XRD pattern of sample after calcinations or after 2 min treatment, see **Figure 4-3** (e), such CO_2 generation is likely attributed to the calcination of possibly remaining $CaCO_3$. Therefore, the weight loss at this temperature seems to be owing to the calcination of the small amount of calcium carbonate.

A significant increase in the CO and CO_2 of the off-gas at ca. 850–1040 °C is attributed to the onset of reduction reaction, **Eq. (5)** and/or **(6)**, at ca. 850 °C after a treatment for 22 min. This result can be supported by detecting Fe phase in the XRD pattern of sample heated to 920 °C, as shown in **Figure 4-3** (c). Rosenqvist [25] also reported that a temperature over 800 °C is required for reduction of FeS-CaO-C mixture owing to the low reactivity of carbon at lower temperatures.

Furthermore, the absence of CO_2 and a dramatic decrease in CO of the off-gas at temperatures over ca. 1040 °C, not only, confirm that the reduction reaction is accomplished at 1040 °C, which causes no significant weight loss at temperatures over 1040 °C, but also, indicate that a greater carbon loss during treatment at temperatures over 1040 °C, as shown in **Figure 4-5**, is attributed to the carbon gasification via the Boudouard reaction, **Eq. (10)**. In

addition, stoichiometric calculations showed that ca. 9.1 mass % carbon remains after reaction whereas the measured carbon contents of samples heated to 1040 and 1290 °C are 9 and 7.4 mass %, respectively. These calculations also confirm carbon consumption via carbon gasification reaction. On the other hand, XRD internal quantitative analysis, shown in **Figure 4-7**, demonstrated a similar ratio of I_{CaS}/I_{Si} (**Figure 4-7** (a)) at temperatures over 1040 °C, confirming the accomplishment of total reaction, **Eq. (7)**, at ca. 1040 °C.

On the other hand, oxygen balance can be calculated according to off-gas analysis. The input oxygen of 0.018 mol was estimated from initial CaO in the sample. The output oxygen of 0.011 mol was calculated from the measured CO/CO_2 in the off-gas. These calculations also indicate oxygen removal during treatment. The difference between input and output oxygen is likely attributed to the presence of CaO in the sample heated to 1295 °C in 35 min, see **Figure 4-3** (a).

Moreover, it is reported that the reduced iron can absorb carbon at temperatures higher than 1200 °C to make molten iron particles during microwave heating [23]. Formation of molten iron particles was confirmed in sample heated to 1290 °C by comparing the optical microscope and SEM-EDX images of samples heated to 1290 and 1040 °C, shown in **Figure 4-8** (a) and (b), respectively. Such behavior was also reported by Hara *et al*. [23] who observed molten iron droplets during microwave heating of a magnetite and graphite mixture at temperatures higher than 1200 °C.

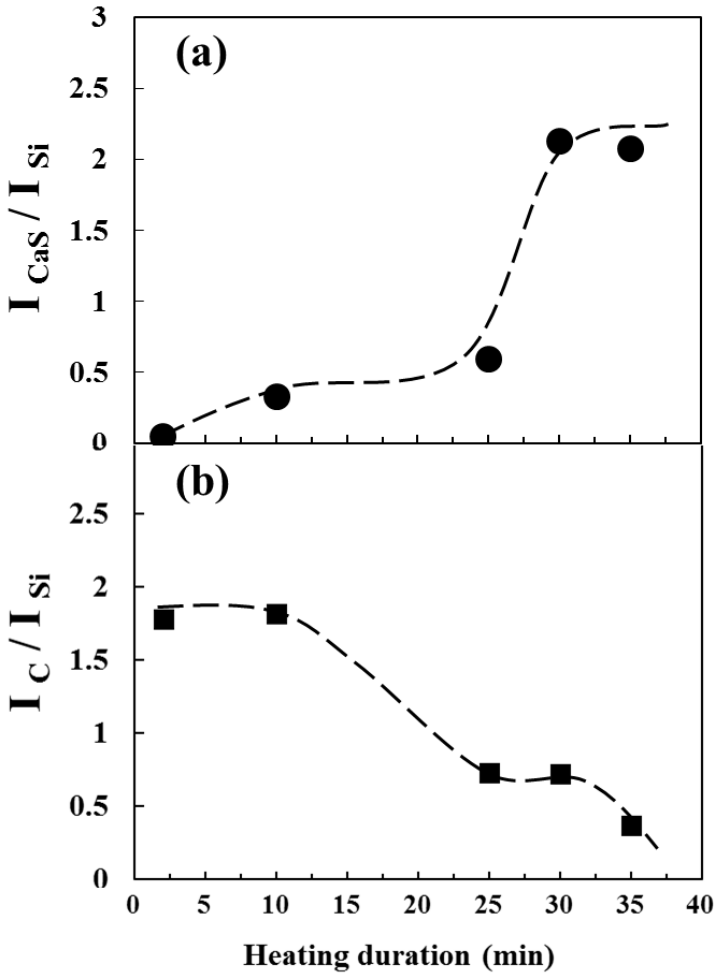

Figure 4-7 (a) I_{CaS}/I_{Si} and (b) I_C/I_{Si} of samples heated to certain temperatures. I_{CaS}/I_{Si} and I_C/I_{Si} were measured according to the XRD internal quantitative analysis by adding 10 mass % Si as standard material to samples.

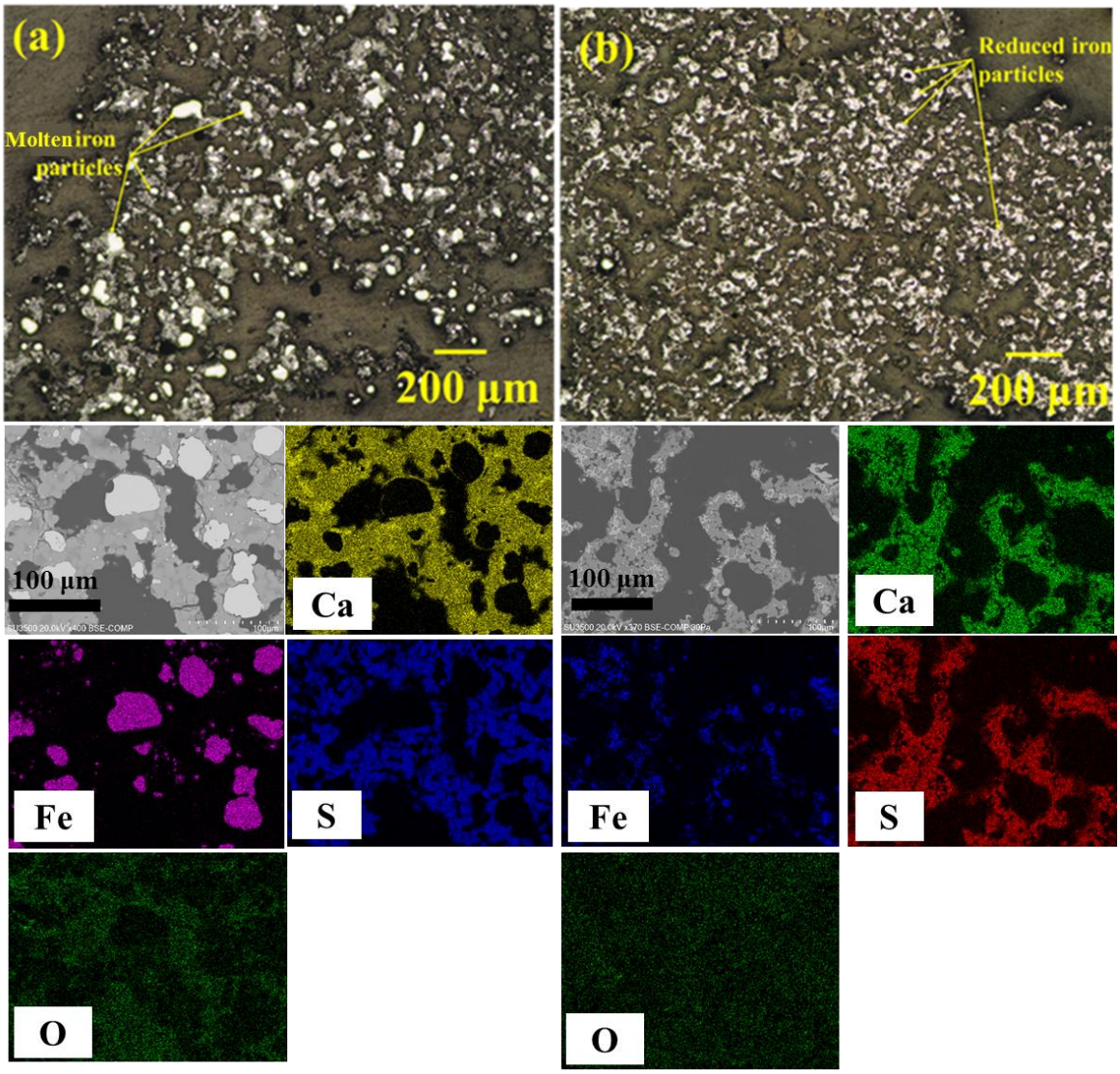

Figure 4-8 Optical microscope and SEM-EDX images of samples heated to (a) 1290 °C in 35 min, and (b) 1040 °C in 30 min via microwave irradiation.

Considering **Figure 4-8**, Fe particles are distributed in a matrix of CaS. This indicates that iron oxide (product of the ion exchange reaction) was also distributed in the CaS matrix before reduction to metallic iron. Therefore, the absence of iron oxide phase despite detection of CaS in the XRD pattern of samples heated up to 645 °C (see **Figure 4-3** (e) and (d)) is likely attributed to a higher weight % of CaS (matrix) compared to the iron oxide particles in the XRD sample. Moreover, after a further progress in the ion exchange reaction at 920 °C, FeO particles cannot be enormously detected owing to the formation of an oxysulfide phase (FeO·CaS) which was detected by both XRD analysis (see **Figure 4-3** (c)) and SEM-EDX observations (**Figure 4-4** (b)).

4-4-2. Effect of Microwave Heating on Reduction Degree

Reduction degree (%) was calculated according to **Eq. (11)**:

$$\text{Reduction degree (\%)} = ([W_i - W_t - W_V] / W_{St}) \times 100 \qquad (11)$$

where W_V (g) is the weight change owing to the removal of volatile materials and dehydration of the sample and W_{St} (g) is the stoichiometric weight change of sample attributed to the removal of CO according to **Eq. (7)**.

Figure 4-9 shows the reduction degree of the FeS:CaO:C = 1:1:2 mixture during microwave heating of samples heated to 1290 °C and that of a mixture with a same mole ratio after conventional heating reported by Jha *et al*. [2] and by Kutsovskaya *et al*. [21].

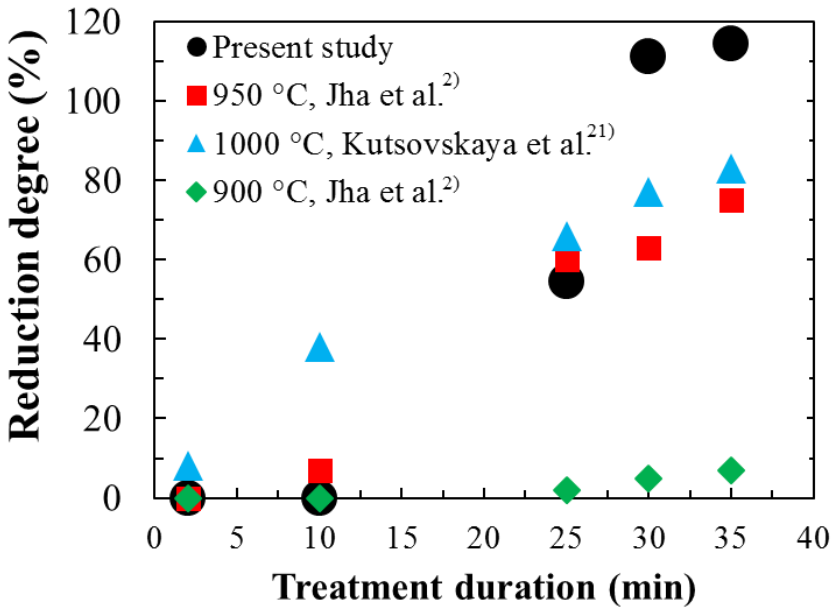

Figure 4-9 Reduction degree of FeS-CaO-C mixture during microwave heating to a certain temperature (circle), after conventional heating at 950 °C for ca. 35 min reported by Jha *et al*. [2] (square), after conventional heating at 1000 °C for ca. 35 min reported by Kutsovskaya *et al*. [21] (triangle).

It was observed that the reduction degree of samples heated for 30 and 35 min is higher than 100 %. Jha *et al*. [2] reported also reduction degree over 100 % and theorized that it is because of the drainage of liquid form pellet. In this study, in addition to the drainage from pellet over 1200 °C, the other possibility is reduction of FeO via **Eqs. (6)** and/or **(12)** followed by carbon gasification via the Boudouard reaction according to **Eq. (10)** which causes a larger weight loss than the stoichiometric weight change. A decrease in carbon contents of sample heated to 1290 °C, despite the accomplishment of the reduction reaction at 1040 °C, confirms the carbon consumption via the Boudouard reaction which can be promoted by microwave irradiation [26].

$$FeO_{(s)} + 1/2\ C_{(s)} = Fe_{(s)} + 1/2\ CO_{2(g)} \qquad (12)$$

Jha *et al*. [2] showed that a minimum 90 min is required to initiate the reduction reaction in a FeS:CaO:C = 1:1:2 mixture at 850 °C during conventional heating whereas Ishizaki *et al*. [27] reported a rapid reduction of FeO to Fe at 870-1200 °C during microwave heating of a magnetite-coal composite pellet. In the present study, as mentioned above, the reduction reaction was initiated at ca. 850 °C after a 20 min microwave heating. It should be mentioned that conventional heating of sample has been conducted at a constant temperature in the literature. It means the sample needs to be heated for certain duration at a specific temperature whereas during microwave heating in the present study, sample properties were studied as a certain temperature was attained, without any holding time. This indicates extraordinary effect of microwave heating on the reaction progress.

This result is in a good agreement with previous investigations [10,16] wherein the carbothermic reduction of iron oxide is conducted in a shorter time and at a lower temperature during microwave heating than the conventional heating. Further, Kashimura *et al.* [12] reported an enhancement in iron production from magnetite and graphite during microwave heating. Also, Hunt *et al.* [26] reported a significant decrease in apparent activation energy of the Boudouard reaction during microwave irradiation compared to the conventional heating. Therefore, the improvement in reaction progress in the present study would be attributed to the effect of microwave irradiation on the chemical reactions [12,26,28,29].

4-5. Conclusions

Carbothermic reduction behavior of FeS:CaO:C = 1:1:2 mixture during microwave heating was investigated using a multi-mode microwave generator at 1050 W at 2.45 GHz. Results can be summarized as follows:

1. FeO consumes via reduction reaction that causes a significant progress in the desulfurization reaction.
2. According to off-gas analysis, reduction reaction initiates at ca 850 °C after microwave heating for ca. 20 min that is shorter than the time required for the carbothermic reduction of FeO to Fe at 850 °C during conventional heating.
3. Reduced iron can absorb carbon during microwave heating at temperatures higher than 1200 °C to make molten iron particles.

4-6. References

[1] A. Amini, T. Maeda, K. Ohno, K. Kunitomo, Carbothermic Reduction Behavior of FeS in the Presence of CaO during Microwave Irradiation, ISIJ Int. 59 (2019), In Press.

[2] A. Jha, P. Grieveson, Carbothermic reduction of pyrrhotite in the presence of lime for the production of metallic iron, Scand. J. Metall. 21 (1992) 50–62.

[3] Y.S.R. Hara, Mineral sulphide-lime reactions and effect of CaO/C mole ratio during carbothermic reduction of complex mineral sulphides, Int. J. Miner. Metall. Mater. 21 (2014) 1–11.

[4] Y.S.R. Hara, A. Jha, Carbothermic reduction of Zambian sulphide concentrates in presence of lime, Miner. Process. Extr. Metall. 122 (2013) 146–156.

[5] Y.R.S. Hara, A. Jha, Energy Efficient Separation of Magnetic Alloy fron the Carbothermic Reduction of NKANA Cu-Co Concentrates, in: Energy Technol. 2015, Springer International Publishing, Cham, 2015: pp. 83–91.

[6] R. Padilla, M.C.C. Ruiz, H.Y.Y. Sohn, Reduction of molybdenite with carbon in the presence of lime, Metall. Mater. Trans. B. 28 (1997) 265–274.

[7] C.A. Crane, M.L. Pantoya, B.L. Weeks, M. Saed, The effects of particle size on microwave heating of metal and metal oxide powders, Powder Technol. 256 (2014) 113–117.

[8] M. Hayashi, Y. Yokoyama, K. Nagata, Effect of particle size and relative density on powdery Fe_3O_4 microwave heating., J. Microw. Power Electromagn. Energy. 44 (2010) 198–206.

[9] M. Hayashi, K. Takeda, K. Kashimura, T. Watanabe, K. Nagata, Carbothermic Reduction of Hematite Powders by Microwave Heating, ISIJ Int. 53 (2013) 1125–1130.

[10] K. Ishizaki, K. Nagata, T. Hayashi, Production of pig iron from magnetite ore-coal composite pellets by microwave heating, ISIJ Int. 46 (2006) 1403–1409.

[11] J. Li, B. Li, J. Han, Z. Cao, J. Wang, A Comparative Study on the Reduction Mechanism of Fe_2O_3 Under Different Heating Methods, Jom. 66 (2014) 1529–1536.

[12] K. Kashimura, M. Sato, M. Hotta, D. Kumar Agrawal, K. Nagata, M. Hayashi, T. Mitani, N. Shinohara, Iron production from Fe_3O_4 and graphite by applying 915 MHz microwaves, Mater. Sci. Eng. A. 556 (2012) 977–979.
[13] N. Standish, W. Huang, Microwave Application in Carbothermic Reduction of lron Ores, ISIJ Int. 31 (1991) 241–245.
[14] Y. Lei, Y. Li, W. Chen, R. Wan, Microwave Carbothermic Reduction of Oolitic Hematite, ISIJ Int. 57 (2017) 791–794.
[15] Q. Ye, H. Zhu, L. Zhang, J. Ma, L. Zhou, P. Liu, J. Chen, G. Chen, J. Peng, Preparation of reduced iron powder using combined distribution of wood-charcoal by microwave heating, J. Alloys Compd. 613 (2014) 102–106.
[16] T. Chun, H. Long, Z. Di, P. Wang, Q. Meng, Influence of microwave heating on the microstructures of iron ore pellets with coal during reduction, Ironmak. Steelmak. 44 (2017) 486–491.
[17] Z. Peng, J.-Y. Hwang, J. Mouris, R. Hutcheon, X. Huang, Microwave Penetration Depth in Materials with Non-zero Magnetic Susceptibility, ISIJ Int. 50 (2010) 1590–1596.
[18] Z. Peng, Z. Li, X. Lin, M. Yang, J.Y. Hwang, Y. Zhang, G. Li, T. Jiang, Microwave Power Absorption in Materials for Ferrous Metallurgy, Jom. 69 (2017) 178–183.
[19] M. Oghbaei, O. Mirzaee, Microwave versus conventional sintering: A review of fundamentals, advantages and applications, J. Alloys Compd. 494 (2010) 175–189.
[20] C.A. Pickles, Microwaves in extractive metallurgy: Part 1 - Review of fundamentals, Miner. Eng. 22 (2009) 1102–1111.
[21] M.L. Kutsovskaya, M.T. Hepworth, J.R. McGaa, Recovery of lime, sulfur, and iron from gypsum and pyrite wastes, Ind. Eng. Chem. Res. 35 (1996) 1736–1746.
[22] K. Nishioka, T. Taniguchi, Y. Ueki, K. Ohno, T. Maeda, M. Shimizu, Gasification and Reduction Behavior of Plastics and Iron Ore Mixtures by Microwave Heating, ISIJ Int. 47 (2007) 602–607.
[23] K. Hara, M. Hayashi, M. Sato, K. Nagata, Pig Iron Making by Focused Microwave Beams with 20 kW at 2.45 GHz, ISIJ Int. 52 (2012) 2149–2157.
[24] A. Jha, S. Tang, A. Chrysanthou, Phase equilibria in the metal-sulfur-oxygen system and selective reduction of metal oxides and sulfides: Part I. The carbothermic reduction and calcination of complex mineral sulfides, Metall. Mater. Trans. B Process Metall. Mater. Process. Sci. 27 (1996) 829–840.
[25] T. Rosenqvist, Phase equilibria in the pyrometallurgy of sulfide ores, Metall. Trans. B. 9 (1978) 337–351.
[26] J. Hunt, A. Ferrari, A. Lita, M. Crosswhite, B. Ashley, A.E. Stiegman, Microwave-specific enhancement of the carbon-carbon dioxide (Boudouard) reaction, J. Phys. Chem. C. 117 (2013) 26871–26880.
[27] K. Ishizaki, K. Nagata, T. Hayashi, Localized Heating and Reduction of Magnetite Ore with Coal in Composite Pellets Using Microwave Irradiation, ISIJ Int. 47 (2007) 817–822.
[28] A. Ferrari, J. Hunt, A. Lita, B. Ashley, A.E. Stiegman, Microwave-Specific Effects on the Equilibrium Constants and Thermodynamics of the Steam − Carbon and Related Reactions, J. Phys. Chem. C. 118 (2014) 9346–9356.
[29] J. Zhou, W. Xu, Z. You, Z. Wang, Y. Luo, L. Gao, C. Yin, R. Peng, L. Lan, A new type of power energy for accelerating chemical reactions: the nature of a microwave-driving force for accelerating chemical reactions, Sci. Rep. 6 (2016) 25149.

Chapter 5: Kinetics of Hydrogen-Reduction of FeS-CaO Mixture: A comparision between Microwave Heating and Conventional Heating

5-1. Abstract

Hydrogen-reduction of FeS-CaO mixture during microwave heating is investigated as a novel idea to combine the advantages of microwave irradiation and using H_2 as reducing agent for a further mitigation of CO_2 emission during iron production. Kinetics of iron production via H_2-reduction of FeS-CaO mixture during both microwave irradiation (at 1275 W (750 °C), 1175 W (570 °C), and 975 W (460 °C) at 2.45 GHz) and conventional heating (at 750, 570, and 460 °C) was investigated to clarify the effect of heating method on the dominant rate-controlling mechanism. Results of microwave treatment revealed that the interfacial chemical reaction is progressed rapidly and gas diffusion in micro pores of reduced metallic iron is dominant rate-controlling mechanism with an activation energy of ~22.3 $kJ.mol^{-1}$ from the onset of microwave irradiation. In conventional heating, the interfacial chemical reaction is the rate controlling mechanism in the first ~500, 800, and 1000 s of treatment at 750, 570, and 460 °C, respectively; while the dominant mechanism is changed to gas diffusion for longer processing time. This is attributed to extraordinary effects of microwave irradiation on speeding up the chemical reactions, especially at lower temperatures, while formation of Fe shell on the surface of FeS particles is responsible for changing the rate controlling mechanism to gas diffusion.

5-2. Introduction

Reduction of sulfide minerals in the presence of lime (CaO) has been studied in previous literature [1,2] to prevent SO_2 emission during production of metal from metal sulfides owing to a high tendency of lime for reaction with sulfur to form CaS in a reducing atmosphere [1,3]. For instance, Hara *et al*. [1] produced metallic Cu, Co and Fe from a sulfide concentrate via a carbothermic reduction in the presence of CaO at 1000 °C. Jha *et al*. [4] showed that the reduction of FeS:CaO:C = 1:1:2 mixture initiates after a heat treatment at 850 °C for > 90 min. Kutsovskaya *et al*. [5] attained a reduction degree of 95 % after treating a FeS:CaO:C = 1:1.1:1.1 mixture at 1050 °C in 30 min.

On the other hand, reduction rate of iron oxide in H_2 is much higher than that in CO [6–9] and also the interdiffusion coefficient of H_2/H_2O gas in iron ore sintered particles is three times higher than that of CO/CO_2 at 500 °C [10]. Such advantages of hydrogen-reduction, in addition to a large demand for eco-friendly ironmaking have resulted in employing H_2 as a reducing agent, instead of carbonaceous materials [6–11], to mitigate CO_2 emission. Moreover, Habashi *et al*. [12] indicated that the CaO favors the hydrogen-reduction of metal sulfides (cupper sulfides and cupper-iron sulfides) at 800 °C. Therefore, hydrogen-reduction of FeS in the presence of lime is likely an alternative method for iron production from iron sulfide minerals that can be considered as a two-stage reaction [3,13]; ion exchange reaction according to **Eq. (4)**, and reduction reaction according to **Eq. (13)**. The total reaction is represented by **Eq. (14)**.

$$FeO_{(s)} + H_{2(g)} = Fe_{(s)} + H_2O_{(g)} \qquad \Delta G_{13}^\circ = 16240 - 8.45\,T \quad J.mol^{-1}\ [14] \qquad (13)$$

$$FeS_{(s)} + CaO_{(s)} + H_{2(g)} = Fe_{(s)} + CaS_{(s)} + H_2O_{(g)} \qquad \Delta G_{14}^\circ = 11625 - 8.655\,T \quad J.mol^{-1} \qquad (14)$$

A higher stability of the metal oxide than metal sulfide demonstrates a greater reactivity of mineral sulfide in the ion exchange reaction [3]. For example, the Gibbs free energy of the ion

exchange reaction between FeS and CaO is negative indicating higher stability of the FeO than FeS. Furthermore, metallization of Fe is restricted by the reduction reaction owing to a higher stability of FeO than metallic iron [3].

In addition, microwave irradiation is an energy-efficient and a rapid-heating method to decrease activation energy of chemical reactions owing to both thermal and non-thermal effects of microwave photons. The non-thermal effect of microwave irradiation on the rate of chemical reactions, has attracted the attention of researchers on microwave irradiation energy in terms of speeding up chemical reactions [15–18]. The thermal effect of microwave irradiation has the potential to mitigate CO_2 emission and decrease the amount of carbonaceous materials required for carbothermic reduction of iron resources due to its specific characteristics, such as rapid and selective heating, volumetric heating, and high-efficiency heating. For example, we have investigated carbothermic reduction of FeS in the presence of lime via microwave heating wherein the results revealed that the average temperature required for attaining a certain reduction degree is lower during microwave heating than in the conventional heating [19].

As a novel idea for a further mitigation of CO_2 emission, hydrogen-reduction of FeS-CaO mixture during microwave irradiation is investigated in the present study to combine the advantages of microwave irradiation and using H_2 as reducing agent during iron production. Such hydrogen-reduction during microwave processing has been also applied for magnetite reduction in our previous work [20]. Furthermore, hydrogen-reduction of FeS-CaO mixture during conventional heating is also conducted in an electric resistance furnace to make a better understanding about the effect of heating method (conventional and microwave) on the kinetics of iron production during reduction reaction.

5-3. Experimental Procedure

5-3-1. Materials

Reagent $CaCO_3$ powder (purity, 99.5%) was calcined at 1300 °C for 600 min followed by crushing and grinding to obtain a CaO with grain size of less than 45 μm. Formation of the CaO after calcination process was confirmed by X-ray diffraction analysis; however, small amount of $CaCO_3$ possibly remain which cannot be detected in the XRD pattern. Reagent FeS (purity, 99%) was crushed and ground to the grain size of less than 45 μm. Then, the crushed CaO and FeS were mixed well by spoon to prepare a powder mixture of FeS:CaO with stoichiometric mole ratio of 1:1. The mixture (2 g) was pressed to a cylindrical shape briquette sample (10 mm diameter, 10 mm height, 2.54 $g.cm^{-3}$ apparent density) using a cold hydraulic press.

5-3-2. Apparatus and procedure

Microwave heating: The prepared briquette samples were subjected to microwave irradiation using a multi-mode microwave generator (in which both the perpendicular magnetic and electric fields contribute to heating) with a maximum output power of 1.5 kW at 2.45 GHz. The reaction progress was estimated based on the weight change of samples during microwave treatment in H_2 (1 NL/min). In the previous literature [14,21–25], a conventional heating apparatus has been equipped with thermobalance to continuously measure weight change during the reduction reactions. In the present study, the microwave heating system was also equipped with thermobalance to prepare a unique apparatus for a novel continuous study of the hydrogen-reduction during microwave irradiation. The sample was placed in a silica basket (silica cannot absorb microwaves and acts as a transparent material during microwave irradiation), and the basket was suspended in a silica tube (inner diameter, 35 mm) by silica chains connected to the thermobalance which installed on top of the microwave apparatus.

Schematic of the microwave heating set-up is illustrated in **Figure 5-1**. The silica tube was purged by H_2 (1 NL.min^{-1}) for ~5 min, then the microwave irradiation was initiated. This time was considered as time zero in weight change measurements during microwave treatment. Temperature of the sample was measured through a window in microwave box above the sample using an infrared radiation thermometer. The measurement temperature range is 330-1500 °C. The experiments were conducted at various temperatures by applying the microwave out-put powers of 1275, 1125, and 975 W. After certain durations, the microwave heating system was turned off and the atmosphere was changed to N_2 (1 NL.min^{-1}) to cool down the sample.

Conventional heating: For treatment of sample during conventional heating, the sample was placed in a silica basket, and the basket was suspended by a Pt wire connected with the thermobalance on top of a vertical electric resistance furnace with alumina tube (inner diameter, 35 mm) to continuously measure weight changes of the sample during treatment. The furnace was heated up to experimental temperatures (same temperatures as used during microwave heating) in flowing N_2 (1 NL.min^{-1}). Then, the silica basket was inserted in the isothermal zone and the atmosphere immediately changed to H_2 (1 NL.min^{-1}). This time was considered as time zero in weight change measurements during conventional heating. The furnace maintained at the experimental temperature by a PID temperature controller for certain duration. Finally, the atmosphere was changed to N_2 (1 NL.min^{-1}) to cool down the sample.

5-3-3. Sample analysis

To identify the phase transformation during heat treatment, the experiment was quitted after a certain duration, then treated sample was subjected to phase analysis using X-ray diffraction (XRD, Cu-$K\alpha$; λ = 1.54 Å; scan speed, 51.9 °/min; power, 3 kW; RIGAKU Smartlab, ZOTK, JAPAN). For this purpose, a portion of the treated sample was ground in a ceramic mortar and pestle. Further, XRD internal quantitative analysis method was applied to study reaction progress by quantitative evaluation of final products after certain treatment durations. For this purpose, 10 mass % reagent Si powder (purity, 99%, grain size, 75 μm) was added as standard material to treated sample, then I_{CaS}/I_{Si} and I_{Fe}/I_{Si} were calculated after X-ray diffraction analysis. I_{CaS}, I_{Fe} and I_{Si} are the intensity of main peaks of CaS, Fe, and Si at 31.4 °, 44.7 °, and 28.4 °, respectively. Moreover, the microstructure of the remaining part of treated samples was analysed using SEM-EDX observation. In addition, stability of sulfur during treatment was confirmed by measuring the sulfur contents of the samples before and after treatment using a carbon/sulfur analyzer (HORIBA Scientific EMIA-320V2 Carbon-Sulfur Analyzer).

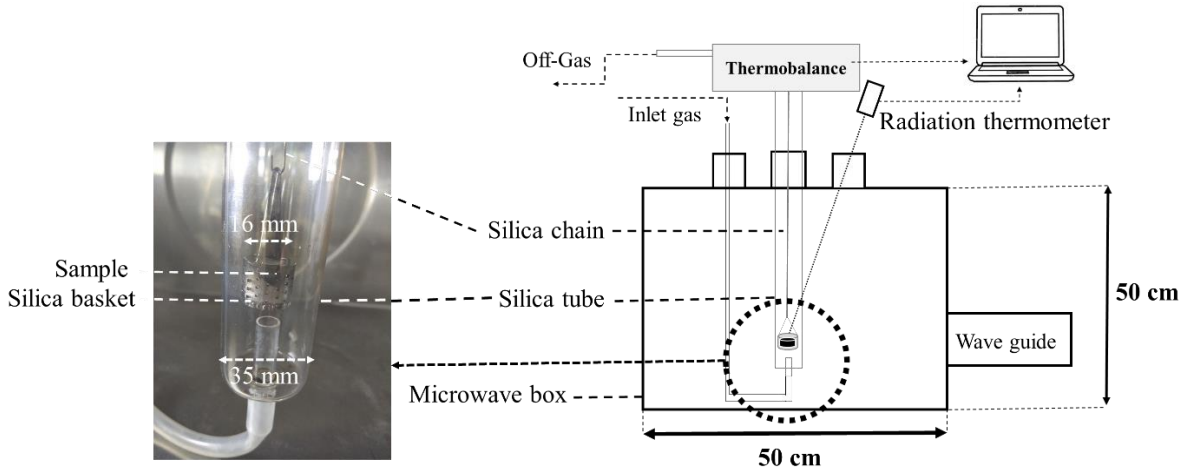

Figure 5-1 Schematic set-up for microwave heating equipped with thermobalance.

5-4. Results and Discussion

5-4-1. Heating profile during microwave treatment

In the present study, the microwave treatment was conducted at least twice at each output power and the average temperature was considered as the temperature corresponding to the applied power. **Figure 5-2** shows average temperature profiles of samples reduced in H_2 during microwave irradiation at powers of 1275, 1125, and 975 W. Error bars represent standard deviations. The average temperature of samples microwave irradiated at 1275, 1125, and 975 W for 1200 s are ~750, 570, and 460 °C, respectively.

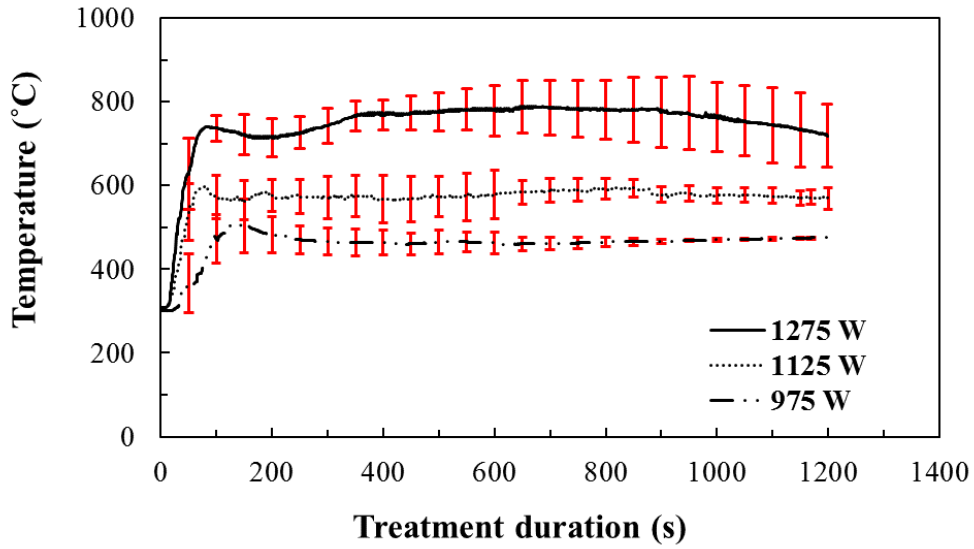

Figure 5-2 Average temperature profiles of samples reduced in H_2 during microwave irradiation at powers of 1275, 1125, and 975 W. Error bars represent standard deviations.

5-4-2. Reduction degree

Reduction degree (X, dimensionless) of sample treated for a certain duration was calculated based on the weight change in the sample, according to **Eq. (15)**:

$$Reduction\ degree\ (X) = \frac{W_i - W_t - W_{ht}}{W_i \times W_O} \quad (15)$$

where W_i (g) is the initial weight of the sample, W_t (g) is the weight of the sample after treatment for t seconds, W_{ht} (g) is the weight change of the sample after treatment for t seconds owing to the dehydration reaction which measured via either microwave or conventional treatment of sample in N_2, and W_O (dimensionless) is the stoichiometric weight ratio of oxygen in the sample, which is 0.111.

Figure 5-3 (a) shows the reduction degree of samples during microwave irradiation in H_2 at powers of 1275 W (750 °C), 1125 W (570 °C), and 975 W (460 °C) for 1200 s. **Figure 5-3** (b) shows the reduction degree of samples in H_2 during conventional heating at 750, 570, and 460 °C for 1200 s. Each experiment was conducted at least twice and error bars represents standard deviations.

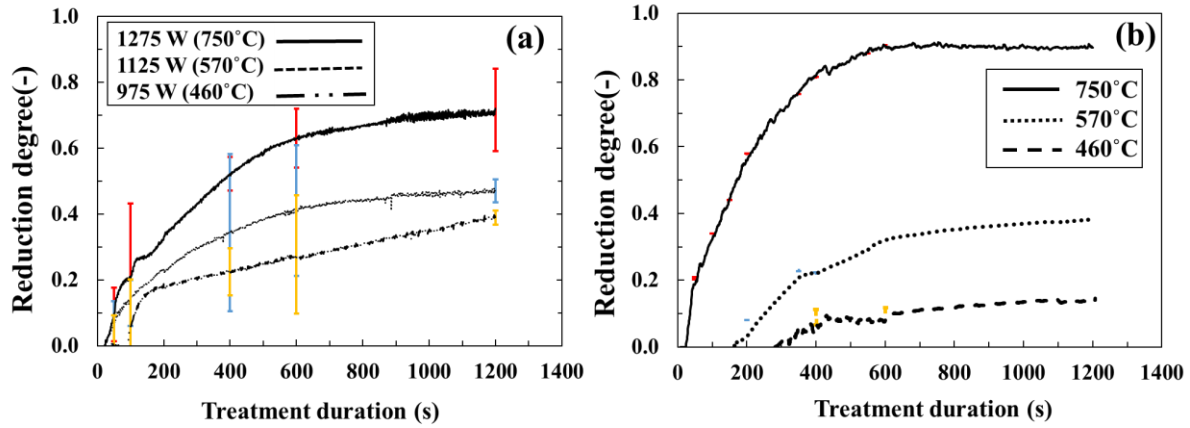

Figure 5-3 Reduction degree of samples (a) microwave irradiated at 1275 W (750 °C), 1125 W (570 °C), and 975 W (460 °C), and (b) conventionally heated at 460 °C, 570 °C, and 750 °C up to 1200 s. Each experiment was conducted at least twice and error bars represents standard deviations.

A noticeable increase in reduction degree was observed in the first 600 s of treatment in H_2 whereas no significant change occurred during a longer processing time. Therefore, in the present kinetic study, the initial 600 s of the treatment was investigated owing to the insignificant change in reduction degree after 600 s. Reduction of the sample during treatment in H_2 is attributed to the oxygen removal as H_2O according to **Eq. (13)** that subsequently results in a phase transformation in the sample. X-ray diffraction pattern of un-treated sample and that of samples treated during microwave irradiation and conventional heating at 750, 570, and 460 °C for 600 s are shown in **Figure 5-4**.

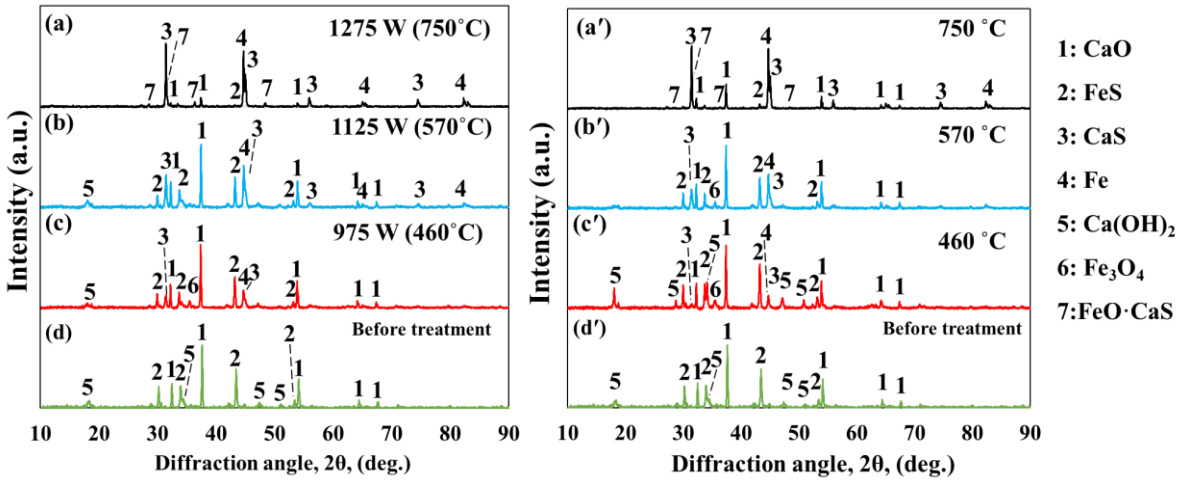

Figure 5-4 XRD patterns of samples treated for 600 s in H_2 during (a) microwave irradiation at 1275 W (750 °C), (b) microwave irradiation at 1125 W (570 °C), (c) microwave irradiation at 975 W (460 °C), (a′) conventional heating at 750 °C, (b′) conventional heating at 570 °C, (c′) conventional heating at 460 °C, (d) and (d′) that of un-treated sample.

$Ca(OH)_2$ was detected in the pattern of un-treated sample (**Figure 5-4** (d) and (d′)), although the crushed CaO powder was kept in a vacuum desiccator chamber to protect it from hydration. This is attributed to the hydration of a portion of CaO during sample preparation steps such as the cold-press of powder mixture. Treatment of sample in the inert gas (N_2, 1 $NL.min^{-1}$) confirmed a decrease in weight of the sample in the first 80 s of microwave treatment at 750 and 570 °C, in the first 100 s of microwave processing at 460 °C, and in the first 30, 180,

and 300 s of conventional heating at 750, 570, and 460 °C, respectively. Therefore, weight change in these times is likely attributed to either reduction reaction or dehydration of $Ca(OH)_2$ according to **Eq. (16)** [26–28].

$$Ca(OH)_{2(s)} = CaO_{(s)} + H_2O_{(g)} \quad (16)$$

CaS and Fe were detected in all patterns indicating a great progress in both ion exchange reaction (**Eq. (4):** $FeS_{(s)} + CaO_{(s)} = FeO_{(s)} + CaS_{(s)}$) and reduction reaction (**Eq. (13):** $FeO_{(s)} + H_{2(g)} = Fe_{(s)} + H_2O_{(g)}$) at 750, 570, and 460 °C in the first 600 s of treatment duration. Moreover, detection of magnetite phase (Fe_3O_4) in the pattern of sample treated at 460 °C for 600 s (**Figure 5-4** (c) and (c′)) is likely attributed to the instability of FeO under 575 °C. Furthermore, an intermediate oxysulfide phase (FeO·CaS) was detected in the XRD pattern of sample treated at 750 °C for 600 s (**Figure 5-4** (a) and (a′)). This phase is an intermediate phase during ion exchange reaction and confirms a great progress in this reaction at 750 °C. Formation of oxysulfide phases is also reported during carbothermic reduction of sulfide minerals in the presence of lime in previous studies.[3,4,29].

In addition, CaO and FeS were also detected as high-intensity peaks in the pattern of samples treated at 570 °C (**Figure 5-4** (b) and (b′)) and 460 °C (**Figure 5-4** (c) and (c′)) demonstrating that a noticeable portion of the treated sample is remained as un-reacted part; although, low-intensity peaks of the CaO and FeS at 750 °C (**Figure 5-4** (a) and (a′)) means a small portion of the treated sample is also remained un-reacted even after treatment for 600 s at higher temperature.

Figure 5-5 shows the SEM-EDX images of large FeS particles from reacted part of a sample treated at 750 °C during microwave irradiation for 600 s. It seems the ion exchange reaction (**Eq. (4)**) is initiated on the surface of FeS particles and forms iron oxide. Then, the iron oxide (product of the ion exchange reaction) is reduced by H_2 to form a layer of metallic iron which surrounds the un-reacted part of FeS particles. This indicates that the un-reacted parts of FeS particles which enclosed by the reduced metallic iron cannot contact/react with CaO particles to continue the ion exchange reaction (**Eq. (4)**). Thus, a portion of FeS and CaO particles remain un-reacted even after treatment for 600 s.

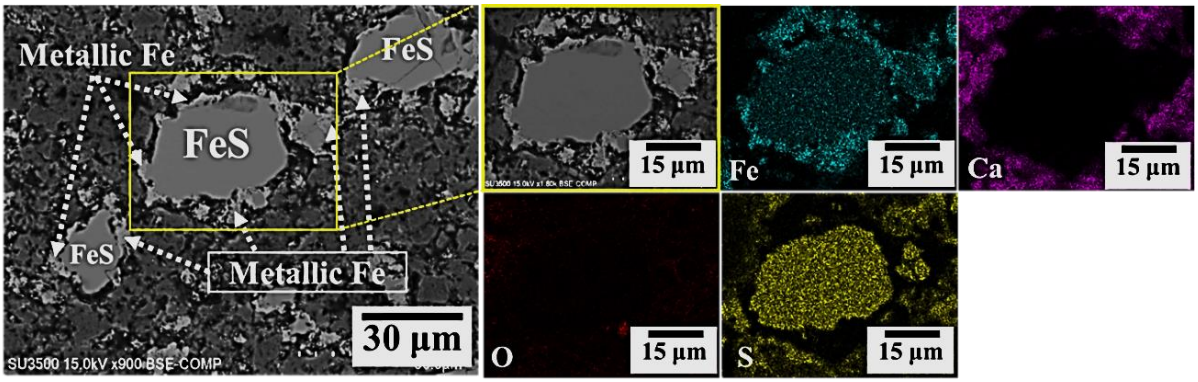

Figure 5-5 SEM-EDX images of large FeS particles in samples microwave treated at 750 °C for 600 s.

5-4-3. Morphology observations

Macroscale observation of samples microwave treated for certain durations at 975 W (460 °C) and 1275 W (750 °C) are illustrated in **Figure 5-6** (a)-(c) and (d)-(f), respectively. A boundary was recognized between the reacted part (bright gray, outer part) and un-reacted core (dark gray). The boundary is moved toward the center of the sample with an increase in processing time that resulted in shrinking of the un-reacted core. This observation indicates

that the total reaction is progressed topochemically and the un-reacted core model can be employed for kinetic study of iron production during microwave treatment of FeS-CaO mixture in H_2.

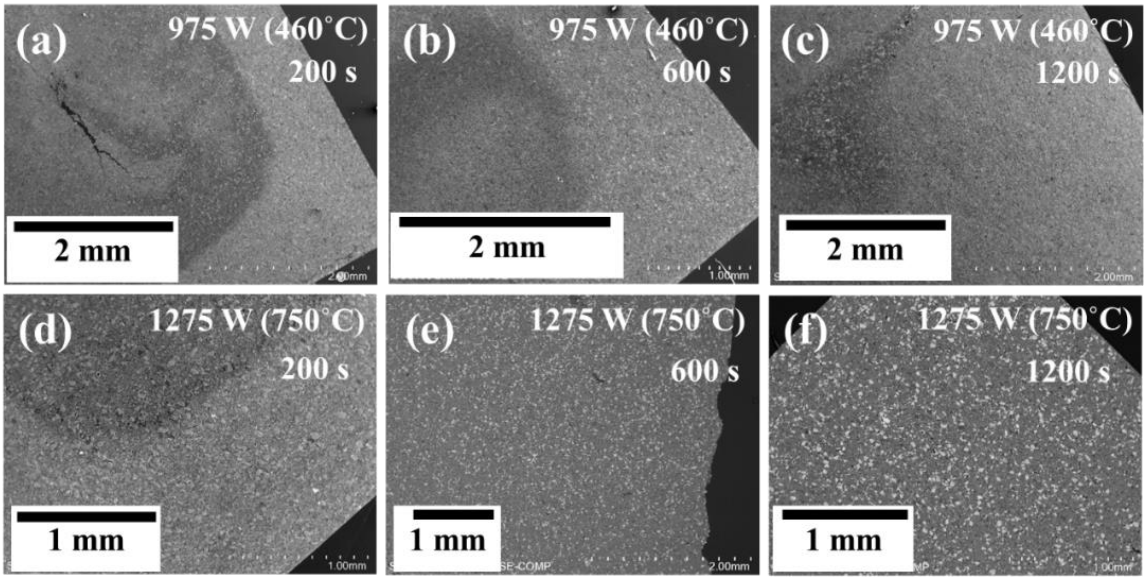

Figure 5-6 SEM macrographs of microwave treated samples at 460 °C for (a) 200 s, (b) 600 s, and (c) 1200 s. SEM macrographs of microwave treated samples at 750 °C for (d) 200 s, (e) 600 s, and (f) 1200 s.

Furthermore, microscale SEM images of samples conventionally treated for 100, 400, and 600 s at 750 and 570 °C are shown in **Figure 5-7** (a)-(c) and (d)-(f), respectively. **Figure 5-7** (a) shows the formation of a noticeable amount of iron oxide in sample conventionally treated at 750 °C for 100 s which confirms a great progress of the ion exchange reaction in this sample. Considering **Figure 5-7** (b) and (c), hydrogen-reduction of the iron oxide (**Eq. (13)**) is progressed during treatment at 750 °C for 600 s to form a metallic iron layer on the surface of the FeS particles. The Fe layer encloses the iron oxide and likely acts as a barrier for gas diffusion during the reduction reaction. Such behavior indicates that the overall reaction is progressed topochemically. Such behavior was also occurred in samples conventionally treated at 570 °C (**Figure 5-7** (d)-(f)) and 460 °C; however, the treatment time required for the formation of a noticeable amount of the iron oxide and Fe layers at 570 and 460 °C (>400 s) is longer than that at 750 °C (<100 s).

A similar behavior also observed in the microwave treated sample (**Figure 5-8**) where a small FeS particle (~15 μm) mostly converted to iron oxide via the ion exchange reaction (**Eq. (4)**) followed by hydrogen reduction of iron oxide (**Eq. (13)**) to make a metallic iron shell on the surface of the particle.

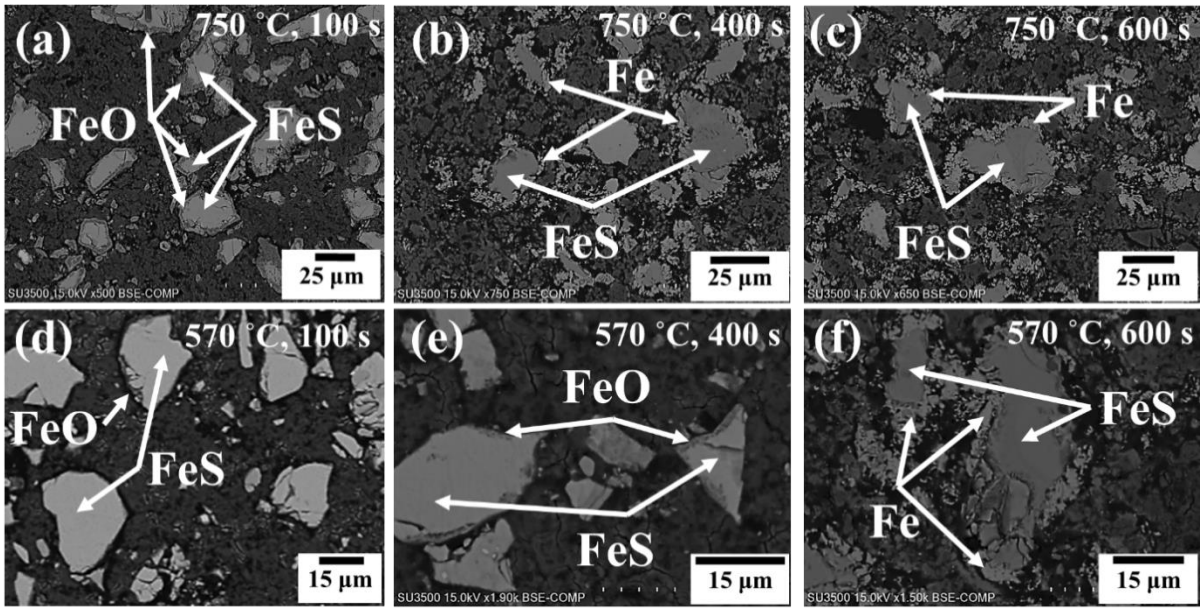

Figure 5-7 SEM images of samples conventionally treated at 750 °C for (a) 100 s, (b) 400 s, and (c) 600 s. SEM images of samples treated at 570 °C for (d) 100 s, (e) 400 s, and (f) 600 s.

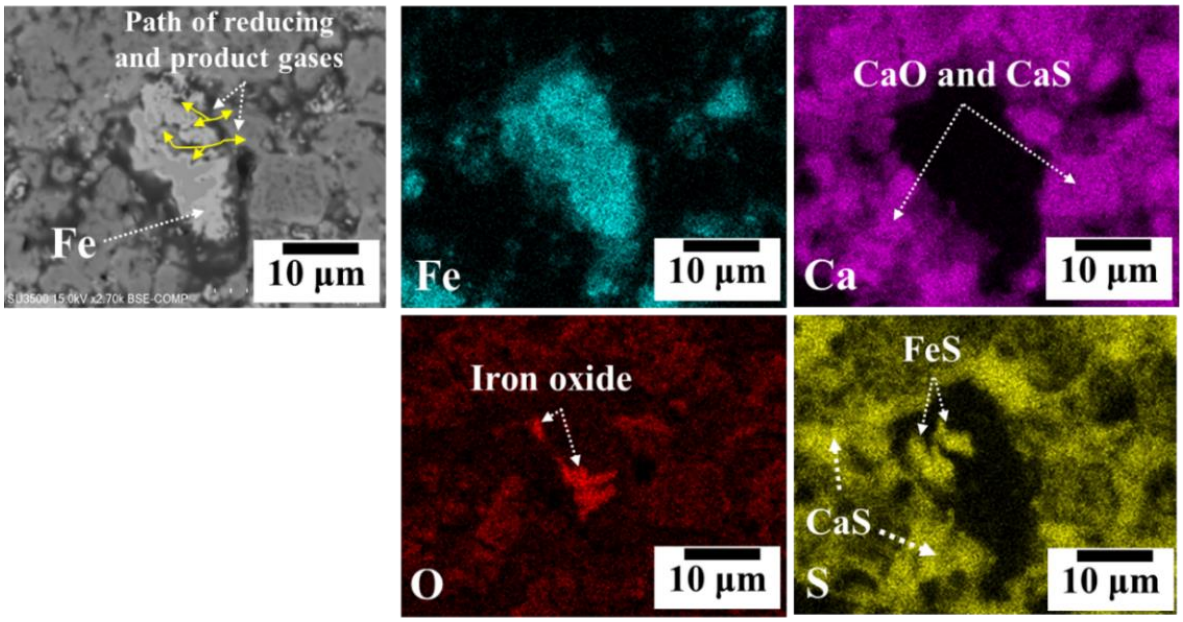

Figure 5-8 SEM-EDX images of the sample microwave treated at 1275 W (750 °C) for 600 s.

5-5. Kinetic Model

Un-reacted core model has been applied widely in previous investigations [25,30] to study the kinetics of chemical reactions which progress topochemically. In this model, four mechanisms can contribute to the reaction progress which are gas diffusion (in micro pores of solid product), gas-solid interfacial chemical reaction, mass transfer (gas diffusion in bulk gas), and mix of these mechanisms. The mechanism with the highest resistance (the lowest rate) controls the rate of overall reaction. To evaluate kinetic parameters in dominant rate-controlling mechanism, mathematical kinetic equations have been derived [31,32] based on the characteristics of reactants and products in gas-solid reactions. **Table 5-1** summarizes the

derived kinetic equations corresponding to the reaction rate-controlling mechanisms for spherical shape particles.

Table 5-1 Kinetic equations corresponding to different reaction rate-controlling mechanisms for spherical particles.

Rate-controlling mechanism	Kinetic equation
Gas diffusion in micro pores (GD)	$1-3(1-X)^{2/3}+2(1-X)=\frac{6D_e}{C_R r_i^2}\left(\frac{K}{1+K}\right)(C_{Ab}-C_{Ae})t$
Interfacial chemical reaction (ICR)	$1-(1-X)^{1/3}=\frac{k(C_{Ab}-C_{Ae})}{C_R r_i}t$
Mass transfer (MT)	$X=\frac{3k_f}{C_R r_i}\left(\frac{K}{1+K}\right)(C_{Ab}-C_{Ae})t$
Mix of GD, ICR, and MT	$\frac{1}{C_R r_i}\left(\frac{K}{1+K}\right)(C_{Ab}-C_{Ae})\frac{t}{f}-\frac{3-3f+f^2}{3k_f}=\frac{r_i}{6D_e}(3f-2f^2)+\frac{K}{k(1+K)}$

Where X (dimensionless) is the reduction degree, K (dimensionless) is the equilibrium constant for reduction reaction, D_e ($cm^2.s^{-1}$) is the effective diffusion coefficient of gas in micro pores, k_f ($cm.s^{-1}$) is the mass transfer coefficient in the gas film, C_{Ab} and C_{Ae} ($mol.cm^{-3}$) are the concentration of reducing gas in bulk and at the equilibrium state, respectively. k ($cm.s^{-1}$) is the rate constant of chemical reaction, t (s) is the treatment duration, r_i (cm) is the radius of sample, and f is equal to $(1-(1-X)^{1/3})$. C_R ($mol.cm^{-3}$) is the concentration of reducible oxygen in the sample, that is 0.0177 $mol.cm^{-3}$.

To recognize the dominant rate-controlling mechanism, left hand side of kinetic equation (**Table 5-1**) is plotted versus t (for the single rate controlling mechanisms) or $3f-2f^2$ (for mix rate-controlling), then the linear relationships of lines in each plot is evaluated by calculating the correlation coefficient [33]. The largest correlation coefficient indicates the dominant rate-controlling mechanism [25,30,33].

5-5-1. Kinetic analysis

With regards to the microscopic observations that confirm the topochemical progress of reaction in the present study, un-reacted core model was employed to clarify the dominant rate-controlling mechanism in reduction reaction (**Eq. (13)**) during treatment under H_2 atmosphere. To simplify calculations, Usui *et al.* [34] suggested that the sample shape (cylinder) can be assumed as a sphere with a volume same as cylindrical sample. Therefore, the radius of the assumed spherical sample (r_i, cm) was calculated based on the radius (r_b, cm) and height (h_b, cm) of the cylindrical shape briquette sample according to **Eq. (17)**:

$$r_i=\left(\frac{3}{4}r_b^2 h_b\right)^{1/3} \quad (17)$$

As mentioned above, weight change during treatment is attributed to the oxygen removal as H_2O via reduction reaction. Therefore, the Gibbs free energy of reduction reaction ($\Delta G_{13}°$) was divided by R (gas constant, $J.mol^{-1}.K^{-1}$) to derive the equilibrium constant (K) of reduction reaction (**Eq. (13)**) as a function of temperature, **Eq. (18)**. The mass transfer coefficient (k_f) was calculated for different temperatures using the Sherwood (*Sh*), Reynolds (*Re*), and Schmidt (*Sc*) dimensionless numbers. The value of K and k_f at different temperatures are presented in **Table 5-2**.

$$lnK=1.016-1953.33T^{-1} \quad (18)$$

Table 5-2 Calculated parameters required for kinetic study at different temperatures.

T (°C)	750	570	460
K (-)	0.409	0.272	0.192
k_f *(cm.s^{-1})*	14.9	10.9	8.69

As mentioned in section 3.2, no significant weight change observed after treatment for >600 s, regarding **Figure 5-3**. Therefore, kinetic study was conducted up to 600 s treatment duration.

Considering the kinetic equations presented in **Table 5-1**, Chemical reaction, mass transfer, gas diffusion, and mixed rate-controlling mechanisms at 750, 570, and 460 °C are plotted for microwave treated and conventionally heated samples in **Figure 5-9** (a)-(d) and **Figure 5-10** (a)-(d), respectively. To compare the linearity of kinetic data in these plots, the correlation coefficient (r) was calculated for each series of data, as suggested by Qu *et al*. [33]. The value of r is between –1 and 1 where –1 and 1 mean a perfect negative and positive linear relationship, respectively. Zero means no linear relationship. In the present study, the absolute value of correlation coefficient ($|r|$) is used to show the linearity of kinetic data after a certain treatment duration, as illustrated in **Figure 5-11**.

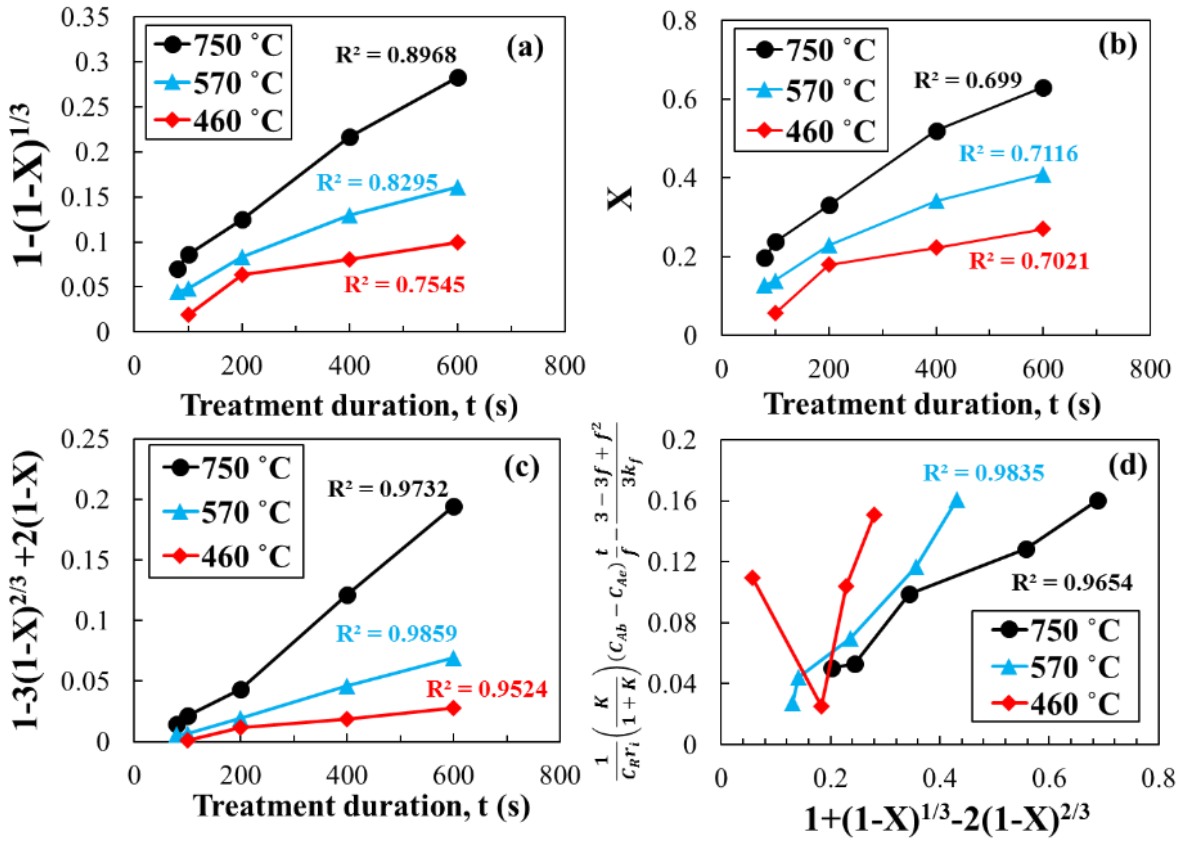

Figure 5-9 Kinetic plots of gas-solid reduction reaction during microwave treatment, (a) interfacial chemical reaction rate-controlling, (b) mass transfer rate-controlling, (c) gas diffusion in micro-pores rate controlling, and (d) mixed control.

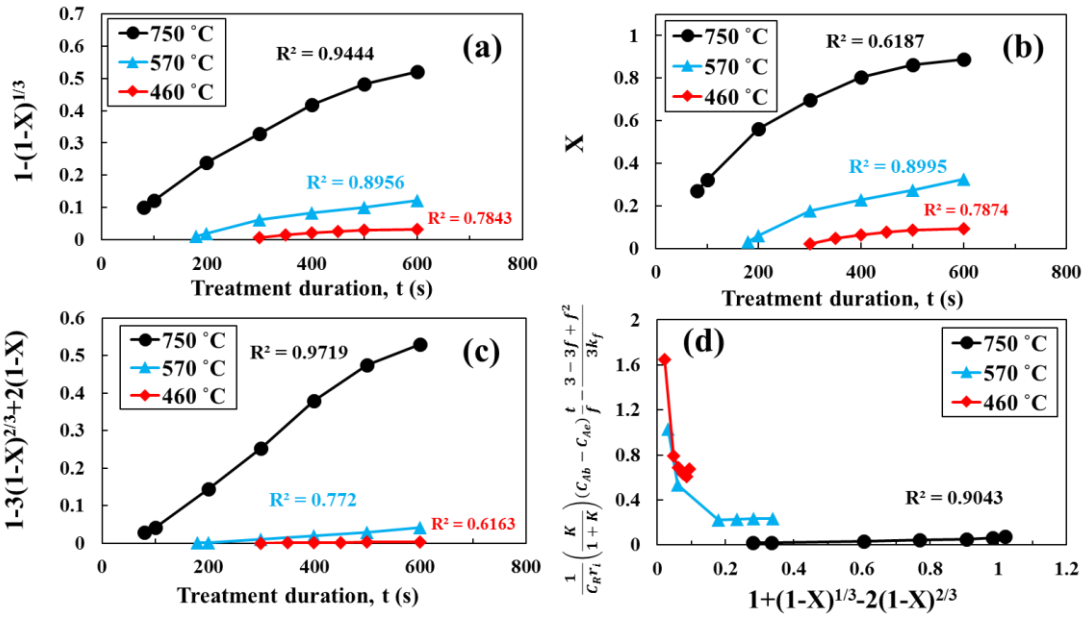

Figure 5-10 Kinetic plots of gas-solid reduction reaction during conventional heating, (a) interfacial chemical reaction rate-controlling, (b) mass transfer rate-controlling, (c) gas diffusion in micro-pores rate controlling, and (d) mixed control.

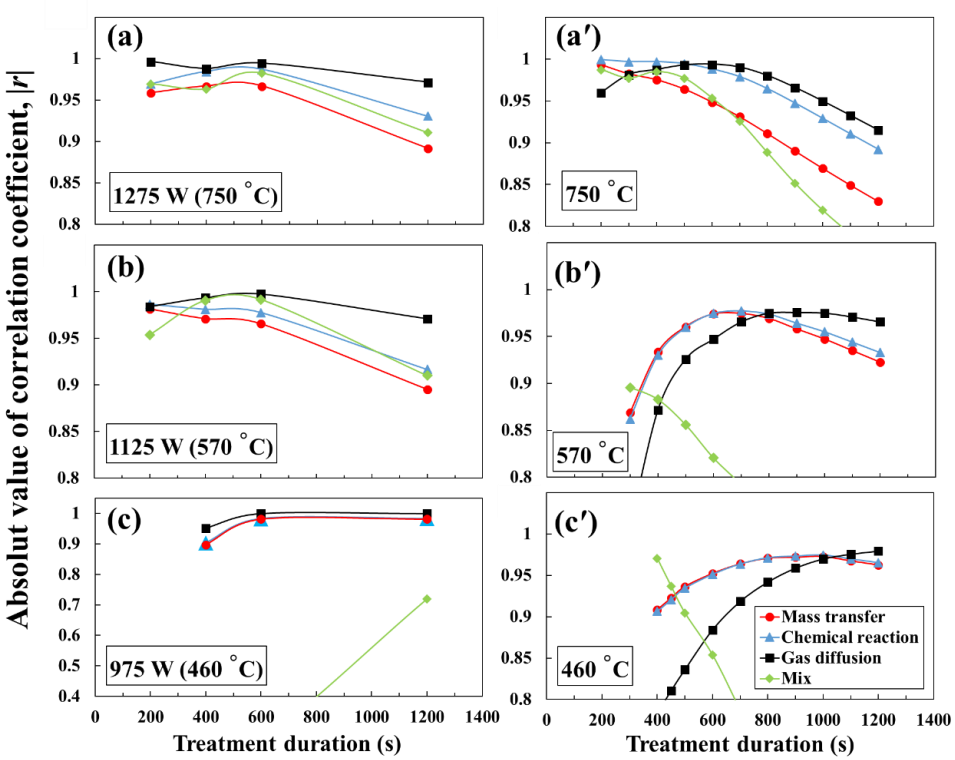

Figure 5-11 Absolute value of correlation coefficient of data corresponding to chemical control, diffusion control, mass transfer control, and mixed control of reduction degree of samples microwave heated at (a) 1275 W (750 °C), (b) 1125 W (570 °C), and (c) 975 W (460 °C) and conventionally heated at (a′) 750 °C, (b′) 570 °C, and (c′) 460 °C.

During microwave heating (**Figure 5-11** (a)-(c)), the correlation coefficient of gas diffusion in micro pores is larger than that of other mechanisms at all temperatures. This indicates that the dominant mechanism for controlling of the reduction rate during microwave irradiation in

H_2 is gas diffusion in micro pores. The path of gaseous reactants and products in the reduced metallic iron (which surrounds the un-reacted wüstite core) is illustrated in **Figure 5-8**.

In the conventional heating, the interfacial chemical reaction controls the rate of overall reaction during treatment up to ~500 s, 800 s, and 1000 s at 750 °C (**Figure 5-11** (a′)), 570 °C (**Figure 5-11** (b′)), and 460 °C (**Figure 5-11** (c′)), respectively. After that, the rate controlling mechanism is changed to the gas diffusion in micro pores. Such changes in rate controlling mechanism is attributed to the formation of Fe shell on the surface of iron oxide, as mentioned in section **3.3**; however, the time required for the formation of this Fe layer is likely shorter at higher temperatures. Comparing the rate-controlling mechanisms during microwave treatment and conventional heating demonstrates that the interfacial chemical reaction acts as the main barrier for the reduction reaction before formation of the metallic Fe shell; while the microwave irradiation enhances the rate of interfacial chemical reaction where the gas diffusion acts as dominant resistance for the reduction reaction from the onset of microwave irradiation. Therefore, the interfacial chemical reaction is progressed rapidly under microwave irradiation, especially at lower temperatures where the kinetic conditions for a great progress in the reaction are not available. This is likely attributed to the non-thermal (catalytic) effect of the microwave irradiation on speeding up the chemical reactions, as reported previously [15–18]. On the other hand, such behavior is likely related to the different interaction between particles and electromagnetic waves provided by either conventional heating or microwave irradiation. In the conventional heating, the thermal energy is usually transferred from heating elements to particle by infrared radiation which has a restricted penetration to the surface of the particle. Hence, the rest of the particle is heated via conduction from the hot surface. In the microwave irradiation, heat can be generated from within the particle (volumetric heating) owing to the penetrative power of microwaves [35].

The XRD internal quantitative analysis was conducted to clarify the progress of both ion exchange (**Eq. (4)**) and reduction (**Eq. (13)**) reactions in samples treated at 750, 570, and 460 °C during both microwave heating and conventional heating. I_{CaS}/I_{Si} (**Figure 5-12** (a) and (a′)) and I_{Fe}/I_{Si} (**Figure 5-12** (b) and (b′)) were considered as an index for the amount of produced CaS (during ion exchange reaction (**Eq. (4)**)) and Fe (during the reduction reaction (**Eq. (13)**)), respectively.

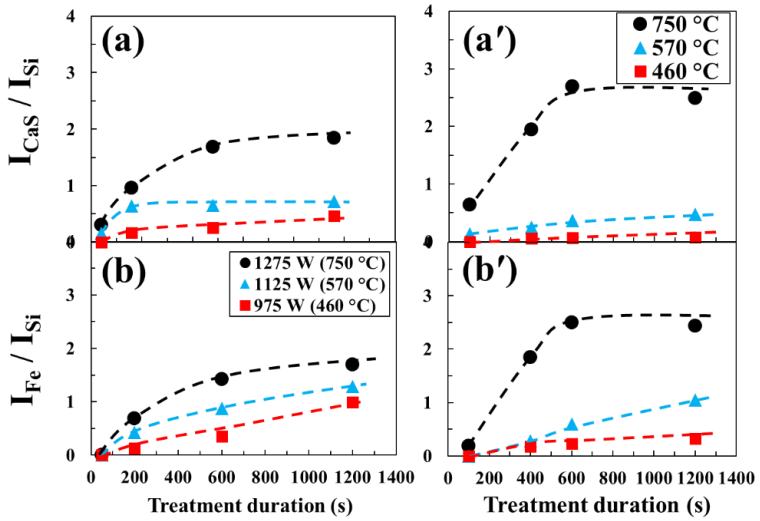

Figure 5-12 (a) and (b) XRD internal quantitative analysis of samples microwave treated at 1275 W (750 °C), 1125 W (570 °C), and 975 W (460 °C) for certain duration. (a′) and (b′) XRD internal quantitative analysis of samples conventionally heated at 750 °C, 570 °C, and 460 °C for certain duration. 10 mass % reagent Si powder was added as standard material to the treated sample, then I_{CaS}/I_{Si} and I_{Fe}/I_{Si} were calculated after X-ray diffraction analysis.

Considering the I_{CaS} / I_{Si}, the ion exchange reaction (**Eq. (4)**) initiated in the first 100 s of either microwave or conventional treatment at 750 and 570 °C whereas a longer processing time is required at 460 °C. This is attributed to the larger amount of energy which rapidly transferred to the sample during treatment at 750 °C (1275 W) and 570 °C (1175 W) than 460 °C (975 W). Further, this reaction progressed greatly in the first 600 s of treatment at 750 °C during either microwave heating or conventional heating, and then stagnated during longer processing up to 1200 s. At 570 °C, the ion exchange reaction progressed rapidly in the first 200 s of microwave treatment and then stagnated whereas during conventional heating, it progressed gradually up to 1200 s. At 460 °C, the ion exchange reaction progressed gradually during microwave irradiation whereas a very small progress was observed during conventional heating.

Variation of I_{Fe}/I_{Si} in **Figure 5-12** (b) showed that the reduction reaction (**Eq. (13)**) cannot progress well in the first 50 s of the microwave treatment (no Fe phase was detected owing to a low reduction degree and a small amount of iron phase) despite the formation of iron oxide via the onset of ion exchange reaction in the first 50 s (**Figure 5-12** (a)) at 1275 W (750 °C) and 1125 W (570 °C). Although the formation of iron oxide via the ion exchange reaction (**Eq. (4)**) is a prerequisite to initiate the reduction reaction (**Eq. (13)**), other conditions such as hydrogen accessibility to iron oxide and kinetics of the reduction reaction are also necessary for production of a a detectable amount of metallic iron by quantitative XRD analysis. It seems such conditions are provided after treatment duration > 50 s. A similar behavior observed in the first 100 s of conventional treatment at 570 and 460 °C (**Figure 5-12** (b′)) where no Fe peak was detected; however, the reduction reaction at 750 °C (**Figure 5-12** (b′)) initiated in the first 100 s of conventional treatment that is likely attributed to the formation of a noticeable amount of iron oxide via a great progress in the ion exchange reaction, regarding **Figure 5-12** (a′).

The quantitative analysis confirms an improvement in reaction progress during microwave irradiation, especially at lower temperatures, where the rate of chemical reaction cannot be sufficiently enhanced by only heating.

5-5-2. Activation energy

Considering the kinetic equation of gas diffusion rate controlling step presented in **Table 5-1**, effective diffusion coefficients (D_e, $cm^2.s^{-1}$) at different temperatures were calculated from slop of linear trend lines in gas diffusion plot, **Figure 5-9** (c), and illustrated in **Figure 5-13**.

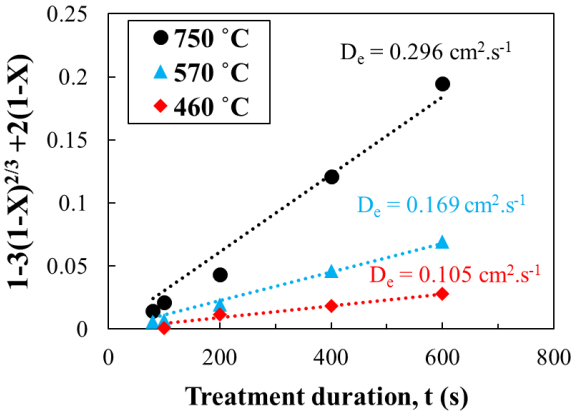

Figure 5-13 Effective diffusion coefficient of gas in micro pores of solid at 750, 570, and 460 °C.

To calculate activation energy for gas diffusion (E_D, $kJ.mol^{-1}$) during the process, the Arrhenius equation was applied. Further, to confirm that the un-reacted core model can be applied for determining of the dominant rate controlling mechanism, Qu *et al*. [33] suggested

that the activation energy can also be calculated by Friedman's method, which is a model free method. For this purpose, lnD_e (Arrhenius equation) and $ln(dX/dt)$ (Friedman's method) were plotted versus $10^4/T$, as shown in **Figure 5-14** (a) and (b), respectively. The slop of lines gives the activation energy calculated from Arrhenius equation and Friedman's method that are 22.3 and 16.9 kJ.mol^{-1}, respectively. No significant difference between the activation energy attained from the Friedman's method and the Arrhenius equation confirms that the un-reacted core mode can be applied in the present study and subsequently, the gas diffusion is the dominant rate controlling mechanism during microwave treatment.

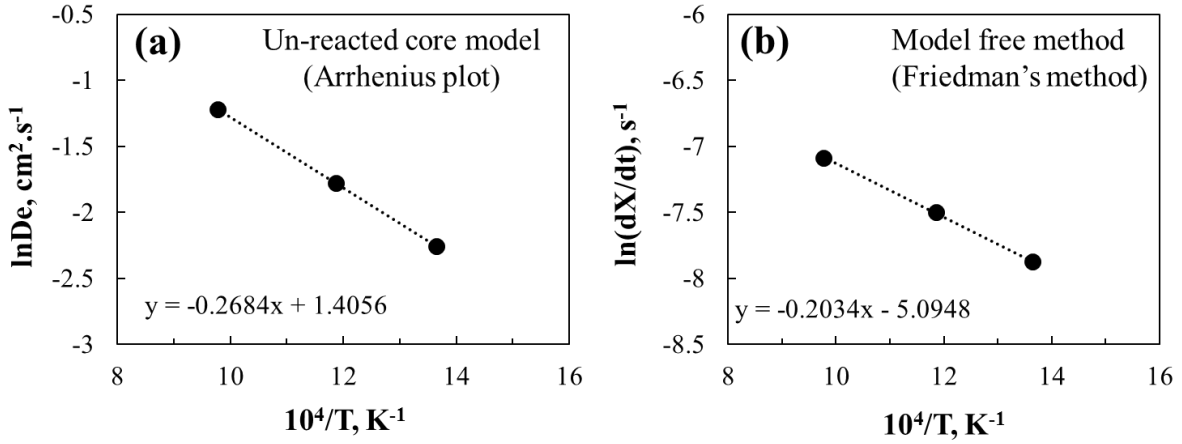

Figure 5-14 (a) Arrhenius and (b) Friedman's method plots for calculating the activation energy of gas diffusion in micro pores of solids during microwave treatment of the samples at 750, 570, and 460 °C.

In the conventional heating, the activation energy cannot be estimated in the present study owing to the change in the dominant rate controlling mechanism at different temperatures. Chatterjee *et al*. [36] have studied hydrogen-reduction of a chalcopyrite concentrate ($CuFeS_2$ and SiO_2) at 900-1050 °C during conventional heating and reported that the interfacial chemical reaction (with activation energy of ~101 kJ.mol^{-1}) is the rate-controlling step in the first 13 min and then the reaction is controlled by gas diffusion in micro pores of Cu and Fe layers (with activation energy of ~76 kJ.mol^{-1}). In the present study, the chemical reaction is likely progressed rapidly during microwave irradiation owing to the extraordinary effects of microwave irradiation (thermal and non-thermal) on speeding up the chemical reactions [15–18] and the overall reaction is controlled by gas diffusion after the onset of microwave irradiation.

5-6. Conclusions

Kinetics of iron production during hydrogen reduction of FeS-CaO mixture was investigated under microwave irradiation and conventional heating to clarify the effect of microwave irradiation on the dominant rate-controlling mechanisms. The results are summarized as follows:

1. Reduction of FeS-CaO mixture in H_2 can be considered as a two-step reaction: An ion exchange reaction between FeS and CaO that forms iron oxide on the surface of FeS particles. Then, H_2 reduces the iron oxide (product of the ion exchange reaction) to form a layer of metallic iron which surrounds the un-reacted part of FeS particles.

2. Hydrogen-reduction of FeS-CaO mixture during either microwave irradiation or conventional heating is a topochemical reaction and un-reacted core model is suitable for kinetic analysis.
3. The interfacial chemical reaction controls the rate of overall reaction in the first ~500, 800, and 1000 s of conventionally treatment at 750, 570, and 460 °C whereas for a longer treatment, the gas diffusion in micro pores is the dominant rate-controlling mechanism. This is attributed to a significant effect of the temperature and the formation of Fe shell on reaction progress during conventional heating.
4. The dominant rate-controlling mechanism from the onset of microwave irradiation is gas diffusion in micro pores with an activation energy of ~22.3 $kJ.mol^{-1}$. This is attributed to the extraordinary effect of microwave irradiation on speeding up the chemical reactions, especially at lower temperatures.

5-7. References

[1] Y.S.R. Hara, A. Jha, Carbothermic reduction of Zambian sulphide concentrates in presence of lime, Miner. Process. Extr. Metall. 122 (2013) 146–156.

[2] Y.R.S. Hara, A. Jha, Energy Efficient Separation of Magnetic Alloy fron the Carbothermic Reduction of NKANA Cu-Co Concentrates, in: Energy Technol. 2015, Springer International Publishing, Cham, 2015: pp. 83–91.

[3] Y.S.R. Hara, Mineral sulphide-lime reactions and effect of CaO/C mole ratio during carbothermic reduction of complex mineral sulphides, Int. J. Miner. Metall. Mater. 21 (2014) 1–11.

[4] A. Jha, P. Grieveson, Carbothermic reduction of pyrrhotite in the presence of lime for the production of metallic iron, Scand. J. Metall. 21 (1992) 50–62.

[5] M.L. Kutsovskaya, M.T. Hepworth, J.R. McGaa, Recovery of lime, sulfur, and iron from gypsum and pyrite wastes, Ind. Eng. Chem. Res. 35 (1996) 1736–1746.

[6] W. Liu, J.Y. Lim, M.A. Saucedo, A.N. Hayhurst, S.A. Scott, J.S. Dennis, Kinetics of the reduction of wüstite by hydrogen and carbon monoxide for the chemical looping production of hydrogen, Chem. Eng. Sci. 120 (2014) 149–166.

[7] A. Pineau, N. Kanari, I. Gaballah, Kinetics of reduction of iron oxides by H_2. Part I: Low temperature reduction of hematite, Thermochim. Acta. 447 (2006) 89–100.

[8] A. Pineau, N. Kanari, I. Gaballah, Kinetics of reduction of iron oxides by H_2. Part II. Low temperature reduction of magnetite, Thermochim. Acta. 456 (2007) 75–88.

[9] K.Y. Kim, E.J. Jang, D.Y. Kim, S.M. Jung, Effect of magnetic field on reduction of magnetite, Ironmak. Steelmak. 44 (2017) 6–16.

[10] T. Murakami, Y. Kamiya, T. Kodaira, E. Kasai, Reduction Disintegration Behavior of Iron Ore Sinter under High H_2 and H_2O Conditions, ISIJ Int. 52 (2012) 1447–1453.

[11] R.J. Fruehan, Y. Li, L. Brabie, E.-J. Kim, Final Stage of Reduction of Iron Ores by Hydrogen, Scand. J. Metall. 34 (2005) 205–212.

[12] F. Habashi, R. Dugdale, The reduction of sulfide minerals by hydrogen in the presence of lime, Metall. Trans. 4 (1973) 1865–1871.

[13] R. Padilla, M.C.C. Ruiz, H.Y.Y. Sohn, Reduction of molybdenite with carbon in the presence of lime, Metall. Mater. Trans. B. 28 (1997) 265–274.

[14] S.K. Kuila, R. Chatterjee, D. Ghosh, Kinetics of hydrogen reduction of magnetite ore fines, Int. J. Hydrogen Energy. 41 (2016) 9256–9266.

[15] A. Ferrari, J. Hunt, A. Lita, B. Ashley, A.E. Stiegman, Microwave-Specific Effects on the Equilibrium Constants and Thermodynamics of the Steam − Carbon and Related Reactions, J. Phys. Chem. C. 118 (2014) 9346–9356.

[16] J. Hunt, A. Ferrari, A. Lita, M. Crosswhite, B. Ashley, A.E. Stiegman, Microwave-specific enhancement of the carbon-carbon dioxide (Boudouard) reaction, J. Phys. Chem. C. 117 (2013) 26871–26880.
[17] J. Zhou, W. Xu, Z. You, Z. Wang, Y. Luo, L. Gao, C. Yin, R. Peng, L. Lan, A new type of power energy for accelerating chemical reactions: the nature of a microwave-driving force for accelerating chemical reactions, Sci. Rep. 6 (2016) 25149.
[18] K. Kashimura, M. Sato, M. Hotta, D. Kumar Agrawal, K. Nagata, M. Hayashi, T. Mitani, N. Shinohara, Iron production from Fe_3O_4 and graphite by applying 915 MHz microwaves, Mater. Sci. Eng. A. 556 (2012) 977–979.
[19] A. Amini, T. Maeda, K. Ohno, K. Kunitomo, Carbothermic Reduction Behavior of FeS in the Presence of CaO during Microwave Irradiation, ISIJ Int. 59 (2019), In Press.
[20] A. Amini, K. Ohno, T. Maeda, K. Kunitomo, Effect of the Ratio of Magnetite Particle Size to Microwave Penetration Depth on Reduction Reaction Behaviour by H_2, Sci. Rep. 8 (2018) 15023..
[21] Z. Wang, J. Zhang, K. Jiao, Z. Liu, M. Barati, Effect of pre-oxidation on the kinetics of reduction of ironsand, J. Alloys Compd. 729 (2017) 874–883.
[22] C. Ding, X. Lv, G. Li, C. Bai, S. Xuan, K. Tang, X. Lv, Isothermal reduction of powdery $2CaO{\cdot}Fe_2O_3$ and $CaO{\cdot}Fe_2O_3$ under H_2 atmosphere, Int. J. Hydrogen Energy. 43 (2018) 24–36.
[23] Y. Man, J. Feng, Effect of iron ore-coal pellets during reduction with hydrogen and carbon monoxide, Powder Technol. 301 (2016) 1213–1217.
[24] J. Oh, D. Noh, The reduction kinetics of hematite particles in H_2 and CO atmospheres, Fuel. 196 (2017) 144–153.
[25] D. Noguchi, K. Ohno, T. Maeda, K. Nishioka, M. Shimizu, Kinetics of Reduction Step of Wustite to Iron of Hematite and Quaternary Calcium Ferrite Mixtures, ISIJ Int. 53 (2013) 1350–1357.
[26] F. Schaube, A. Wörner, R. Tamme, High Temperature Thermochemical Heat Storage for Concentrated Solar Power Using Gas–Solid Reactions, J. Sol. Energy Eng. 133 (2011) 031006.
[27] F. Schaube, L. Koch, A. Wörner, H. Müller-Steinhagen, A thermodynamic and kinetic study of the de- and rehydration of $Ca(OH)_2$ at high H_2O partial pressures for thermo-chemical heat storage, Thermochim. Acta. 538 (2012) 9–20.
[28] I. Fujii, M. Ishino, S. Akiyama, M.S. Murthy, K.S. Rajanandam, Behavior of $Ca(OH)_2$/CaO pellet under dehydration and hydration, Sol. Energy. 53 (1994) 329–341.
[29] A. Jha, S. Tang, A. Chrysanthou, Phase equilibria in the metal-sulfur-oxygen system and selective reduction of metal oxides and sulfides: Part I. The carbothermic reduction and calcination of complex mineral sulfides, Metall. Mater. Trans. B Process Metall. Mater. Process. Sci. 27 (1996) 829–840.
[30] M.-H. Bai, H. Long, S.-B. Ren, D. Liu, C.-F. Zhao, Reduction Behavior and Kinetics of Iron Ore Pellets under H_2–N_2 Atmosphere, ISIJ Int. 58 (2018) 1034–1041.
[31] J. Wiley, K. Hepburn, O. Levenspiel, Chemical Reaction Engineering, 1964.
[32] M.S. Valipour, Mathematical Modeling of a Non-Catalytic Gas-Solid Reaction : Hematite Pellet Reduction with Syngas, Sci. Iran. 16 (2009) 108–124.
[33] Y. Qu, Y. Yang, Z. Zou, C. Zeilstra, K. Meijer, R. Boom, Reduction Kinetics of Fine Hematite Ore Particles with a High Temperature Drop Tube Furnace, ISIJ Int. 55 (2015) 952–960.
[34] T. Usui, M. Ohmi, S. Hirashima, N. Kitagawa, Kinetic Analysis on the Rate of Stepwise Reduction of a Single Sinter with CO-CO_2-N_2 Gas Mixture, Tetsu-to-Haganè. 73 (1987) 1956–1963.
[35] M. Gupta, E. Wong Wai Leong, Microwaves and Metals, John Wiley & Sons, 2007.

[36] R. Chatterjee, D. Ghosh, Kinetics of Hydrogen Reduction of Chalcopyrite Concentrate, Metall. Mater. Trans. B. 46 (2015) 2692–2705.
[37] C.R. Wilke, A Viscosity Equation for Gas Mixtures, J. Chem. Phys. 18 (1950) 517–519.

Appendix

$R_{(s)} + a\ A_{(g)} = p\ P_{(s)} + b\ B_{(g)}$

- Interfacial chemical reaction rate controlling:

$$-R_{AS} = k(C_{Ab} - C_{Ae})$$

$$-R_{AP} = 4\pi {r_t}^2\ (-R_{AS})$$

$$-R_{AP} = 4\pi {r_t}^2 k(C_{Ab} - C_{Ae})$$

$$-R_{RP} = -\frac{R_{AP}}{a}$$

$$-R_{RP} = -\frac{d}{dt}\left(\frac{4}{3}\pi {r_t}^3 C_R\right) = -4\pi {r_t}^2 C_R \frac{dr_t}{dt}$$

Where r_t is the radius of un-reacted core at time t.

$$-\frac{dr_t}{dt} = \frac{k(C_{Ab} - C_{Ae})}{aC_R}$$

$$\frac{r_t}{r_i} = 1 - \frac{k(C_{Ab} - C_{Ae})}{aC_R} t$$

$$X = \frac{W_i - W_t}{W_i} = 1 - \left(\frac{r_t}{r_i}\right)^3$$

$$1 - (1 - X)^{1/3} = \frac{k(C_{Ab} - C_{Ae})}{aC_R r_i} t$$

- Mass transfer between gas and solid rate controlling:

$$-\dot{n}_{Af} = 4\pi r_i^2 k_f (C_{Ab} - C_{AS})$$

$$\dot{n}_{Bf} = 4\pi r_i^2 k_f (C_{BS} - C_{Bb})$$

$$-R_{AP} = -\dot{n}_{Af} = \dot{n}_{Bf}$$

$$-R_{AP} = 4\pi r_i^2 k_f \left(\frac{K}{1+K}\right)(C_{Ab} - C_{Ae})$$

$$-R_{RP} = \frac{-R_{AP}}{a}$$

$$-R_{RP} = -\frac{d}{dt}\left(\frac{4}{3}\pi {r_t}^3 C_R\right) = -4\pi {r_t}^2 C_R \frac{dr_t}{dt}$$

$$-R_{AP} = a(-R_{RP}) = -4\pi {r_t}^2 a C_R \frac{dr_t}{dt}$$

$$-\frac{dr_t}{dt} = \frac{k_f}{aC_R}\left(\frac{K}{1+K}\right)(C_{Ab} - C_{Ae})(\frac{r_i}{r_t})^2$$

$$\int_{r_i}^{r_t}[-\left(\frac{r_i}{r_t}\right)^{-2}]dr_t = \int_0^t [\frac{k_f}{aC_R}\left(\frac{K}{1+K}\right)(C_{Ab} - C_{Ae})]dt$$

$$1 - (\frac{r_t}{r_i})^3 = \frac{3k_f}{aC_R r_i}\left(\frac{K}{1+K}\right)(C_{Ab} - C_{Ae})t$$

$$X = \frac{W_i - W_t}{W_i} = 1 - \left(\frac{r_t}{r_i}\right)^3$$

$$X = \frac{3k_f}{aC_R r_i}\left(\frac{K}{1+K}\right)(C_{Ab} - C_{Ae})t$$

- Gas diffusion in micro pores rate controlling:

Mass transfer rate A:

$$-\dot{n}_A = 4\pi r_i^2 (D_A)_{eff} \frac{dC_A}{dr}$$

Integration from r = r_t ($C_A = C_{Ai}$) to r = r_i ($C_A = C_{AS}$)

$$-\dot{n}_A = (D_A)_{eff} \frac{4\pi r_i r_t}{r_i - r_t}(C_{Ab} - C_{Ae})$$

$$\dot{n}_B = (D_B)_{eff} \frac{4\pi r_i r_t}{r_i - r_t}(C_{Be} - C_{Bb})$$

$$-R_{AP} = -\dot{n}_A = \dot{n}_B$$

$$K = \frac{C_{Be}}{C_{Ae}}$$

$$\frac{1}{D_e} = \frac{K}{1+K}\left(\frac{1}{(D_A)_{eff}} + \frac{1}{(D_B)_{eff}}\right)$$

$$-R_{AP} = D_e\left(\frac{4\pi r_i r_t}{r_i - r_t}\right)\left(\frac{K}{1+K}\right)(C_{Ab} - C_{Ae})$$

$$-R_{RP} = \frac{-R_{AP}}{a}$$

$$-\frac{dr_t}{dt} = \frac{k(C_{Ab} - C_{Ae})}{aC_R}$$

$$-\frac{dr_t}{dt} = \frac{D_e}{aC_R}\left(\frac{K}{1+K}\right)(C_{Ab} - C_{Ae})\frac{r_i}{r_t(r_i - r_t)}$$

Integration from t = 0 ($r_t = r_i$) to t = t ($r_t = r_t$) if r_i be constant:

$$1 - 3\left(\frac{r_t}{r_i}\right)^2 + 2\left(\frac{r_t}{r_i}\right)^3 = \frac{6D_e}{aC_R r_i^2}\left(\frac{K}{1+K}\right)(C_{Ab} - C_{Ae})t$$

$$X = \frac{W_i - W_t}{W_i} = 1 - \left(\frac{r_t}{r_i}\right)^3$$

$$1 - 3(1-X)^{2/3} + 2(1-X) = \frac{6D_e}{aC_R r_i^2}\left(\frac{K}{1+K}\right)(C_{Ab} - C_{Ae})t$$

- Mixing rate controlling

$$-R_{AP} = \frac{4\pi {r_i}^2 \left(\frac{K}{1+K}\right)(C_{Ab} - C_{Ae})}{\frac{1}{k_f} + \frac{1}{D_e}\cdot\frac{r_i(r_i - r_t)}{r_t} + \frac{K}{k(1+K)}\left(\frac{r_i}{r_t}\right)^2}$$

$$-R_{AP} = a(-R_{RP}) = -4\pi {r_t}^2 aC_R\frac{dr_t}{dt}$$

$$-\frac{dr_t}{dt} = \frac{\frac{1}{aC_R}\left(\frac{K}{1+K}\right)(C_{Ab} - C_{Ae})}{\frac{1}{k_f}\left(\frac{r_t}{r_i}\right)^2 + \frac{1}{D_e}\cdot\frac{r_t(r_i - r_t)}{r_i} + \frac{K}{k(1+K)}}$$

Integration from t = 0 ($r_t = r_i$) to t = t ($r_t = r_t$):

$$\frac{1}{3k_f}\left[1 - \left(\frac{r_t}{r_i}\right)^3\right] + \frac{r_i}{6D_e}\left[1 - 3\left(\frac{r_t}{r_i}\right)^2 + 2\left(\frac{r_t}{r_i}\right)^3\right] + \frac{K}{k(1+K)}\left[1 - \frac{r_t}{r_i}\right] = \frac{1}{aC_R r_i}\left(\frac{K}{1+K}\right)(C_{Ab} - C_{Ae})t$$

$$X = \frac{W_i - W_t}{W_i} = 1 - \left(\frac{r_t}{r_i}\right)^3$$

$$\frac{X}{3k_f} + \frac{r_i}{6D_e}\left[1 - 3(1-X)^{2/3} + 2(1-X)\right] + \frac{K}{k(1+K)}\left[1 - (1-X)^{1/3}\right] = \frac{1}{aC_R r_i}\left(\frac{K}{1+K}\right)(C_{Ab} - C_{Ae})t$$

$$\boldsymbol{f = \frac{r_i - r_t}{r_i} = \left[1 - (1 - X)^{1/3}\right]}$$

$$\boldsymbol{\frac{1}{aC_R r_i}\left(\frac{K}{1+K}\right)(C_{Ab} - C_{Ae})\frac{t}{f} - \frac{3 - 3f + f^2}{3k_f} = \frac{r_i}{6D_e}(3f - 2f^2) + \frac{K}{k(1+K)}}$$

$$r_i = \left(\frac{3}{4} r_b^2 h_b\right)^{1/3}$$

r_b and h_b represent radius and height of briquette sample, respectively.
Gas concentration in bulk:

$$C_{Ab} = \frac{n}{V_b}$$

Gas concentration at equilibrium state:

$$C_{Ae} = \frac{n}{V_e}$$

$$\frac{n}{V_x} = \frac{P_x}{RT}$$

P_b = 1 atm

Gas flow rate at temperature T:

$$v_T = \frac{v_{298} \times T \times 1000}{298 \times 60}$$

$$u_\infty = \frac{v_T}{\pi r^2}$$

$$u_\infty = 6.3486 \times 10^{-3}\, T$$

v_T ($cm^3.s^{-1}$) is the gas flow rate at temperature T, v_{298} ($L.min^{-1}$) is the gas flow rate at 25 °C, u_∞ ($cm.s^{-1}$) is the gas velocity, r (cm) is the radius of reaction tube.

Oxygen density in the sample, C_R ($mol.cm^{-3}$), calculated as follow:

$$C_R = \frac{W_i\left(\frac{M_O}{M_O + M_{Fe} + M_{Ca} + M_S}\right)}{M_O V_{app}}$$

M_O, M_{Fe}, M_{Ca}, and M_S ($g.mol^{-1}$) represent the molar weight of oxygen, iron, calcium, and sulfur, respectively. V_{app} (cm^3) is the apparent volume of briquette samples (π×[radius]^2× height).

Equilibrium constant, K (dimensionless), can be calculated according to:

$$\Delta G° = -RT\,lnK$$

Substituting of $\Delta G°$ from **Eq. (13)** gives the following equation:

$$lnK = 1.016 - 1953.33T^{-1}$$

Mass transfer coefficient, k_f (cm.s^{-1}),

$$Sh = \frac{k_f L}{D_{H_2-H_2O}}$$

$$Sh = 2 + 0.6\, Re_P^{1/2}\, Sc^{1/3}$$

$$Re_P = \frac{\rho u_\infty L}{\mu}$$

$$Sc = \frac{\mu}{\rho D_{H_2-H_2O}}$$

$$k_f = \frac{2D_{H_2-H_2O}}{L} + \frac{0.6\, u_\infty^{1/2}\, \rho_{H_2-H_2O}^{1/6}\, D_{H_2-H_2O}^{2/3}}{L^{1/2}\, \mu_{H_2-H_2O}^{1/6}}$$

$$L = 6 \times \frac{\pi r_b^2 h_b}{2\pi r_b^2 + 2\pi r_b h_b}$$

Joseph O. Hirschfelder:

$$D_{H_2-H_2O} = 1.8583 \times 10^{-3} \frac{T^{3/2}}{P\, \sigma_{H_2-H_2O}^2\, \Omega_{H_2-H_2O}} \left(\frac{1}{M_{H_2}} + \frac{1}{M_{H_2O}}\right)^{1/2}$$

where σ is the intermolecular distance that gives $\Phi = 0$ in the "Lennard-Jones12-6 potential".

$$\phi_{H_2-H_2O} = 4\, \varepsilon_{H_2-H_2O} \left[\left(\frac{\sigma_{H_2-H_2O}}{r}\right)^{12} - \left(\frac{\sigma_{H_2-H_2O}}{r}\right)^{6}\right]$$

$$\sigma_{H_2-H_2O} = \frac{1}{2}\left(\sigma_{H_2} + \sigma_{H_2O}\right)$$

$$\varepsilon_{H_2-H_2O} = \sqrt{\varepsilon_{H_2} \varepsilon_{H_2O}}$$

In case of no data:

$$\sigma = 2.44 \left(\frac{T_c}{P_c}\right)^{1/3} \qquad [\text{Å}]$$

$$\frac{\varepsilon}{k_B} = 0.77\, T_c \qquad [\text{K}]$$

where T_c and P_c are the critical temperature and pressure, respectively. k_B is the Boltzman's constant.

Collision integral, Ω, can be evaluated as a function of k_B T/ε from Table

Density:

$$\rho = \frac{\left(x_{H_2}\, M_{H_2} + x_{H_2O}\, M_{H_2O}\right)P}{RT}$$

$$P_i = P\, x_i$$

$$\rho = \frac{\left(P_{H_2}\, M_{H_2} + P_{H_2O}\, M_{H_2O}\right)}{RT}$$

Viscosity of mixture gas: Wilke equation [37]

$$\mu_{mix} = \sum_{i=1}^{n} \left[\frac{x_i \mu_i}{x_i + \sum_{j=1, j\neq i}^{n} x_j \phi_{ij}} \right]$$

$$\phi_{ij} = \frac{\left[1 + \left(\frac{\mu_i}{\mu_j}\right)^{1/2} \left(\frac{M_j}{M_i}\right)^{1/4}\right]^2}{\sqrt{8}\left[1 + \frac{M_i}{M_j}\right]^{1/2}}$$

$$\mu_{H_2-H_2O} = \frac{x_{H_2}\, \mu_{H_2}}{x_{H_2} + x_{H_2O}\, \phi_{H_2-H_2O}} + \frac{x_{H_2O}\, \mu_{H_2O}}{x_{H_2O} + x_{H_2}\, \phi_{H_2O-H_2}}$$

The viscosity of pure gas, Hirschfelder's equation:

$$\mu_i = 2.6693 \times 10^{-5}\, \frac{\sqrt{M_i T}}{\sigma_i^2 \Omega_\mu}$$

Table 5-3 Lennard-Jones Parameters

	σ [Å]	ε / k_B [K]		σ [Å]	ε / k_B [K]
H_2	2.915	38.0	CO	3.590	110
Fe	2.44	3520	CO_2	3.996	190
Ar	3.418	124	SO_2	4.290	252
Air	3.617	97.0	O_2	3.433	113
N_2	3.681	91.5	CH_4	3.822	137

Table 5-4 Critical temperature (T_C) and critical pressure (P_C)

	T_C [K]	P_C [atm]		T_C [K]	P_C [atm]
H_2	33.3	12.8	CO	133.2	34.5
H_2O	647.4	218.3	CO_2	304.2	72.9
Ar	151.2	48.0	SO_2	430.7	77.8
Air	132.5	37.2	O_2	154.8	50.1
N_2	126.2	33.5	CH_4	191.1	45.8

Chapter 6: SUMMARY

A novel pre-treatment of high sulfur iron ore via employing both hydrogen and microwave irradiation was experimentally investigated in different steps and the following results were achieved:

First, the interaction between microwaves and Fe_3O_4 particles in N_2 was studied at both high temperatures (T>585 °C) and temperatures lower than the Curie point (T<585 °C). Results showed that at T>585 °C, the particle size of Fe_3O_4 has no effect on the microwave absorption. At T<585 °C, small particles fall in the transparent region and cannot absorb microwaves whereas larger particles act as a microwave susceptor and heat well. Therefore, microwave irradiation can be used as an efficient heating source for magnetite treatment owing to a good coupling of microwaves and magnetite particles; however, an optimum ratio of magnetite particle size to microwave penetration depth is required for a maximum microwave absorption by particles.

Next, the atmosphere was changed to H_2 to combine the advantages of microwave heating and using H_2 as a reducing agent, for the first time in the world, to investigate an eco-friendly hydrogen-reduction of Fe_3O_4 under microwave treatment for a further mitigation of CO_2 emission. Such novel technique can open a new window to the world of microwave treatment and solid-gas reactions. Results revealed that the formation of FeO via reduction reaction ($Fe_3O_{4(s)}+H_{2(g)}=3FeO_{(s)}+H_2O_{(g)}$) increases the microwave absorption of the sample while the formation of metallic iron ($FeO_{(s)}+H_{2(g)}=Fe_{(s)}+H_2O_{(g)}$) results in less absorption of microwaves. Further, a lower reduction degree was obtained in small particles which have a very low ratio of particle size to microwave penetration depth (d/δ), and behave as a transparent material that heated via convection and/or conduction instead of the microwave heating.

Then, carbothermic reduction and desulfurization of FeS−CaO−C was investigated during microwave heating to confirm the effect of microwave irradiation on these reactions. Results demonstrated that the carbothermic reduction of iron oxide can be conducted in a shorter time and at a lower temperature during microwave heating than the conventional heating.

Finally, the effect of sulfur on the iron oxide reduction during microwave treatment in H_2 was studied by adding FeS, as sulfur source, and CaO, as desulfurizer, to the Fe_3O_4 sample. For this purpose**,** the microwave heating system was equipped with thermobalance to prepare a unique apparatus for a continuous study of the hydrogen reduction during microwave irradiation. Results showed that a reduction degree similar to the pure Fe_3O_4 is attained wherein the CaO acts as a good desulfurizer via an ion exchange reaction ($FeS_{(s)}+CaO_{(s)}=FeO_{(s)}+CaS_{(s)}$) and prevents SO_2 emission. Moreover, comparing the kinetics of iron production from treatment of FeS−CaO mixture in H_2 during both microwave irradiation and conventional heating demonstrated that the rate controlling mechanism in conventional heating is chemical reaction in the beginning of the treatment and then it is changed to gas diffusion. In case of using microwave heating, the rate controlling mechanism is gas diffusion from the onset of microwave irradiation that is attributed to the extraordinary effect of microwave irradiation on the rate of chemical reactions, especially at lower temperatures.

According to the results of the present study, both hydrogen, as a reducing agent, and microwave irradiation can be employed during treatment of iron ore such as reduction and desulfurization. If so, a further mitigation of CO_2 emission and speeding up the chemical reactions are expected.

Acknowledgments

I want to thank my Father and Mother who spent their life and their youth to teach me how to live. I wish to thank them for all they did for me to achieve my dreams.

I want to thank my wife, for all she did to prepare good conditions for me to do only research without any other concern. I have to thank her for times that she pushed me forward when I was disappointed and tired of bad experimental results.

I would like to appreciate Prof. Kunitomo, Prof. Ohno, and Prof. Maeda for giving me the chance of being a member of their group and giving me many valuable advices during my PhD course. I wish to represent my gratitude to them for preparing any required conditions for me to do research, attend conferences and publish papers.

I want to thank my Father and Mother in law, and my sisters and brother and my brother in law for their moral support and their positive energy that always give me.

I would like to thank all of my friends who taught me how to use facilities in the laboratory and helped me.

I wish to thank the Kyushu University and Ministry of Education, Culture, Sports, Science and Technology (MEXT) of Japan for accepting me as a MEXT PhD scholar.

Ahmadreza Amini